The Dissertation Committee for Michaela T. Huynh Certifies that this is the approved version of the following Dissertation:

Persistent Oxidative Damage Accounts for the Origin of Mutations Observed in Uterine Pathology

Committee:

Sandra Hatch, MD, Supervisor

Lawrence C. Sowers, PhD

Lisa Elferink, PhD

Tapas Hazra, PhD

Matthew Anderson, MD, PhD

Dean, Graduate School of Biomedical Sciences

Persistent Oxidative Damage Accounts for the Origin of Mutations Observed in Uterine Pathology

by

Michaela Thanh Tra-Mi Huynh, BS

Dissertation

Presented to the Faculty of the Graduate School of

The University of Texas Medical Branch

in Partial Fulfillment

of the Requirements

for the Degree of

Doctor of Philosophy

The University of Texas Medical Branch

September 2016

Persistent Oxidative Damage Accounts for the Origin of Mutations Observed in Uterine Pathology

Michaela Thanh Tra Mi Huynh, PhD

The University of Texas Medical Branch, 2016

Supervisor: Lawrence C. Sowers

Endometrial adenocarcinoma and leiomyomas are prevalent disorders of the same organ. Endometrial cancer, the most prevalently diagnosed gynecological cancer, is associated with mutated PTEN tumor suppressor gene. The type I endometrial cancer PTEN hotspot mutation involves a cytosine to guanine transversion. The mechanism for C to G transversions in endometrial tissue has not been previously explained. For the first time, we show that the CpG dinucleotide of codon 130 is methylated, which increases the likelihood of oxidative damage to the adjacent guanine. 8oxoG, in the presence of peroxynitrite, can form guanidinohydantoin or spiroiminodihydantoin and mispair with guanine, explaining C:G>G:C mutations. We show that uterine tissue is persistently exposed to peroxynitrite, which can also generate nitrotyrosine by interaction with proteins. We have also detected nitrated proteins in benign human uterine tissue, and for the first time identified the predominantly nitrated protein as ACTBL2.

Leiomyomas are frequently observed and are a common indication for hysterectomy. Leiomyomas are known to contain MED12 codon 44 mutations at high frequency, involving all 6 possible guanine substitutions in the codon GGT. We show that myometrium is persistently exposed to peroxynitrite, as is endometrium. Oxidative guanine damage, promoted by peroxynitrite exposure, explains the prevalence of guanine mutations observed in leiomyomas.

Benign human endometrial tissue and normal myometrium are persistently exposed to peroxynitrite, indicating similar mutagenic pathways in both uterine tissues.

TABLE OF CONTENTS

List of Tables

List of Figures

List of Abbreviations

8oxoG	8-oxo-7,8-dihydroguanine
COSMIC	Catalogue of Somatic Mutations in Cancer (cancer.sanger.ac.uk)
EIN	Endometrial intraepithelial neoplasia
Gh	Guanidinohydantoin
MPO	Myeloperoxidase
MSI	Microsatellite instability
PP_i	Pyrophosphate
Sp	Spiroiminodihydantoin

Chapter 1 Introduction

Uterine Tissue

The uterus is a pear-shaped reproductive organ, which lies posterior to the bladder and anterior to the rectum. Fallopian tubes extend from the uterus toward the ovaries, serving as the conduit of an ovum to the uterus, in which a fertilized ovum implants. The uterus is composed of an inner endometrial layer. The endometrium is composed of two compartments: the functionalis and the basalis (Fig. 1.1). The functionalis is highly responsive to hormonal stimulation and sheds each month if an egg is not implanted, resulting in menses. The basalis is not shed during menses and instead houses the stem cells that proliferate to form the functionalis during the next menstrual period. The functionalis and basalis are histologically distinct: the functionalis is highly responsive to hormone stimulation and its histological appearance fluctuates as the menstrual cycle progresses (Fig. 1.2), whereas the basalis appears consistent throughout the menstrual cycle. Both compartments contain glands and intervening stroma. The endometrial glands are lined by epithelial cells, which secrete a glycogen-rich material into the lumen. This material aids in embryo implantation and growth.

The basalis lies adjacent to the myometrium, composed primarily of smooth muscle. The myometrium undergoes hypertrophy to accommodate a growing fetus in the womb. The myometrium also functions in forceful contractions to expel the fetus. The myometrium extends to the outermost wall of the uterus, covered by a serosal lining.

Menstrual Cycle

The menstrual cycle is dated by the first day of menses. The first half of a typical 28-day cycle is the proliferative phase; during which the the basalis rapidly proliferates to form the functionalis. If an egg is not implanted into the endometrium, the uterus proceeds into the secretory phase. This phase lasts 2 weeks and precedes menstruation. During the secretory phase,

the endometrial glands secrete a variety of nutrients intended to support an implanted embryo (1).

As the menstrual cycle progresses, changes in histologic structures in the functionalis can be observed. These findings were reported by Noyes (2) and have been used to date uterine tissue according to a 28-day menstrual cycle. Representative characteristics can be seen in Fig. 1.2. For instance, proliferative phase glands are linear, whereas secretory phase glands are tortuous and branching. The stroma periodically appears edematous then shows decidual changes towards the end of the secretory phase. Characteristics of secretory phase glands can be used to determine menstrual cycle dating: the position of the nucleus in relation to secretory vesicles varies with time. Because these changes do not occur stochastically, dating can be narrowed down to a window of a few days based on any one histological characteristic and refined by considering additional histological criteria. During the proliferative phase, histologic changes are more subtle than in the secretory phase, so dating can be narrowed down to early, middle, or late rather than day by day.

Endometrial adenocarcinoma

Endometrial adenocarcinoma is the most frequently diagnosed gynecological cancer in the United States (3,4). Endometrial carcinoma is subdivided into Type I and Type II endometrial cancer based on histological characteristics. Type I endometrial cancer is diagnosed based on the histological determination of endometrial glands which maintain endometrioid morphology but over-proliferate relative to the surrounding stroma. Type II endometrial cancer arises in the setting of endometrial hyperplasia and risk of development is related to unopposed estrogen exposure. This is in opposition to Type II endometrial adenocarcinoma cases, which include endometrial tissue of clear cell, serous, or mixed morphology and typically present in the setting of endometrial atrophy. The two subtypes differ in a number of respects, including prognosis and known mutation spectrum. When diagnosed at an early stage, Type I endometrial cancer prognosis is good, with a 83-97% five year survival rate which falls drastically as cases

progress to later stage (5,6) whereas the five-year survival rate of patients with Type II is less than 70%. Currently, cost-effective sensitive and specific screening tools are not available for diagnosis of endometrial cancer (7). Women typically present for diagnosis when they experience abnormal uterine bleeding. We aim to contribute to early diagnostic techniques and prevention by contributing an understanding of the factors that lead to carcinogenesis.

Type I endometrial adenocarcinoma was thought to progress from endometrial hyperplasia. Endometrial hyperplasia was divided into 4 subcategories: simple hyperplasia without nuclear atypia, simple hyperplasis with nuclear atypia, complex hyperplasia without nuclear atypia and complex hyperplasia with nuclear atypia. As nuclear complexity increases and the presence of nuclear atypia is observed, the likelihood of progression to endometrial cancer increases.

More recently, it has been debated that type I endometrial adenocarcinoma arises from endometrial intraepithelial neoplasia (EIN) (8). EIN is characterized by an increased gland to stroma ratio affecting an area greater than 1 mm with the glands having altered cytologic appearance from the background glands. EIN is a more accurate predictor of progression to endometrial cancer than the hyperplastic conditions mentioned above.

The most prevalently observed mutations in Type I cases are mutations in the PTEN gene, followed by mutations in genes which encode for other proteins active in the PI3K pathway. PTEN is also most frequently observed to be mutated in endometrial cancer cases, in comparison to any other cancer set (COSMIC). According to COSMIC, PTEN mutations make up 44% of the mutations observed in endometrioid carcinoma samples with ranges of 26-69.3% (9–11) reported in the literature. PTEN mutation has been observed in 55% of EIN (12) and >9.6% of endometrial hyperplastic precancers (10,13), and even in benign endometrial tissues (14). Not only do PTEN mutations contribute to endometrial carcinogenesis, mutation of PTEN occurs early along the progression of normal to cancer, with the potential for null glands to involute or progress to EIN and cancer (14,15).

Type II cases predominantly contain p53 mutations, which are not observed in early stage Type I cases but are observed in late stage Type I cases. Early detection of molecular changes that lead to endometrial cancer will lead to targeted therapies to prevent progression of lesions to a cancerous state. We sought to explain how molecular factors which promote mutagenesis arise or accumulate in endometrium by studying benign human endometrial tissues.

PTEN

Various genes are known to be mutated in Type I endometrial cancer. The genes mutated predominantly upregulate the PI3K-AKT pathway, resulting in dysregulated cellular proliferation and decreased apoptosis. The predominant gene mutated in type I endometrial cancer is PTEN (11,16).

PTEN, a tumor suppressor gene, functions as a protein tyrosine phosphatase (PTP) and lipid phosphatase. The lipid phosphatase activity inhibits cellular signaling through the PI3K-AKT pathway by catalyzing the conversion of PIP3 into PIP2, reversing the action of PI3K. This effectively decreases AKT phosphorylation and increases apoptosis. PTEN is encoded on by a gene found at chromosome 10q23, comprising 9 exons. The PTEN protein contains 403 amino acids which make up an unstructured N terminal, PIP2-binding domain, phosphatase domain, C2 domain, a unstructured C terminal tail (17,18). The PIP2-binding domain is found at the N-terminus of the protein. The phosphatase domain spans residues 15-185 and contains the P loop (residues 123-130) used in PIP3 dephosphorylation (19,20). The C2 domain is reported to function in post-translational regulation of PTEN PIP3 phosphatase function (18). Whether the C2 domain (residues 186-351) also participated in membrane-recruitment is debated (21). Recently is has been reported that phosphorylation at the C-terminal tail impairs binding at the phospholipid membrane (22) and that the C-terminal tail stabilizes homodimerization of PTEN (23).

As endometrial cancer is one of the characteristic developments of Lynch syndrome, many groups have studied whether microsatellite instability (MSI) plays a role in sporadic

endometrial carcinogenesis as it does in Lynch syndrome. MSI is defined by detected insertion/deletion mutations at multiple DNA repeat loci, as measured by sequencing of five National Cancer Institute recommended sequences (24), MSI has been detected in up to 44% of sporadic EC cases (9) and cases of hyperplasia with MSI are more likely to contain mutations in PTEN than in microsatellite stable hyperplasia (13). MSI, which is thought to result from the dysregulation of mismatch repair genes such as MLH1, MSH2, MSH6, and PMS2 would explain a subset of PTEN mutations observed in sporadic endometrial carcinoma, such as insertion/deletion mutations at polyA tracks (25). But, rather than MSI causing PTEN mutations, Zhou et al. suggest that PTEN mutations precede mismatch repair defects and microsatellite instability (26). Given the controversy of ascribing PTEN mutations to MSI, we instead seek to explain the origins of PTEN substitution mutations, which has not previously been elucidated in sporadic endometrial carcinoma.

The most frequently mutated PTEN codon in type I endometrial adenocarcinoma is codon 130 (Fig 1.3).R130 is the last residue of the P loop and is necessary for the lipid phosphatase catalytic function of PTEN (19). Mutation at R130 to R130G results in loss of lipid phosphatase activity (27). Due to homodimerization of PTEN, mutated PTEN can act in a dominant negative manner, suppressing the action of bound wild type PTEN (27,28). It has also been suggested that PTEN function is dose dependent, with a small downregulation of expression leading to an increase in tumor risk (29).

At codon 130, a C>T mutation would result in p.R130X and a G>A mutation would result in p.R130Q. PTEN p.R130X results in a truncated PTEN protein which is unstable and rapidly degraded, causing the cell to mimic a heterozygous PTEN state (27). Loss of one allele of PTEN does not dictate progression to endometrial cancer, as described by Podsypanina et al. (30). This phenomenon is also supported by Mutter et al.'s study concerning the involution of PTEN-null glands observed in benign endometrium (14). But presence of a PTEN mutation promotes endometrial carcinogenesis in the event of a second hit, either to the second PTEN allele (31) or another gene affecting mTOR signaling (32). In cell culture, PTEN p.R130Q

results in increased detected phospho-AKT (27), resulting from PTEN dysfunction. Loss of PTEN function allows cells a selective advantage over wildtype cells by dysregulation of PIP3 signaling, allowing mutant cells to proliferate.

A confounding factor of PTEN studies is the existence of a PTEN pseudogene, found on chromosome 9 (33,34). The pseudogene aligns with the exonic sequence of PTEN, without intervening intronic sequences. Amplification and sequencing of PTEN requires attention to the hazard of mistakenly sequencing the PTEN pseudogene. Sequencing studies have addressed this hazard by designing primers which bind to the intronic/exon border or bind to the intervening intronic sequences.

Cancer comparison

PTEN, as a tumor suppressor gene, is mutated in a variety of cancers such as primary glioblastoma. PTEN hotspot mutations appear in both type I endometrial carcinoma and primary glioblastoma cases, and while some of the hotspots observed in glioblastoma are also seen in endometrial cancer, the spectrum of mutations observed is different. This can be seen in (Fig. 1.4), generated from data curated from the Catalogue of Somatic Mutations in Cancer (COSMIC) data base (cancer.sanger.ac.uk/cosmic/browse/tissue). The top 3 Type I EC substitution hotspots occur at codon positions 130, 233, and 173 whereas the top 5 glioblastoma PTEN substitution hotspot locations are 105, 130, 173, 233, and 335. We note, for the first time, that the majority of these hotspots, with the exception of codon 105, contain CpG dinucleotides. We also note that C>T and G>A mutations are observed at all of these sites, two mutations that could be attributed to deamination of methyl-cytosine. But is not known whether the CpG dinucleotide at the PTEN hotspots are methylated. We, herein, focus on PTEN codon 130 as it is most frequently mutated in endometrial cancer. C:G to G:C mutations comprise 51.7% of PTEN codon 130 substitution mutations in endometrial adenocarcinoma, but only 18.2% of such in gliomas. The difference in mutation spectrum between endometrial cancer and glioblastoma points to a difference in the microenvironment which promotes C>G mutations in endometrial

cancer and C>T mutation in glioma. As of yet, the origin of C:G>T:A mutations observed in endometrial carcinoma have not been elucidated.

Sample selection

Rather than study tissue obtained from pathological samples, we concentrated our efforts on benign human uterine tissue to study molecular changes that occur prior to the onset of pathology. Knowing the mechanism of mutation will lead to development of techniques for prevention.

By studying precursors to tumor formation, we will contribute to earlier diagnosis and preventative measures.

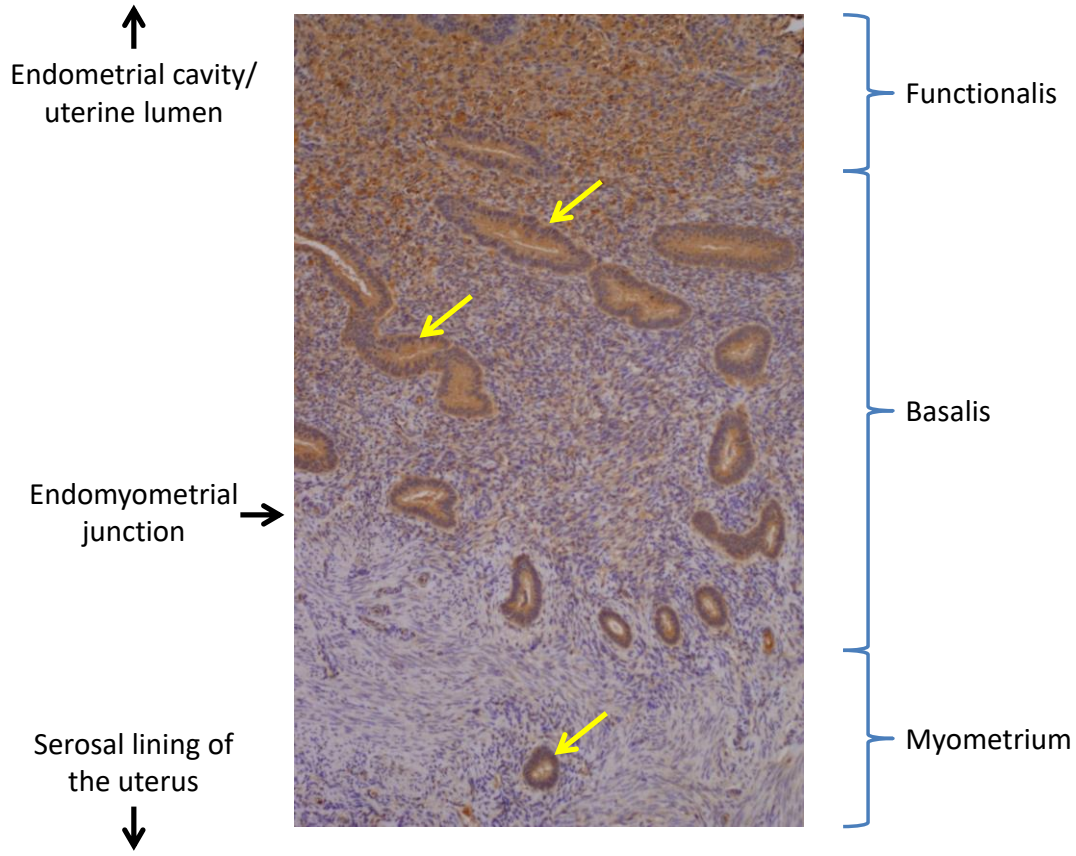

Figure 1.1: Cross section of uterine tissue.

Endometrium is adjacent to myometrium in the human uterus. The endometrium is subdivided into the functionalis and basalis, the former sheds during menses and the latter contains the stem cells that proliferate to reform the functionalis.

The endometrium lines the uterine cavity and is surrounded by smooth muscle (myometrium). The endometrium contains endometrial glands and stroma. Eutopic glands can be visualized in the endometrium, and seen invaginating into the myometrium. Section is representative of proliferative phase uterine tissue. Image is captured at 10x magnification.

Brown staining denotes nitrotyrosine immunoreactivity and blue staining results from the Harris heamatoxylin counterstain for DNA.

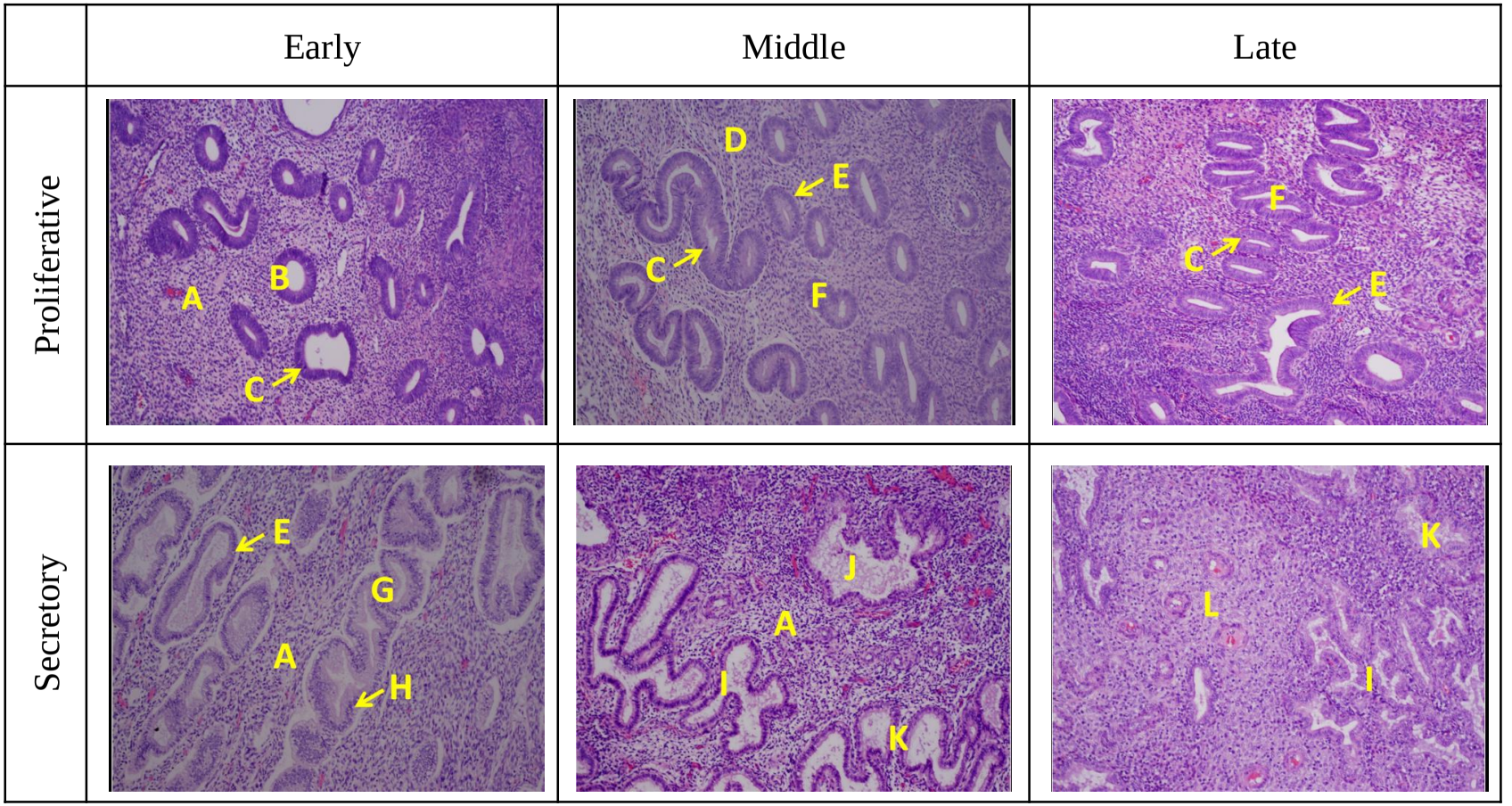

Figure 1.2: Characteristics of the endometrial functionalis throughout the menstrual cycle.

Histological characteristics of endometrial glands and stroma are used to date cycling endometrium. A=stromal edema, B=non-coiled glands, C=glandular mitosis, D=stromal mitosis, E=nuclear pseudostratification, F=coiled glands, G=tubular glands with infolding, H=basal vacuoles, I=branching glands, J=luminal secretions, K=basal vacuoles no longer present, L=decidualization around arterioles. Images are captured at 10x magnification.

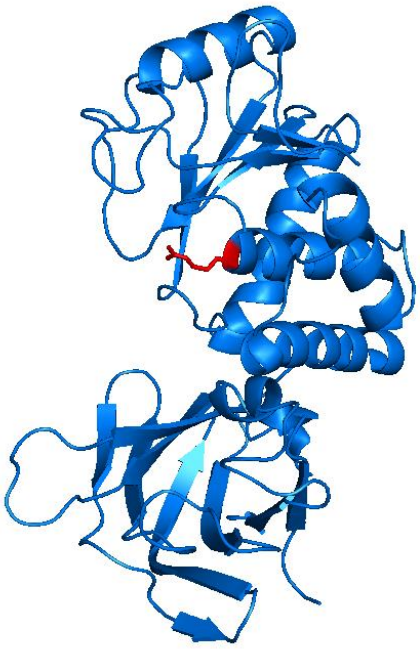

Figure 1.3: PTEN protein structure.

PTEN is the most frequently mutated protein in endometrial cancer. The lipid phosphatase activity of PTEN is hindered by mutation of the R130, which is highlighted in red. R130 lies in the catalytic pocket – the P loop – and is the most frequently PTEN residue in endometrial cancer.

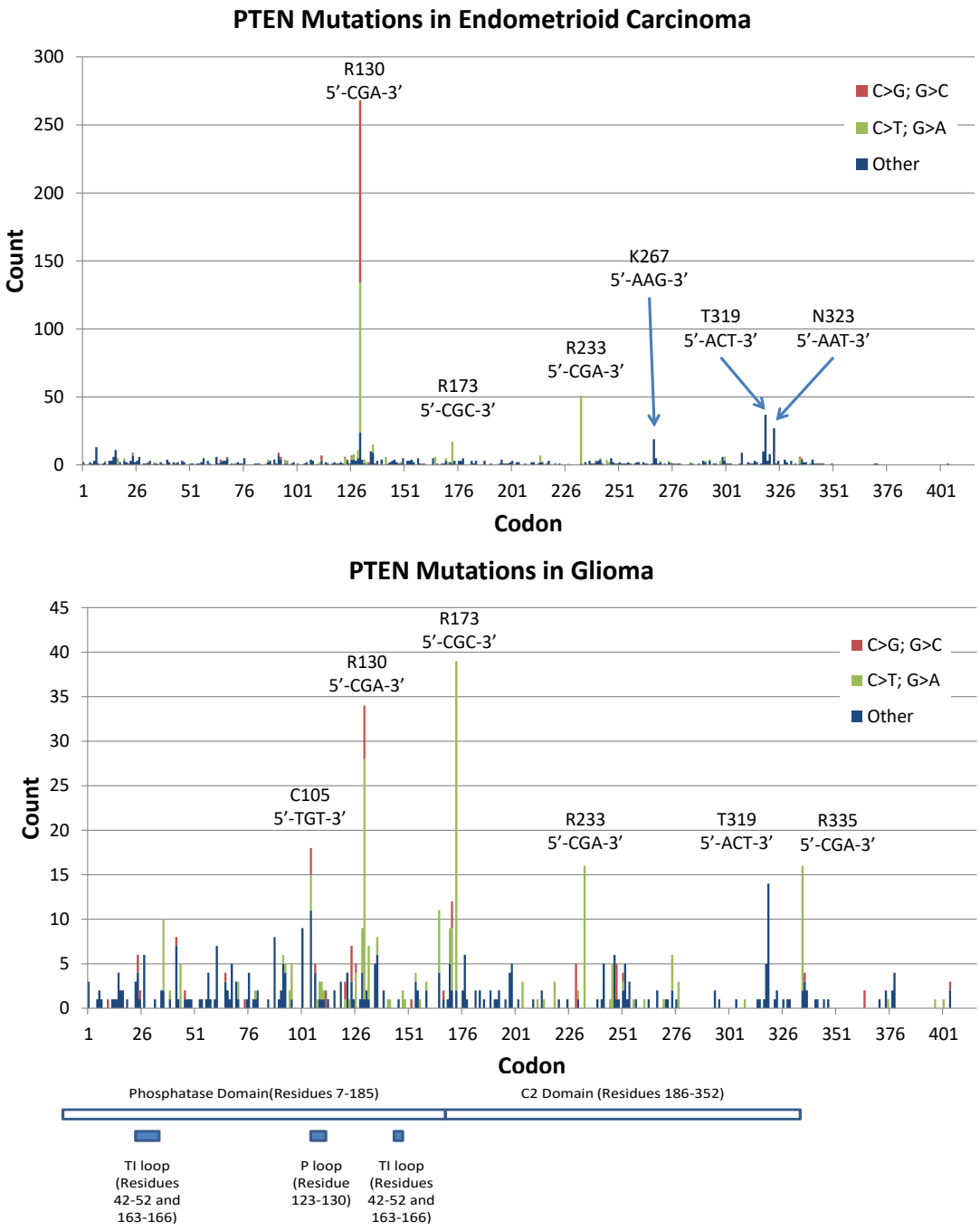

Figure 1.4: PTEN is mutated in endometrial cancer and glioblastoma

PTEN mutations are observed in endometrioid carcinoma and in glioma, as curated by COSMIC (06/2016). Endometrioid carcinoma and glioma display different frequencies of hotspot mutations from the other. Noticeably, endometrioid hotspot mutations are composed of a greater percentage of C:G>G:C mutations than are glioma at the same locus. The difference in mutation spectra between the two diseases suggests that different processes are responsible for the generation and accumulation of PTEN mutations in endometrioid carcinoma from gliomas.

The mutation hotspot R130, which is a highly conserved residue in the P loop which is required for lipid phosphatase activity. The R130, R173, and R233 substitution hotspots contain a CpG site. R130 substitutions most frequently result from C:G>G:C mutations in endometrial cancer, whereas it is not in glioma.

Blue samples include insertion, deletion, and not otherwise specified substitution mutants.

Chapter 2 Methylation as a driver of mutagenesis in endometrial tissue

BACKGROUND

Endometrial cancer is the most frequently diagnosed gynecologic cancer in the United States each year. The PTEN gene is the most frequently mutated gene in Type I endometrial adenocarcinoma. We are interested in explaining the mutations observed at codon 130 of the PTEN gene in type I endometrial adenocarcinoma. Many detected mutations at codon 130 are consistent with deamination of methylcytosine (^{m}C:G->T:A), but it is not known whether the CpG site of PTEN codon 130 is mutated. We used bisulfite pyrosequencing to query the methylation status of PTEN codon 130 in benign human endomyometrial tissue.

Methylation as a driver of mutation

There is a high frequency of C:G>T:A mutations in human disease (35). Studies of hotspot mutations in the p53, FBXW7, and NF1 have shown correlation with the presence of methyl-cytosine at the hotspot codon (36–39). Pfeifer reported that p53 hotspot mutations at sites of CpG dinucleotides are methylated in the benign state (37,40), a correlation which contributes to our understanding of C>T mutation occurrence. It has also been noted that ^{m}C promotes adduct formation at the nearby guanine residue (41) above the rate of mutation of non-methylated cytosine (40,42). In vitro study of the deamination rate of ^{m}C and C demonstrate that ^{m}C deaminates to T at a rate of 5.8×10^{-13} s^{-1} in double stranded DNA whereas C deaminates to U at a rate of 2.6×10^{-13} s^{-1} in the same conditions (42). Presence of uracil in DNA is not standard, and is rapidly repaired by uracil glycosylase (43). A T:G mispair is repaired by thymine glycosylase, which less efficiently recognizes mispairs when compared with uracil glycosylase (44).

As many observed mutation occurring at PTEN codon 130 are consistent with deamination of ^{m}C (9,45), we seek to determine the methylation status of PTEN exon 5 (involving CpG sites at codons 130 and 142) in benign endometrial tissue.

We aim to address the question of why R130 is a hotspot mutation site. To learn whether methyl-cytosine may play a role, we used bisulfite pyrosequencing to query the methylation status of PTEN codon 130 in exon 5.

Methylation status analysis

Bisulfite treatment was first described by Frommer in 1992 (46). Frommer et al. described the conversion of C>U upon exposure to sodium bisulfite. The presence of a methyl group at the 5-position of cytosine prevented bisulfite-mediated conversion. This chemical property can be used to distinguish ^{m}C from C. DNA, converted or not, can be PCR amplified, effectively converting U>T and ^{m}C>C. Sequencing of the gene of interest then reveals the methylation status.

Use of pyrosequencing adds a layer of information to traditional sequencing, allowing quantification of base incorporated at a site (47). Pyrosequencing takes advantage of the 1:1 release of pyrophosphate (PP_i) for each base incorporated. ATP sulfurylase converts PP_i into ATP, which is then used by luciferase to emit a detectable light signal. The pyrosequencing software generates a pyrogram, showing a quantified amount of light emitted for each base incorporated. When analyzing CpG sites which technique allows for quantification of methylated and non-methylated cytosine. During sequencing, a location which originally contained C will be detected as T, whereas an original mC will be detected as C. The quantification abilities of pyrosequencing, allows for calculation of the relative amount of DNA strands containing methylated-C or containing C at any C site.

To validate complete bisulfite conversion and sequencing technique, pyrosequencing includes internal and external controls. Within any human gene sequence of interest, it is anticipated that all C outside of a CpG dinucleotide is expected to be 0% methylated and therefore will be bisulfite-converted to U and sequenced as T. These sites are used to determine whether the original sequence was fully bisulfite converted.

This method is not without limitations. Though relative amount of ^{m}C to C containing DNA strands can be calculated, the distribution of methylated cytosine is unclear in a mixed population. For instance, given a 50% methylation status at one locus of human DNA, it is unclear whether one allele is 100% methylated and the other is 0% methylated or if both alleles are partially methylated. Given a stretch of DNA with multiple CpG dinucleotides, it is unclear whether any one strand of DNA is methylated at multiple locations, not at all, or methylated at one but not another site. Such concerns may be addressed with more time and resource-consuming methods of sequencing.

At this time, we are interested in the aggregate methylation status of the CpG mutational hotspot in exon 5 of PTEN (codon 130 and 142). To demonstrate methylation status, we used bisulfite treatment and pyrosequencing to demonstrate the methylation status of PTEN exon 5 and the degree to which the 2 exon 5 CpG sites are methylated.

MATERIALS AND METHODS

Specimen collection

Specimens were collected with IRB approval (IRB # 12-282, PI: Pooja Patel, MD) from 4 women treated at the University of Texas Medical Branch in 2013-2014. The samples were collected following hysterectomy for various gynecological conditions, including abnormal uterine bleeding, adenomyosis, and leiomyomas. Categorization of samples into proliferative or secretory phase of the menstrual cycle and histological diagnosis of uterine pathology was determined by pathologists at UTMB and validated by Dr. Eduardo Eyzaguirre and myself. All

health information is coded and de-identified. The patients ranged in age from 39 to 46 with an average BMI of 43 ±4.9.

Isolate DNA

Unfixed, unfrozen samples were collected from surgical pathology and stored at -80°C until tissue lysis and genomic DNA isolation.

Between 30 and 86 mg of endomyometrial tissue were incubated with 100 µL 1M Tris pH 8.5, 10 µL 0.5M EDTA, 10µL 20% SDS, 40 µL 5M NaCl, 5 µL 20mL/mL Proteinase K, 1.67 µL 10 mg/mL RNAse, and 840 µL ddH_2O overnight at 37°C at an agitation rate of 600 rpm using an Eppendorf Thermomixer.

The sample volumes were split into two samples each, to which 37.5 µL of 8M ammonium acetate and 350 µL of phenol/chloroform/isoamyl alcohol were added. Samples were inverted multiple times to promote mixing. The aqueous layer was transferred to a new container containing 750 µL of 100% ethanol. DNA was precipitated by centrifugation for 10 minutes at 12,000 rpm, 4°C. Ethanol was removed and samples allowed to air dry prior to resuspension with 100 µL of ddH_2O.

Bisulfite treatment

A representative sample from each patient was selected for pyrosequencing based on A260/280 ~1.8 (for DNA free of protein and phenol) and A260/230 ~2.0 (for DNA free of phenol). Bisulfite treatment was performed on 1 µg of each gDNA sample. Samples were incubated with bisulfite mix, DNA protect buffer, and RNase-free water according to recommendation from the manufacturer (Qiagen, EpiTect Bisulfite kit, cat#59104).

Bisulfite conversion was performed on a Peltier Thermal Cycler with the following conditions: 95°C 5 minutes, 60°C 20 min, 95°C 5 min, 60°C 85 min, 95°C 5 min, 60°C 175 min, 95°C 5 min, 60°C 120 min. Following conversion, DNA was purified by the cleaning procedure recommended by Qiagen (EpiTect Bisulfite kit).

A control sample purchased from Qiagen (EpiTect PCR Control DNA Set, cat#59695) was also bisulfite treated.

Amplification of PTEN, Exon 5

PCR was performed using 15 ng of bisulfite treated DNA per reaction. Each PCR reaction contained 5 µL of 10xPCR buffer (included in Qiagen kit cat#203203), 1 µL 200uM/L dNTP mix (Qiagen kit cat#203203), 1 µL 10 µM forward primer, 1 µL 10 µM reverse primer, 0.4 µL 5U/µL HotStar Taq polymerase (Qiagen kit cat#203203) in a total volume of 50 µL.

The following primers were used to amplify exon 5 of human PTEN: forward primer for coding strand 5'-ATGGTTAAGTGAAGATGATAATTATGT-3', reverse primer for coding strand 5'-Biosg-TCTATTTTCCAATAAATTCTCAAATCCA-3', forward primer for noncoding strand 5'-GATTTAGGAAGAGGAAAGGAAAAATAT-3', reverse primer for noncoding strand 5'-Biosg-TAACCCACCACAACTAAAAC TTATCAA-3'. The primers were designed to bind to exon/intron borders to mitigate binding to the PTEN pseudogene.

Amplification was performed using the following thermocycler conditions: 95°C for 15 min, followed by 50 cycles of 94°C for 30 seconds, 52°C or 30 seconds, and 72°C for thirty seconds. The protocol was followed by a 10 minute hold at 72°C. Amplicon size was verified by agarose gel electrophoresis.

Pyrosequence

Pyrosequencing was performed using a Qiagen PyroMark Q24 with PyroMark Q24 software, version 2.0.6. Pyrosequencing reactions were performed on 10-16 µL of PCR product. Biotinylated PCR products were annealed to streptavidin-coated sepharose beads by agitating the PCR product, 2 µL of streptavidin-coated sepharose beads (GE Healthcare cat#17-5113-01), 40 µL binding buffer (Qiagen cat#979006), and RNase-free H_2O to a total volume of 80 µL for 15 minutes at 1400 rpm on an IKA MS 3 Digital. Immediately following agitation, the beads were adhered to the PyroMark filter probe, washed with 70% ethanol, denaturing solution (Qiagen

cat#979007), and wash buffer (Qiagen cat#979008) in sequence. Beads were next deposited into the wells of a plate containing 0.75 µL 10 µM sequencing 24.25 µL primer and annealing buffer (Qiagen cat#979009). The mixture was incubated at 80°C for 2 minutes to disrupt secondary structure and promote primer binding to the template DNA. The plate is then loaded onto the PyroMark Q24. The enzymes DNA polymerase, ATP sulfurylase, luciferase, and apyrase (Qiagen cat#970802); substrates adenosine 5' phosphosulfate and luciferin (Qiagen cat#970802); and nucleotides (Qiagen cat#970802) are loaded into a cartridge for use with the Q24 (Qiagen cat#979202).

Sequencing primers for exon 5 of PTEN are as follows: coding strand 5-GTAAAGTTGGAAAGGG-3' and noncoding strand 5'-AGGGTTTTTTGTGTTTTT AA-3'.

Two control samples purchased from Qiagen (EpiTect PCR Control DNA Set, cat#59695) were also PCR amplified and pyrosequenced: a bisulfite treated fully methylated human DNA control and a bisulfite treated fully unmethylated human DNA control.

RESULTS: CPGS ARE METHYLATED IN EXONIC REGIONS OF PTEN

The methylation status of exon 5 of PTEN was examined by pyrosequencing of bisulfite-treated genomic DNA purified from histologically normal human endometrium. We find that PTEN codons 130 and 142 are predominantly methylated in 4 samples of benign human endometrial tissue.

Pyrosequencing of PTEN exon 5 was performed using bisulfite treated genomic DNA isolated from benign endomyometrial tissue. Methylation status was determined for codon 130 and 142, in both the coding and noncoding strands. The codon 130 cytosine found in the coding strand was methylated at 72% ± 3.5% (SD) while the non-coding strand cytosine was methylated at 70% ± 4.4% (SD). The codon 142 cytosine in the coding strand was methylated at 91% ± 2.0% (SD) and that in the noncoding strand at 94% ± 2.1% (SD). As methylation in human tissue is maintained by DNMT1, which propagates methylation across hemimethylated DNA, we anticipated that methylation on the coding and non-coding strands would be similar across each

CpG dinucleotide. Our results are as expected across PTEN codon 130 and codon 142: that is, that methylation percentage in the coding strand is similar to that in the non-coding strand. There was only a 0-6% variation between coding and non-coding methylation percentage within the sequencing runs for each patient, which is within the error range plausible as determined by sequencing the control templates. With precise clustering of measurements, we are confident that the percent methylation measured is an accurate representation of PTEN exon 5 methylation status in human endometrial tissue.

For each sequence of PTEN exon 5 analyzed, cytosine bases not in the CpG context were examined for complete bisulfite conversion. Two non-CpG cytosine were sequenced in the PTEN coding strand and 3 in the noncoding strand. At all sites, 0% C and 100% T as the sequencing readout would represent complete bisulfite sequencing of the templating DNA. We expect a small fraction of cytosine to thymine, as bisulfite conversion is performed to completion would risk non-specific conversion reactions of ^{m}C to T. In our samples, the maximum C/(C+T) detected was 9.9% at a non CpG site, indicated that bisulfite conversion was performed to >90% completion.

Pyrosequencing of the coding strand of PTEN from fully methylated commercially-available control DNA yielded an average of 86.67% ± 1.5% (SD) and 88.33% ± 1.5% (SD) methylation at PTEN, codon 130 and 142, respectively. Pyrosequencing of the commercially-available fully unmethylated control DNA yielded an average of 2.33% ± 0.6% (SD) and 5.33% ± 0.6% (SD) methylation at PTEN codon 130 and 142, respectively. These measurements define the range of confidence for measurement of methylation status.

In comparing the methylation status of PTEN codon 130 to codon 142, codon 142 is more frequently methylated than is codon 130 in benign human endomyometrial tissue. The difference in average methylation status of codon 142 and codon 130 of each patient is greater than 15%, representing a greater percentage of sample methylated at codon 142 than 130.

DISCUSSION

To explain C>T mutations at PTEN codon 130, we asked whether the CpG dinucleotide at PTEN codon 130 is methylated in benign tissue. Determination of methylation status would help explain a mechanism of PTEN codon 130 mutation accumulation. The methylation status of PTEN exon 5 has not been previously shown. We have shown that the CpG sites at codons 130 and 142 of the PTEN gene are predominantly methylated in benign endomyometrial tissue. Based on literature concerning the methylation status of other genes mutated in cancer at sites of CpG methylation, we hypothesized that a PTEN mutation hotspot would be methylated in benign tissue. As PTEN is highly mutated at codon 130 and infrequently mutated at codon 142 in endometrial cancer (9), we anticipated that methylation of the CpG site at codon 130 would be more frequent than that at codon 142. A complementary explanation for the accumulation of mutations at codon 130 as opposed to codon 142 may lie in functionally important residues. PTEN includes a HCXXGXXR motif, in which R130 and C124 are necessary for the lipid phosphatase catalytic function of PTEN (19). An inactivating mutation at R130 would promote cellular proliferation and allow propagation of the inciting PTEN mutation.

Though the sample size was small, the PTEN codon 130 and 142 methylation status appears independent of patient race or menstrual cycle phase because of the precise clustering of measurements between the samples. The four patients included in this study were similar in age and all pre-menopausal, so no conclusions can be drawn about age-related methylation accumulation

The results of the fully methylated and fully unmethylated controls should be considered. Pyrosequencing of the bisulfite treated fully methylated control was expected to yield a result of 100% methylation while the fully unmethylated control was expected to yield 0%. The reported detection limit of bisulfite pyrosequencing is 5% (48). We were able to detect 87.5% methylation of cytosine in fully methylated controls and 3.8% methylation of fully unmethylated controls. The methylation status of cytosine in benign endomyometrial genomic DNA may have an error of up to 13%. The discrepancy could be related to degradation of the aged sample. The results from our study were consistent through multiple replicates of testing and methylation status of

the coding and noncoding strand were similar to each other at each codon. We confidently conclude that codons 130 and 142 of PTEN exon 5 are predominantly methylated in benign human endomyometrial tissue.

Proposed pathway of mutations

We propose that the predominance of methylated cytosine at CpG sites in PTEN contribute to C>T mutations observed in endometrial cancer. ^{m}CpG have been observed at hotspot mutations sites of various genes commonly mutated in a variety of cancers (36,49).

Cytosine has been shown to deaminate to uracil at a rate of $2.6x10^{-13}$ s^{-1}, whereas methyl-cytosine deaminates to thymine more quickly, at a rate of $5.8x10^{-13}$ s^{-1} at 37°C in the context of double stranded DNA (42). U:G mispairs have been reported to be repaired more quickly than T:G mispairs (50). These two factors together help to explain how methylation of cytosine can promote mutation over non-methylated cytosine.

Further study of PTEN methylation status could aid in explaining other C:G>T:A observed at hotspot mutation sites in endometrial adenocarcinoma and precancers. For instance, C>T and G>A mutations are observed at PTEN R173 and R233 in endometrial cancer. They have also been observed in benign human endometrial glands immunohistochemically negative for PTEN expression (14) and their prevalence may result from deamination of ^{m}C to T or C to U.

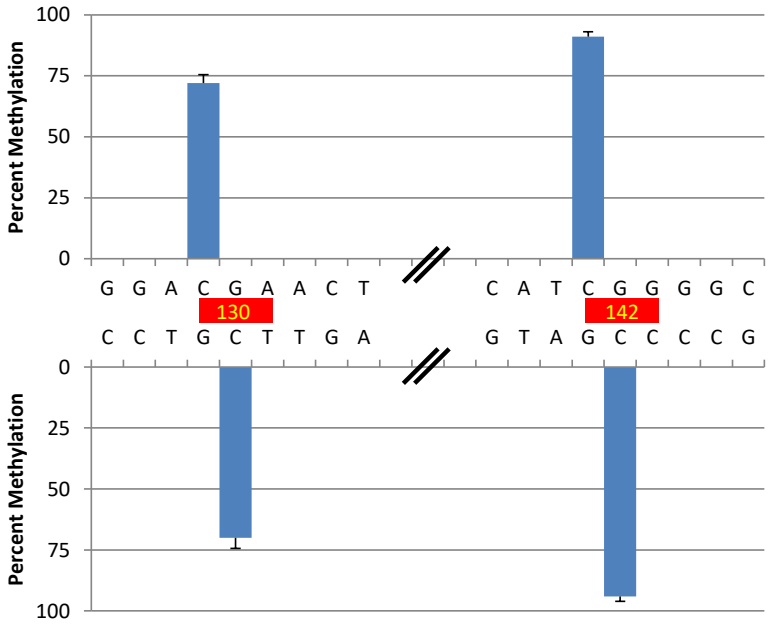

Figure 2.1: CpG sites in exon 5 of PTEN are predominantly methylated.

PTEN exon 5 CpG sites are predominantly methylated in benign endometrial samples (n=4). Codons 130 (left red line) and 142 (right red line) of the PTEN gene are predominantly methylated at the involved CpG site, assessed by pyrosequencing of the coding (top graph) and non-coding (bottom graph) strands. The range of methylation percentage at each site spanned 11% and 10% for codons 130 and 142, respectively, with standard deviations <5%.

Chapter 3 Nitrotyrosine in human endometrial tissues

BACKGROUND

To further understand PTEN mutations observed in endometrial cancer, we sought to explain the preponderance of C>G mutations observed at PTEN codon 130. The formation of secondary oxidation products of guanine (guanidinohydantoin and spiroiminodihydantoin) are known form from exposure of DNA to peroxynitrite and to promote G>C mutations. We detected the presence of nitrotyrosine in benign human endometrial tissue, showing that endometrial tissue is persistently exposed to agents capable of forming Gh and Sp. As nitrated proteins have not yet been identified in benign human endometrium, we used nanoLC-MSMS to identified ACTBL2 as the predominately nitrated species in these tissues. Our studies contribute understanding physiological exposure that can lead to pathological mutagenesis.

PTEN C>G mutations are observed most frequently

The majority (52%) of endometrial carcinoma mutations observed at PTEN codon 130 are C:G>G:C mutations. This is of interest, given that C>G mutations infrequently observed, compared to other substitution mutations (51). The only known route of C:G>G:C mutation occurs through the generation of guanidinohydantoin (Gh) or spiroiminodihydantoin (Sp) (52). We seek to show that this is the likely route of mutation in endometrial tissue.

Oxidative damage at guanine results in the formation of 8-hydroxydeoxyguanosine (8oxoG). 8oxoG is a stable product, detectable by a variety of experimental means (53,54); as such, it has been widely studied in the context of human disease such as ischemia reperfusion, liver pathology, UV damage, among other pathologies (55–59). 8oxoG has even been detected in benign uterine pathology and histologically normal uterine tissue (60). de Carvalho and colleagues observed 8oxoG in uterine pathology at higher immunoreactive intensity than in matched normal female reproductive tissue (60). Gh and Sp are formed as secondary oxidation

products from the reaction of peroxynitrite with oxidized guanine (61–63), and both are associated with mutations more frequently than 8oxoG (61,64). Gh and Sp are able to mispair, notably with guanine (65,66); following replication, such a mispair would result in G:C>C:G.

Guanine, which has the lowest redox potential of the typical nucleobases (67) is particularly susceptible to oxidative damage and is further targeted if base paired with ^{m}C (68) or is adjacent to ^{m}C (69). It has also been noted that the rate of oxidation of 8oxoG is accelerated when base paired with ^{m}C, in comparison to 8oxoG:C (68). We have thus far shown that CpG at PTEN codon 130 is predominantly methylated in endometrial tissue. Because PTEN codon 130 C:G>G:C mutations are prevalent in endometrial cancer and since benign endometrial tissue is methylated at PTEN codon 130, we ask whether nitrosative damage at guanine basepaired to the methylated cytosines at codon 130 is possible and likely. We then sought to determine whether nitrosative damage, which leads to the formation of secondary guanine oxidation products was detectable in benign uterine tissue. Due to the difficulty of detecting secondary guanine oxidation products in the context of tissue, we instead sought to determine the presence of $ONOO^{-}$ induced damage in uterine tissue by detecting protein nitration. Herein, we describe our investigation of the nitrated proteins benign human endometrial tissues as we seek to explain the higher than anticipated C>G mutation frequency observed in endometrial carcinoma.

Menstrual cycle

The endometrium proliferates every month in preparation for the implantation of a fertilized egg. Menstrual cycling occurs in response to ovarian hormones, namely estrogen and progesterone. The menstrual cycle can be divided into two phases: proliferative and secretory (Fig. 1).

Histological characteristics associated with menstrual cycle progression are seen in the functionalis, the luminal two-thirds of the endometrium (Fig 1). Such characteristics as stromal edema, cellular localization of epithelial cell nuclei, glandular morphology, and stromal decidualization can be used to date the endometrium by menstrual cycle phase (2). During the

proliferative phase, the endometrial glands progress from being short and narrow during early proliferative phase to longer, curving glands, and finally to tortuous glands during the late proliferative phase (2). During the secretory phase, endometrial gland cells secrete acidophilic material into the lumen (2). The endometrium then undergoes predecidual changes in preparation for egg implantation. If no egg is fertilized and implanted, the functionalis of the endometrium sheds and the cycle begins again. The process of proliferation and shedding of the endometrium has been likened to wound healing, with inflammatory cell influx and activation followed by regrowth of the tissue (70).

Previous reports estimate that inflammatory cells make up as much as 45% of the endometrial cells during the day leading up to menstruation (70). Though this process is regulated, the consistent, cyclical nature of inflammatory cell influx and activation may result in collateral damage to surrounding tissues as would be expected in chronic inflammatory conditions. We anticipated that chronic exposure of DNA to inflammatory mediators would result in accumulation of mutations. We explored this potential by assessing myeloperoxidase (MPO) and nitrotyrosine in benign endometrial tissue.

The basalis, the layer of endometrium adjacent to the myometrium (Fig 2), houses the endometrial stem cells. The basalis is maintained through menstruation and proliferates to regenerate the functionalis during each menstrual cycle. Collateral damage to the DNA of cells of the basalis could be propagated as the basalis proliferates, leading to aberrant endometrial cells.

Role of NO in the endometrium

Nitric oxide (NO) is a diffusible gas with many biological functions, such as promoting vascular dilation, angiogenesis and inhibiting platelet aggregation (71–73). NO is thought to play a role in menstruation and in embryo implantation through its effects on the endometrium (74,75); for instance, by promoting the formation of spiral arteries in the endometrium. Additionally, nitric oxide is thought to play a role in inflammation, wound healing (76), and even

regulate endometrial epithelial cell apoptosis (77). Aside from its physiological effects, NO exposure can result in detrimental changes. NO, as a radical species easily reacts with other radicals, such as superoxide. In the presence of superoxide, NO can be converted into peroxynitrite. $ONOO^-$ is capable of causing lipid peroxidation, protein nitration, and DNA damage. In vivo exposure of DNA to peroxynitrite donors results in secondary guanine oxidation products, which are known to lead to mutation in vivo.

NO has been studied in explants of animal tissue (78), but directly measuring NO in human tissues has proven difficult due to the transient nature of NO presence.

Evidence that NO production is prompted by ovarian hormone exposure has been presented in equine endometrial tissue (78). Others have observed that intraperitoneal NO donor administration can modulate immune response, by decreasing plasma levels of IFN-γ, IL-2, and IL-4 (79).

What has been seen before (NOS)

NO is produced by conversion of L-arginine to L-citrulline by the activity of nitric oxide synthase (NOS). NOSs have been found to exist as three isoforms: endothelial NOS (eNOS), inducible NOS (iNOS), and as brain NOS (bNOS). The NOS enzymes have also been reference as constitutive and inducible, but this status varies with tissue distribution. In the uterine endometrium, eNOS and iNOS have been detected at varying concentrations throughout the menstrual cycle (74,80–82) and even vary in their distribution between endometrial glands and stroma (83). Kamada et al. reports that eNOS is intensely immunoreactive in secretory phase endometrium, and not in proliferative phase endometrium when analyzed by immunohistochemistry. According to Wang et al., a Western blot analysis of endometrial eNOS expression showed a progressive rise in eNOS expression during the proliferative phase, peaking during the late proliferative and a variable amount of eNOS during the secretory phase with a peak during the mid-secretory phase (80). This trend matches the serum estrogen concentration

for the same cohort (80). NOS has been shown to be regulated by ovarian sex hormones: positively regulated by estrogen with an inverse effect upon progesterone exposure (84).

What has been seen before (Nitrotyrosine)

Downstream breakdown products of peroxynitrite can act as reactive species and cause damage to surrounding proteins, DNA, and lipids. Reactive nitrogen species can react with oxidized guanine to generate a variety of secondary oxidation products with high mutagenic potential (63).

When peroxynitrite reacts with tyrosine residues, nitrotyrosine is formed. As a stable product, nitrotyrosine can be used as a marker of peroxynitrite presence and activity. A study of nitrotyrosine content in the gastric mucosa of Japanese patients evaluated for gastritis found higher levels of nitrotyrosine and iNOS expression in the gastric mucosa of patients infected with *Helicobacter pylori*, and expression was higher in those that later developed gastric cancer as compared to patients negative for H. pylori and those that did not develop gastric cancer (85).

Nitrotyrosine immunoreactivity has previously been observed in uterine tissue. For instance, Kamada et al. and Hickey et al. assessed endometrial tissue for nitrotyrosine immunoreactivity. Kamada and colleagues observed positive immunuoreactivity in glandular and stromal cells in secretory, but not in proliferative phase eutopic endometrium (83). The Kamada study included a small subset of patients and grouped them either into proliferative or secretory phase, neglecting the possibility of variation amongst subphases. Analysis of a larger cohort with attention to the menstrual cycle subphases would enhance our understanding of $ONOO^-$ exposure with greater discrimintation of timing. Hickey et al. report positive nitrotyrosine immunoreactivity in secretory phase endometrium as well (86). A study of nitric oxide synthases (NOS) and nitrotyrosine has revealed that proliferative glands in the endometrium (normal or eutopic glands) differ in NOS expression and nitrotyrosine presence as compared to adenomyotic glands in the myometrium (ectopic glands) (83).

The proteins nitrated in endometrium have not been previously identified nor their role in endometrial tissue elucidated.

Proteomic profile of endometrial tissue

While endometrial samples have been shown to contain nitrotyrosine, the nitrated proteins have yet to be identified in benign human endometrium. Previous reports identify non-nitrated proteins in normal endometrium have used 2D gel electrophoresis followed by mass spectrometry (87,88). Due to relatively large amount of sample required and the progression of technology available, we instead used nano-liquid chromatography-tandom mass spectrometry (nanoLC-MSMS) to perform our analysis of the nitroproteome of benign endometrial tissue. We expected that $ONOO^-$ would non-specifically interact with proteins, as the reaction is chemically mediated, rather than enzyme dependent.

MATERIAL AND METHODS

Obtaining and preparing tissues

Specimens were collected with IRB approval (IRB # 12-282, PI: Pooja Patel, MD) from 33 women treated at the University of Texas Medical Branch in 2013-2014 (Table 3.1). The samples were collected following hysterectomy for various gynecological conditions, including abnormal uterine bleeding, adenomyosis, cervical cancer or dysplasia, incontinence, organ prolapse, and leiomyomas. Categorization of samples into proliferative or secretory phase of the menstrual cycle and histological diagnosis of uterine pathology was determined by pathologists at UTMB and confirmed by myself and Dr. Eduardo Eyzaguirre. Samples were further categorized by subphase by Dr. Eyzaguirre and myself based on glandular and stromal characteristics described by Noyes (2). Demographic information was obtained from the medical records for participating patients. All health information is coded and de-identified.

Unfixed, unfrozen samples were collected from surgical pathology and stored at -80°C until fixation in 10% neutral buffered formalin. Samples remained in formalin approximately 48 hours to one week prior to processing.

Additional endomyometrial samples were collected from 15 patients in 2014-2015, flash frozen in cold isopentane, and stored at -80^{O}C until fixation and processing. Due to the large size of the tissue samples, fixation in 10% neutral buffered formalin was extended to 5 days. After embedding in paraffin, 5 µm sections were cut and adhered to positively charged slides as described above. Staining was performed the day after sectioning.

Three additional samples were obtained from the surgical pathology department at UTMB. The samples were immediately placed in formalin and were processed and embedded by the histology department at UTMB. These three samples were selected for inclusion based on the menstrual cycle subphase (late secretory).

Tissue preparation

Samples were processed to facilitate dehydration and preparation for paraffin embedding. Processing was performed by the following method on a Shandon PathCentre: 30 minutes in 10% neutral buffered formalin, 30 minutes in 70% ethanol, 30 minutes in 80% ethanol, 30 minutes in 95% ethanol, 3 washes of 100% ethanol for 30 minutes each, 3 washes of xylene for 30 minutes each all at room temperature. This is followed by 2 incubations in 60°C paraffin for 30 minutes each and two additional incubations in 60°C paraffin for 60 minutes each. These steps are performed under vacuum and pressure to facilitate dehydration of the tissues.

Samples were embedded in paraffin and sectioned at a thickness of 5 µm. Sections were either stored at -80°C for later use or immediately placed at 58°C to melt away paraffin. Sections remained at 58°C overnight to promote adherence of the tissue sections to positively charged slides.

H&E Staining

Tissue sections were stained with hematoxylin and eosin (H&E) to facilitate and confirm the orientation of tissues in the paraffin block. H&E staining was performed on tissue sections used in the menstrual cycle dating of samples. Slides of 5 μM thick sections were baked overnight in at 58°C to promote paraffin melting and adherence of tissue to the slide. The slides were stained with the use of a Shandon Varistain® Gemini. Sections were rehydrated by 3 successive washes in xylene (5 minutes per wash), followed by 2 washes in 100% ethanol (1 minute each) and 1 wash in 95% ethanol (1 minute). The slides were rinsed in running water prior to a 3 minute incubation in Harris heamatoxylin. The slides were rinsed in running water and then differentiated by an incubation in acid alcohol for 20 seconds. The slides were rinsed in running water then washed in 95% ethanol before blueing in 0.25% ammonia water. The slides were rinsed in running water, followed by 95% ethanol prior to counterstaining in eosin-phloxine. The slides are dehydrated by successive washes in 95%, 95%, 100%, then 100% ethanol and 4 changes in xylene in preparation for coverslipping and tissue analysis.

Immunohistochemical Staining

Sections of 5 μm were deparaffinized in 3 washes of xylene then rehydrated in 4 washes of 100% ethanol, followed by a wash in distilled water. Antigen retrieval was performed by incubating the slides in 10 mM citrate, pH 6 at 95°C (using a steamer) for 20 minutes. Slides were removed from the steamer, but left in the citrate buffer for 20 minutes to allow the solution to cool towards room temperature. After a 10 minute incubation in 3% H_2O_2 to quench endogenous peroxidase activity, slides were rinsed in distilled water.

Slides were immunohistochemically stained for nitrotyrosine presence by the following method. All steps were performed at room temperature using a DAKO autostainer with washes of Tris-buffered saline between each step. Slides were incubated with avidin for 15 minutes, followed by biotin for 15 minutes in order to block non-specific binding. The primary antibody (1:2000, anti-nitrotyrosine purified in rabbit, Millipore, cat#06-284, lot 2420453) was diluted in DAKO antibody diluting solution with background reducing components. The slides were

incubated with 200 uL of primary antibody for 1 hour. The slide was incubated with secondary antibody, LSAB2-link, for 15 minutes followed by 15 minutes with LSAB-HRP, and finally for 5 minutes with the chromagen, diaminobenzidine. Slides were counterstained with filtered Harris heamatoxylin for 15 seconds. All slides were dehydrated with 3 quick washes in 100% ethanol and 4 quick washes in xylene then coverslipped using Permount solution.

Sections from the additional samples (those stored after flash freezing in isopentane and those obtained from surgical pathology) were rehydrated and blocked as described above. Due to concerns about inactivity of the secondary antibody and linker reagent which are no longer commercially available, alternative reagents were used: 1:200 diluted biotinyated anti-rabbit IgG, made in goat and affinity purified (Vector, cat# BA-1000, lot Z1203) and streptavidin, horseradish peroxidase (HRP) (Vector, SA-5704, lot ZA021).The secondary antibody was applied to the sections for 15 minutes and the streptavidin-HRP was applied for 30 minutes. The subsequent steps were performed as described above.

Immunohistochemical staining for ACTBL2 was performed similarly to nitrotyrosine IHC. IHC for ACTBL2 was performed on never-frozen tissue, ACTBL2 (1:100 for IHC or 1:300 for IF, Abcam, #ab100869) was incubated for1 hour at room temperature followed by incubation with goat anti-rabbit secondary antibody and streptavidin-HRP (Vector).

Images were captured using an Olympus BX51 microscope with a mounted digital camera system.

IHC quantification

The immunostaining of the endometrium was determined by scoring the intensity of staining of glandular cells in the basalis of the endometrium. Intensity was scored as negative, weak, moderate, or strong. The scoring scheme is typical of semi-quantitative analysis of immunohistochemical staining. In comparison, Kamada et al. uses an evaluation nonogram based on staining intensity and frequency to score immunohistochemical immunoreactivity (83). The scoring scale used in this study is typical of the scale used in histopathological clinical diagnosis.

Statistical analysis

Chi-squared analysis of the immunohistochemically stained samples was performed using GraphPad Prism 6 to determine statistical significance, set at $p<0.05$.

Dual staining and confocal microscopy

Tissue sections of 5 μm thickness were incubated at 58°C overnight to melt off paraffin and adhere sections to positively charged slides. The tissue was rehydrated by 3 successive 5 minute washes in xylene followed by 4 successive 5 minute washes in 100% ethanol then 5 minutes in distilled water. Antigen retrieval was performed by incubating the slides in 200 mL of 10 mM citrate, pH 6, 95°C for 20 minutes. The slides were allowed to cool towards room temperature for 20 minutes. This was followed by a 30 minute incubation in 0.1% Sudan Black B in 70% ethanol to block background fluorescence. The slides were washed 3 times in PBS for 5 minutes at a time.

The first primary antibody was applied at 200 uL per slide (nitrotyrosine 1:2000 at room temperature for 1 hour; myeloperoxidase 1:4000 overnight at 4°C). The slides were washed 3 times in PBS for 5 minutes at a time. The fluorescent secondary antibody (AlexaFluor 488, 1:250) was applied at 200 uL per slides and the slides were incubated for 30 minutes at room temperature. The slides were washed 3 times in PBS for 5 minutes at a time. This procedure was repeated for the second primary antibody (ACTBL2 1:300 at room temperature for one hour or chlorotyrosine at 1:50 at room temperature for 2 hours) and fluorescent secondary antibody (AlexaFluor 594, 1:250) combination.

A working solution of DAPI (Sigma, 0.5 μg/mL) was applied to the slide for 5 minutes at 200 uL per slide, followed by a quick wash in dH_2O. The slides were coverslipped and kept at 4°C until confocal imaging was performed.

Confocal imaging was performed with a Zeiss LSM510META.

Proteomics

Proteomics were performed on endomyometrial samples collected, as described above. Samples were selected based on nitrotyrosine immunohistochemistry results: two samples of high nitrotyrosine staining intensity and one sample of low nitrotyrosine staining intensity were selected to maximize nitrated protein detection and to verify nitrated species level and identity, respectively. A typical proteomics work flow is diagramed in Fig 3.1.

PROTEIN ISOLATION AND PREPARATION

Endomyometrial tissue (50-100 mg) was homogenized in 2 mL of lysis buffer (Pierce™ RIPA buffer, supplemented with a 1:50 dilution of ThermoFisher Scientific Halt™ Protease and Phosphatase inhibitor cocktail, and 1 mM ThermoFisher Scientific phenylmethylsulfonyl fluoride) using a Polytron® PT 10-35 GT. The homogenized sample was incubated on ice with 50 units of ThermoFisher Scientific Pierce universal nuclease for 30 minutes and then centrifuged (20 min, 15000 g, 4ºC) to separate the soluble protein from insoluble cellular matter.

The soluble fraction was divided into 200 µg aliquots, and the aliquots diluted to 1 µg/µL with 50 mM triethylammonium bicarbonate buffer, pH 8.5 (TEAB). To this solution, 10 µL of 200 mM Bond-Breaker™ 0.5M tris(2-carboxyethyl)phosphine (TCEP) solution, neutral pH to reduce disulfide bonds upon heating at 55ºC for 1 hour at 650 rpm. The sample was then alkylated by incubating the sample for 45 minutes with 10 µL of 375 mM iodoacetamide in 50 mM TEAB at room temperature, 500 rpm. The proteins were precipitated by addition of 4 volumes of -20ºC mass spectrometry grade acetone (880 µL acetone per 200 µg aliquot) and incubated at -20ºC overnight. The sample was centrifuged for 20 minutes at 4ºC, 16000 rpm to pellet the protein.

The pellet was reconstituted with 30 µL freshly prepared of 8M urea by sonication and vortexing of the sample. Proteins were digested with 8 µg sequencing grade, modified porcine trypsin by incubating the sample at 37ºC, 500 rpm for 16 hours.

A C18 Sep-Pak Vac 1 cc cartridge connected to a vacuum manifold was used for peptide purification. The cartridge was equilibrated with 3 x 1 mL optima grade acetonitrile, followed by

3 x 1 mL 0.25% trifluoroacetic acid. The sample of peptides was adjusted to 1% trifluoroacetic acid and mixed to precipitate the peptides. The peptide mixture is applied to the Sep-Pak cartridge and the solution was eluted by gravity flow, minimizing the flow speed to enhance peptide binding to the resin. The cartridge is washed with 4 x 1mL 0.25% trifluoroacetic acid. Then, the peptides were eluted by gravity flow in 1mL 80% optima grade acetonitrile, 0.1% LC-MS grade formic acid. The solvent is evaporated to leave a pellet of peptides.

LIQUID CHROMATOGRAPHY-MASS SPECTROMETRY

The peptide mixtures were analyzed by nanoflow liquid chromatography-tandem mass spectrometry (nanoLC-MS/MS) using a nano-LC chromatography system (UltiMate 3000 RSLCnano, Dionex), coupled on-line to a Thermo Orbitrap Fusion mass spectrometer (Thermo Fisher Scientific, San Jose, CA) through a nanospray ion source (Thermo Scientific). Chromatographic columns were made from 75 µm ID polyimide-coated fused silica capillary (Polymicro Technologies, Phoenix, AZ) packed with 5 µm Zorbax SB-C18 reversed-phase packing (Agilent, Santa Clara, CA) to a length of 15 cm by using a Pressure Injection Cell (NextAdvance, Averill Park, NY). The trap column was prepared in the same manner but to a length of 1 cm. After equilibrating the column in 98% solvent A (0.1% formic acid in water) and 2% solvent B (0.1% formic acid in acetonitrile), the samples (1 µL in solvent A) were injected onto the trap column and subsequently eluted (400 nL/min) by gradient elution onto the C18 column as follows: isocratic at 2% B, 0-5 min; 2% to 8% B, 5-8 min; 8% to 33% B, 8-98 min; 33% to 45% B, 98-105 min; 45% to 90% B, 105-107 min; isocratic at 90% B, 107-112 min; 90% to 2% B, 112-114 min; and isocratic at 2% B, 114-120 min.

All LC-MS/MS data were acquired using XCalibur, version 2.1.0 (Thermo Fisher Scientific) in positive ion mode using a top speed data-dependent acquisition (DDA) method with a 3 sec cycle time. The survey scans (*m/z* 350-1600) (MS) were acquired in the Orbitrap at 120,000 resolution (at *m/z* = 400) in profile mode, with a maximum injection time of 100 msec and an AGC target of 200,000 ions. The S-lens RF level was set to 60. Isolation was performed

in the quadrupole with a 1.6 Da isolation window, and HCD MS/MS acquisition was performed in profile mode using rapid scan rate with detection in the ion trap, with the following settings: parent threshold = 5,000; collision energy = 28%; maximum injection time 250 msec; AGC target 20,000 ions. Monoisotopic precursor selection and charge state filtering were on, with charge states 2-6 included. Dynamic exclusion was used to remove selected precursor ions, with a +/- 10 ppm mass tolerance, for 60 sec after acquisition of one MS/MS spectrum.

PEPTIDE IDENTIFICATION AND VERIFICATION

Tandem mass spectra were extracted and charge state deconvoluted by Proteome Discoverer (Thermo Fisher, version 1.4.1.14). Deisotoping was not performed. All MS/MS spectra were searched against a Uniprot/SwissProt Human database (April 2014 version, 88,708 entries) using Mascot (Matrix Science, London, UK; version 2.3.02). Searches were performed with a parent ion tolerance of 10 ppm and a fragment ion tolerance of 0.60 Da. Trypsin was specified as the enzyme, allowing for two missed cleavages. Fixed modification of carbamidomethyl (C) and variable modifications of oxidation (M) and nitration (Y) were specified in Mascot.

Scaffold (version Scaffold_4.4.8, Proteome Software Inc., Portland, OR) was used to validate MS/MS based peptide and protein identifications. Peptide identifications were accepted if they could be established at greater than 95.0% probability by the Scaffold Local FDR algorithm. Protein identifications were accepted if they could be established at greater than 99.0% probability and contained at least 2 identified peptides. Protein probabilities were assigned by the Protein Prophet algorithm (89). Proteins that contained similar peptides and could not be differentiated based on MS/MS analysis alone were grouped to satisfy the principles of parsimony. Proteins sharing significant peptide evidence were grouped into clusters.

Nitrotyrosine-containing peptides identified by Mascot and passing the 95% Scaffold Local FDR algorithm were manually verified by comparing observed *m/z* values in the .raw data

files (XCalibur) for parent and fragment ions with theoretical values obtained from the MS-Product utility of the Protein Prospector website (http://prospector.ucsf.edu).

Western Blotting

Western blotting was used to confirm the results received from proteomic analysis of benign human endomyometrial tissue.

Endomyometrial tissue (50-100 mg) was homogenized in 2 mL of lysis buffer (Pierce™ RIPA buffer, supplemented with a 1:50 dilution of ThermoFisher Scientific Halt™ Protease and Phosphatase inhibitor cocktail, and 1 mM ThermoFisher Scientific phenylmethylsulfonyl fluoride) using a Polytron® PT 10-35 GT . The homogenized sample was incubated on ice with 50 units of ThermoFisher Scientific Pierce universal nuclease for 30 minutes and then centrifuged (20 min, 15000 g, 4ºC) to separate the soluble protein from insoluble cellular matter.

The protein concentration of the soluble fraction was measured by BCA. The soluble fraction was divided into 200 µg aliquots and dried. Pellets of 200 µg protein, isolated from human endometrium were resuspended in buffer to a concentration of 2 µg protein/uL. The buffer consisted of FLAG-IP lysis buffer (50 mM Tris HCl, pH 7.4, 150 mM NaCL, 1 mM EDTA, 1% Triton X-100), cOmplete mini EDTA-free phosphatase inhibitor cocktail, and PhosSTOP EASY pack phosphatase inhibitor cocktail tablet, and Laemmli sample buffer. Samples were heated at 90ºC to promote protein solubilization and denaturing.

Samples were loaded and run on a 10% acrylamide SDS-PAGE gel with a 5% stacking gel layer. The gel was rinsed in dH_2O to wash away excess SDS. Proteins were transferred from the gel to a PVDF membrane using by semi-dry transfer Bio-Rad Trans-Blot® SD Semi-Dry Transfer Cell.

Membranes were stained with Ponceau stain to visualize transferred proteins and then washed 3 times with dH_2O.

Membranes were blocked with PBST-milk (5% non-fat dry milk, 1X PBS, 0.1% Tween20) with agitation for 15 minutes prior to an overnight, 4ºC incubation with agitation with the primary antibody (nitrotyrosine 1:2000 or ACTBL2 1:1000).

Membranes were washed 3 times with PBST at 15 minutes per wash with agitation, followed by a 1.5 hour incubation with secondary antibody (goat anti-rabbit IgG, H&L chain specific HRP conjugate, 1:10,000) at room temperature, agitated. Excess secondary antibody was washed away with three 15 minute washes in PBST.

Chemiluminescent HRP substrate (SuperSignal West PICO or Immobilin Chemiluminescent HRP Substrate) was applied to the membrane. This substrate emits a light, which is registered on film. The film is developed on a Konica Minolta SRX-101A for visualization.

RESULTS

Nitrotyrosine content varies throughout the menstrual cycle

Nitrotyrosine immunoreactivity was observed throughout the menstrual cycle. In both proliferative phase and in secretory phase, a wide range of nitrotyrosine staining intensity was observed (Fig 3.2). The endometrial glands of the basalis had a lower average nitrotyrosine staining intensity (Fig. 3.3) during the secretory phase, as compared to the proliferative phase ($p<0.0001$). Samples in the proliferative phase display a range of intensity, from no staining to strong staining. Samples in the early and mid-secretory phase have a small range of intensity, primarily staining with weak intensity.

Staining was performed in three batches. The initial sample set included samples from 33 women. The sample set contains many early proliferative and mid-proliferative samples, but relatively few late proliferative and secretory subphase samples. To discern whether the trend in menstrual cycle subphase versus nitrotyrosine content was accurate, addition of late proliferative and of secretory samples was pursued. Samples from 15 additional women were included, with

samples comprised of late proliferative, early secretory, mid-secretory, and late secretory samples. The addition of samples did not dramatically change the trends seen in the original data set. A third set of 3 samples obtained and processed by pathology were added in order to include additional late secretory samples.

In the glands of the basalis, proliferative sub-phase samples show a range of nitrotyrosine immunoreactivity, from negative to strong intensity. The glands of early and mid-secretory endometrium are primarily weak in nitrotyrosine immunoreactivity with a large range of nitrotyrosine immunoreactivity again appearing in late secretory samples. A comparison of basalis glandular epithelium nitrotyrosine immunoreactivity and race revealed a non-statistically significant trend: African-American women displayed more intense nitrotyrosine immunoreactivity than Caucasian women. Analysis of nitrotyrosine immunoreactivity by smoking status, parity, BMI, and age was non-significant.

We observed positive nitrotyrosine immunoreactivity in all samples. In the one sample negative for glandular nitrotyrosine staining in the basalis, the surrounding stoma was positive for staining.

Proteomics

To identify nitrated proteins, proteomic analysis of the soluble proteins isolated from 3 benign human endomyometrial samples (Table 3.2) was performed. This led to identification of 1631proteins at a false discovery rate of 1% and a peptide threshold of 95% with at least 2 peptides per protein identified.

Cytoplasmic and nuclear proteins were identified. Within the set of proteins identified, various non-nitrated actin isoforms were present, including alpha skeletal actin, beta actin, and gamma enteric smooth muscle actin. Filtering for nitrated peptides yielded one candidate: ACTBL2.

Identification of nitrated ACTBL2

Of the proteins identified, 1 nitrated peptide was predominantly identified. A peptide TTGIVMDSGDGVTHIVPIyEGYALPHAILR was identified as ACTBL2 residues 149-178, containing nitrated Y167 (lower case) (Fig. 3.4). The peptide was identified in all three tissue samples with a Mascot identity score of >28.8. The sequence was manually verified. The peptide is unique to ACTBL2, containing I163 in place of asparagine or threonine in the homologous position in other actin isoforms. Nitration of ACTBL2 has not been previously reported, nor has nitration of any other actin isoform at the same tyrosine site. Other actin isoforms identified in our proteomic analysis were not nitrated.

ACTBL2

ACTBL2 VARIES THROUGH THE MENSTRUAL CYCLE

To determine whether nitrotyrosine immunoreactivity varies according to $ONOO^-$ exposure or ACTBL2 expression level, we sought to determine whether ACTBL2 expression varies with the menstrual cycle, as nitrotyrosine immunoreactivity does.

Immunohistochemical analysis of endometrial glands of the basalis was performed and scored on the same scale as nitrotyrosine immunoreactivity. As observed with nitrotyrosine immunoreactivity, ACTBL2 immunoreactivity in the endometrial glands of the basalis is less intense in secretory phase than in the proliferative phase (Fig 3.5A) ($p<0.05$). When the proliferative and secretory phases are divided into subphases, ACTBL2 immunoreactivity fluctuates between subphases (Fig 3.5B) in a trend that resembles nitrotyrosine immunoreactivity.

ACTBL2 COLOCALIZES WITH NITROTYROSINE IN TISSUE

To validate the proteomic identification of ACTBL2 as nitrated and verify that identified ACTBL2 was not a contaminant, we sought to demonstrate that ACTBL2 immunoreactivity and nitrotyrosine immunoreactivity colocalized in tissue. Nitrotyrosine immunoreactivity was observed to colocalize with ACTBL2 (Fig. 3.6), whereas ACTBL2 predominantly colocalized

with nitrotyrosine but was also observed without colocalizing. As anticipated of a cytoskeletal protein, ACTBL2 immunoreactivity was observed in the cytoplasmic compartment. Non-nitrated actin was observed on the luminal side of the endometrial glandular cells, where cilia can be observed.

ACTBL2 AND NITROTYROSINE IN PROTEIN EXTRACTS

To confirm the nanoLC-MSMS identification of nitrated ACTBL2, the same extract isolated for proteomics was used in Western blot analysis. Membranes run in parallel were blotted with an antibody against ACTBL2 or against nitrotyrosine, The membrane blotted for ACTBL2 expression displayed a predominant band at the expected molecular weight of actin, 42 kDa. The low nitrotyrosine sample in lane 1, blotted with the antibody against ACTBL2, also revealed a smaller molecular weight band, which we attribute to a degradation product. The three samples blotted for nitrotyrosine showed multiple bands, though the predominant band is also observed at 42 kDa (Fig. 3.7).

The expression level of ACTBL2 does not match the quantification obtained from proteomics. The Western blotting was used to confirm MSMS identity, rather than for quantification. As such, a loading control was not deemed necessary for standardization of protein loading. Additionally, the relative intensity of nitrotyrosine bands does not match IHC results. The IHC results reported are specific to the endometrial epithelium, whereas the Western blot sample contains proteins isolated from the glands, stroma, and adjacent myometrium.

DISCUSSION

We show that nitrotyrosine content in the endometrium varies with the menstrual cycle and is predominantly corresponds to ACTBL2 nitration.

NO is normal in endometrium

Nitric oxide plays a physiologically relevant role in endometrial tissue, but its presence also results in damage to macromolecules. $ONOO^-$, a product of the reaction of NO with superoxide, can interact with DNA to form highly mutagenic base analogues (90) or with proteins, forming nitrotyrosine (91). Peroxynitrite-mediated DNA damage is the part of the only known route by which C:G>G:C mutations form. We sought to show that peroxynitrite-induced damage can be found in uterine tissues and can explain the predominance of C:G>G:C mutations observed in PTEN in endometrial cancer.

Our findings lay in contrast to inflammation induced damage, which we previously thought induced endometrial cancer associated mutagenesis. We compared the nitrotyrosine staining pattern with that of myeloperoxidase, an enzyme released from activated neutrophils, and chlorotyrosine, a damage product that results from the interaction of proteins with HOCl generated by myeloperoxidase. In contrast to widespread nitrotyrosine damage, chlorotyrosine and myeloperoxidase were discreet and focal in endometrial tissues (Fig 3.8). This leads us to believe that $ONOO^-$ damage is not mediated solely by inflammation, not is it confined to areas affected by leukocytes.

Nitrotyrosine level varies throughout the menstrual cycle

In this study, endometrial glands and stroma were found to stain positively for nitrotyrosine by immunohistochemistry, irrespective of menstrual cycle phase. This observation disagrees with work published by Kamada et al., in which it is reported that over 71% of the secretory samples analyzed have immunoreactive glands whereas no eutopic proliferative glands showed immunoreactivity against nitrotyrosine. Wang et al. report varying levels of eNOS even within the proliferative and within the secretory phase when phases are divided into early, middle, and late, suggesting that endometrial tissue is persistently exposed to NO. The trend of eNOS presence reported by Wang mimics cyclic changes in estrogen presence (80), indicting an association of eNOS with estrogen and potentially a link between nitrotyrosine presence and estrogen level. We expected nitrotyrosine immunoreactivity to follow a similar trend as NOS

expression because of the mechanistic cornnection of NOS activity with $ONOO^-$ formation. We instead detected ranges of nitrotyrosine immunoreactivity that contrasted with reported Western blot assayed expression for eNOS. The discrepancy between nitrotyrosine content seen in this study and studies of NOS presence may be attributable to rates of NOS turnover and rates of nitrotyrosine-containing protein turnover. A different in staining technique may also contribute to the discrepancy.

As has been reported previously, we were able to observe nitrotyrosine staining in the endometrial glands and stroma. To the best of our knowledge, accumulation of nitrotyrosine in endometrial tissues has not been reported with discrimination the functionalis and the basalis. The range of nitrotyrosine immunoreactivity observed throughout the proliferative phase suddenly narrows as the menstrual cycle progresses into the secreotyr phase. Endometrial glandular cell intensity decreases as menstrual cycle subphases progress into secretory phase. An influx of inflammatory cells during menstruation is likely to contribute to oxidative damage which peaks during the early proliferative subphase. As the menstrual cycle progresses, exposure to inflammatory cells is lower (70). But estrogen exposure prompts NOS expression, contributing to nitrotyrosine formation. A dilutional effect may occur with damage products such as nitrotyrosine which are not repaired, dispersing nitrated proteins as cells proliferate and accounting for the decrease in intensity of nitrotyrosine staining observed during the secretory phase. Estrogen also mediates cellular migration through PI3K signaling and actin remodeling (92). Cellular migration involves the breakdown and build up of actin networks. As actin nitration inhibits actin depolymerization (93), nitration may affect estrogen-driven cellular motility. In addition to these processes, it has been reported that nitrated proteins are turned over more quickly than unmodified proteins (94), potentially outpacing the generation of nitrogenated proteins as the menstrual cycle progresses. Proteosomal degradation could contribute to the decrease in nitrotyrosine observed, as proteins and amino acids are recycled.

Towards the end of the secretory phase, a greater range of immunoreactivity is again observed. An influx of inflammatory cells late in the secretory phase, preceding menstrual

shedding may account for the accumulation of peroxynitrate damage products in the basalis during the late secretory subphase. A similar mechanism may account for the observed trend in stromal nitrotyrosine immunoreactivity seen (not shown). The immunoreactivity of the stroma in the basalis trends downward as the proliferative phase progresses and increases during the secretory phase as inflammatory cells are expected to invade the endometrium and become activated.

$ONOO^-$ level is mediated by enzymes that metabolize superoxide. Expression of catalase (95) and of superoxide dismutase (SOD) (96) have been studied in endometrial tissue. Presence of such enzymes which catalyze the reaction of reactive products into unreactive products may account for variations of nitrotyrosine observed in our samples. With upregulated metabolism of superoxide, peroxynitrite content is expected to decrease and result in decreased accumulation of oxidative damage products, including nitrotyrosine. SOD converts superoxide into O_2 and H_2O_2, protecting the cell from $ONOO^-$. SOD activity in the endometrium varies throughout the menstrual cycle, increasing as the proliferative phase progresses then increasing through the mid-secretory phase before decreasing in the last secretory phase (97). The trend of SOD activity aligns with the trend of nitrotyrosine throughout the menstrual cycle observed in this study. Along this metabolic pathway, catalase metabolizes H_2O_2 into oxygen and water. Catalase has been observed to be low during the early proliferative subphase and high during the late secretory phase (95).

The intensity of nitrotyrosine staining in glands in the basalis is lower in the non-Hispanic Caucasian population of this study than the black/African American population and the Hispanic population (Fig 3.3). This finding contrasts with anticipated trend of higher accumulation of nitrotyrosine in the Caucasian population. In previous studies, white populations were found to have a high incidence of uterine corpus (including endometrial carcinoma) cancers as compared to Hispanic and African American women (98–100). We anticipated that higher risk of cancer development may be linked to higher exposure to reactive oxidative species, and accumulation of damage products such as nitrotyrosine. But mechanistically, the nitrotyrosine

intensity trend aligns with what has been observed concerning estrogen level and NOS activity in different populations. African-American women, as compared to Caucasian women ont eh same diet, has statistically significantly higher levels of E_1, E_2, free E_2, and andronstendione (101). Many studies have suggested a link between NOS expression and estrogen (80), and even shown so in cell culture (102).

Telfer et al. addresses the difference in NOS expression intensity between functionalis and basalis endometrial glands (74). In addition to analyzing the variation in NOS immunoreactivity between the glands of the functionalis and of the basalis, the endometrial stroma of the two compartments was also compared. In agreement with the Telfer results, we observed a difference in intensity of nitrotyrosine in endometrial glands in the functionalis and in the basalis (not shown).

Irrespective of menstrual cycle phase, demographic, obstetric history, or reported exposures, at least one endometrial compartment was positive for nitrotyrosine immunoreactivity. Presence of nitrotyrosine in the endometrial glands and the stroma in the functionalis and basalis points to broad exposure to peroxynitrite. Further studies will address presence of oxidative damage products and relation to RNS exposure. It is of interest to study ROS and RNS exposure concurrently to assess the synergistic potential for DNA damage and mutation accumulation in the face of increased chemical insult.

Studies were performed to identify the proteins nitrated and assess whether the identity of nitrated proteins changes as the menstrual cycle progresses.

Endometrial proteome

Previous reports demonstrate gene expression profiles (103) and proteomic analysis (104,105) of endometrial tissue, but proteomic data has not yet been mined for nitrated proteins. We selected a subset of samples stained for nitrotysine immunoreactivity for nitroproteomic analysis. We identified ACTBL2 as the predominantly nitrated protein in benign human endomyometrial tissue.

Previous literature has identified cytoplasmic β-actin, cytoplasmic γ-actin, and presumptively identified aortic smooth muscle actin or alpha skeletal muscle actin in cycling endometrium (104–107). In a comparison of normal to endometrial cancer tissue, cytoplasmic β-actin was identified to be differentially expressed (87).

We were able to identify a comparably large number of proteins (>1000), in opposition to other studies , by the use of LC-MS/MS rather than 2-D gel electrophoresis based proteomics. We were able to identify various non-nitrated actins, including cytoplasmic β-actin, γ-enteric smooth muscle actin, and α skeletal muscle actin. Both β and α actin was identified in all three samples analyzed, which γ actin was identified in the 2 samples selected for high nitrotyrosine immunoreactivity. While we identified nitrated ACTBL2, we did not detect non-nitrated ACTBL2. ACTBL2, an actin isoform, has also been referred to as kappa actin and has been found in hepatocellular carcinoma (108). ACTBL2 has not yet been identified in endometrium.

While it was expected that multiple proteins would be nitrated, due to the non-specific chemical nature of $ONOO^-$ reactions, we were surprised to find that one protein was predominantly nitrated in three human endomyometrial samples. The predominant nitrated peptide comprised residues 149-178 of ACTBL2, an actin isoform. ACTBL2 has not previously been reported to be nitrated, particularly at Y167 (Fig 3.9).

The specificity of nitration on ACTBL2, and not other actin isoforms or other proteins (at least within the bounds of this study), points to biological significance of ACTBL2 nitration.

Physiological significance of actin nitration

Though multiple actin isoforms have been detected, it is unclear whether the actin isoforms have independent or overlapping roles. Actin plays multiple roles, including mediation of cellular structure, division, and motility (109) using a treadmilling polymerization (110)(111). Actin polymerization and depolymerization plays a role in endothelial cell apoptosis (112), as actin polymerization inhibitors inhibit apoptosis (113). As an actin isoform, ACTBL2 is

predicted to function as other actins. It is currently unclear what role ACTBL2 plays in the endometrium, as compared to other actin isoforms.

G-actin (globular form) combines to form F-actin (filament form) (114), in a process regulated protein binding (114) and exposure to peroxynitrite (115). It is believed that the effect peroxynitrite exerts on actin polymerization relates to the formation of nitrotyrosine in actin (116). Nitrated actin promote F-actin over G-actin (93).

The specificity of nitrated of ACTBL2 in endometrial tissue is likely to serve a physiological role. As Y167 lies in a binding interface between two actin monomers in F-actin structure (114,109), nitration at Y167 likely disrupts F-actin formation and depolarization as nitration of other actin isoforms have been shown to do (115,117) in contrast to the statements made by Aslan (93) .

Cyclical variation of nitrotyrosine correlates with ACTBL2 expression

Having identified ACTBL2 as the predominant nitrated protein in endomyometrial tissue, we then asked whether the observed fluctuation in N-tyr immunoreactivity was 1) due to fluctuation in ACTBL2 expression or 2) fluctuation in $ONOO^-$ exposure.

To answer the former, we determined the ACTBL2 immunoreactivity of tissues obtained from the same patients assessed for nitrotyrosine immunoreactivity. ACTBL2 immunoreactivity in the glands of the basalis fluctuated, with a similar trend as nitrotyrosine immunoreactivity in the same compartment. As ACTBL2 has been identified as the predominant nitrated protein because ACTBL2 and nitrotyrosine immunoreactivity follow similar trends, it appears that the detected level of nitrotyrosine immunoreactivity in benign endometrial tissue is a result of ACTBL2 protein expression. We have confirmed ACTBL2 as the predominantly nitrated protein in benign human endometrium by nanoLC-MSMS (peptide identification), immunofluorescence (showing that nitrtyrosine predominantly colocalizes with ACTBL2), and Western blot.

In reference to the possibility of $ONOO^-$ exposure being the predominant effector of nitrotyrosine immunoreactivity, we asked if factors which contribute to $ONOO^-$ formation vary with the menstrual cycle. Others have assessed NOS and arginase expression in endometrial tissues. While these determinations were made based on the endometrial as a whole, without discrimination between the functionalis/basalis or glands/stroma, the findings provide us with clues that can be related to our own findings. For instance, arginase has been observed in endometrial glandular cells and observed to be present in higher quantity during the secretory phase than proliferative phase (118). Arginase competes with NOSs for arginine usage. With less arginase present during the proliferative than the secretory phase, there is arguable more arginine available for NOS-mediated generation of NO. A higher level of nitric oxide during the proliferative phase may help explain the seemingly higher amount of exposure of endometrial glandular cells to peroxynitrite during this menstrual phase

NO is a signaling molecule with a physiological role in the uterus

As every sample stained displayed nitrotyrosine immunoreacitivyt, it is evident that endometrial tissue is perisitently exposed to $ONOO^-$. Formation of $ONOO^-$ utilizes NO and superoxide. Rather than being pathologic, NO serves a physiological role in human endometrial tissue (119): mediating angiogenesis, preventing platelet aggregation, causing vasodilation and maintaining myometrial quiescence of the nearby smooth muscle tissue. But NO also reacts with superoxide to form $ONOO^-$, which can then nitrate protein residues. It is, of yet, unclear whether protein nitration widely affects protein function as it does actin function. Further study will elucidate the cellular role of protein nitration.

Proposed pathway of mutations

We sought to explain the prevalence of C:G>G:C mutations observed in endometrial carcinoma. We proposed that persistent exposure to ONOO- promotes the formation of guanine secondary oxidation damage products which are known to be highly mutagenic (Fig 3.10).

It has been previously observed that 8oxoG can be detected in benign endometrial tissues (59). While G has the lowest redox potential of the standard four bases, 8oxoG is further susceptible to oxidation (66,67,120).

We show that benign endometrial tissue is persistently exposed to ONOO-, identifying ONOO- mediated damage protein products by multiple means. We extrapolate this finding to infer that macromolecules in endometrial tissue are at risk of ONOO- mediated damage, including DNA bases.

8oxoG exposed to ONOO- results in Gh and Sp formation (62,63). Gh and Sp are more mutagenic than 8oxoG, which is itself mutagenic (64). Gh and Sp are able to mispair with G (64,65), and through repair escape and replication, C can be incorporated in place of the damaged G. The formation of secondary guanine oxidation products form from the reaction of $ONOO^-$ with 8oxoG and can mispair with A,T,C, or G. NEIL1 is capable of removing Gh and Sp from DNA, opposite any of the normal bases. When this occurs opposite guanine, a cytosine could be erroneously inserted to prompt a G>C mutation.

Table 3.1: Clinical information for patients included in the study and staining results.

Tissue was collected from 51 patients who underwent hysterectomy for a variety of clinical indications. Nitrotyrosine immunoreactivity and ACTBL2 immunoreactivity varied with menstrual cycle subphase.

Patient #	Menstrual Phase	Age	Ethnicity	Indication for surgery	Staining intensity score of basalis glands	
					Nitrotyrosine	ACTBL2
1	Early proliferative	30	White	Endometriosis, pelvic pain	Weak	Moderate
2	Early proliferative	49	White	Urinary stress incontinence, rectocele, perineocele, uterine prolapse, cystocele	Weak	Moderate
3	Early proliferative	36	White	Abnormal uterine bleeding	Weak	Strong
4	Early proliferative	45	White	Menorrhagia	Moderate	Weak
5	Early proliferative	43	Black/AA	Mixed incontinence, uterovaginal prolapse	Moderate	Moderate
6	Early proliferative	47	Hispanic/Latino	Fibroid , menorrhagia, mixed incontinence	Moderate	Moderate
7	Early proliferative	37	Black/AA	Fibroids, menorrhagia	Moderate	Moderate
8	Early proliferative	41	Black/AA	Menorrhagia	Moderate	not stained
9	Early proliferative	37		Dysplasia	Moderate	not stained
10	Early proliferative	39	Black/AA	Fibroids	Strong	Moderate
11	Early proliferative	49	Black/AA	Cystocele, rectocele, incontinence	Strong	Moderate
12	Early proliferative	46	Hispanic/Latino	Fibroids, menorrhagia	Strong	Moderate
13	Early proliferative	42	White	Pelvic pain, dysmenorrhea , endometriosis. Possible adenomyosis	Strong	Moderate
14	Early proliferative	35	Black/AA	Menorrhagia	Strong	not stained
15	Mid-proliferative	32	White	Utero-vaginal prolapse	Weak	Weak
16	Mid-proliferative	41	Hispanic/Latino	Menorrhagia	Weak	Weak
17	Mid-proliferative	42	Black/AA	Abnormal uterine bleeding, fibroids	Moderate	Weak
18	Mid-proliferative	36	White	Cervical dysplasia	Moderate	Moderate
19	Mid-proliferative	36	Black/AA	Cervical cancer	Moderate	Moderate
20	Mid-proliferative	41	White	Menorrhagia	Strong	Weak
21	Mid-proliferative	27	Hispanic/Latino	Bladder exstrophy, uterine prolapse	Strong	Weak
22	Mid-proliferative	57	Black/AA	Metrorrhagia, recurrent polyps	Strong	Moderate
23	Mid-proliferative	27	White	Cervical dysplasia	Strong	Moderate
24	Late proliferative	47	White	Fibroids	Negative	Moderate
25	Late proliferative	32		Pelvic organ prolapse	Weak	Weak
26	Late proliferative	42	Hispanic/Latino	Endometriosis, dysmenorrhea	Moderate	Moderate
27	Late proliferative	31	White	Pelvic pain	Moderate	Moderate
28	Late proliferative	37	Hispanic/Latino	Pelvic organ prolapse	Moderate	Moderate
29	Late proliferative	47	White	Abnormal uterine bleeding	Moderate	Moderate
30	Late proliferative	48	Black	Fibroids	Moderate	Moderate
31	Late proliferative	46	Hispanic/Latino	Fibroids	Strong	Moderate
32	Early secretory	47	Black/AA	Uterovaginal prolapse, cystocele, rectocele, incontinence	Weak	Weak
33	Early secretory	46	White	Menorrhagia	Weak	Weak
34	Early secretory	36	White	Menorrhagia, menometrorrhagia	Weak	Weak
35	Early secretory	46	Black	Uterine fibroids, menometrorrhagia, anemia	Weak	Weak
36	Early secretory	39	White	Stress incontinence, cystocele, rectocele.	Weak	Moderate
37	Early secretory	48	White	Cystocele, midline incontinence	Weak	Moderate
38	Early secretory	30	White	DCIS with a family history of breast and ovarian cancer	Weak	Moderate
39	Early secretory	49	Hispanic/Latino	Menorrhagia	Moderate	Weak
40	Mid-secretory	37	White	Pelvic pain, dysmenorrhea	Weak	Weak
41	Mid-secretory	44	Hispanic/Latino	Fibroids, menorrhagia	Weak	Weak
42	Mid-secretory	40	White	Menorrhagia, fibroids	Weak	Weak
43	Mid-secretory	39	White	Mixed incontinence, fecal incontinence,	Weak	Weak
44	Mid-secretory	40	Hispanic/Latino	Cervical dysplasia	Weak	Weak
45	Mid-secretory	46	Hispanic/Latino	Fibroids, pelvic pain, menorrhagia	Weak	Weak
46	Late secretory	31	White	Prolapse, incontinence	Weak	Weak
47	Late secretory	28	White	Abnormal uterine bleeding, cystocele	Weak	Weak
48	Late secretory	32	White	Cervical dysplasia	Moderate	Weak
49	Late secretory	43	Black	Menometrorrhagia	Strong	Negative
50	Late secretory	32	Hispanic/Latino	Cervical dysplasia	Strong	Weak
51	Late secretory	45	Thite	Abnormal uterine bleeding, chronic pelvic pain	Strong	Weak

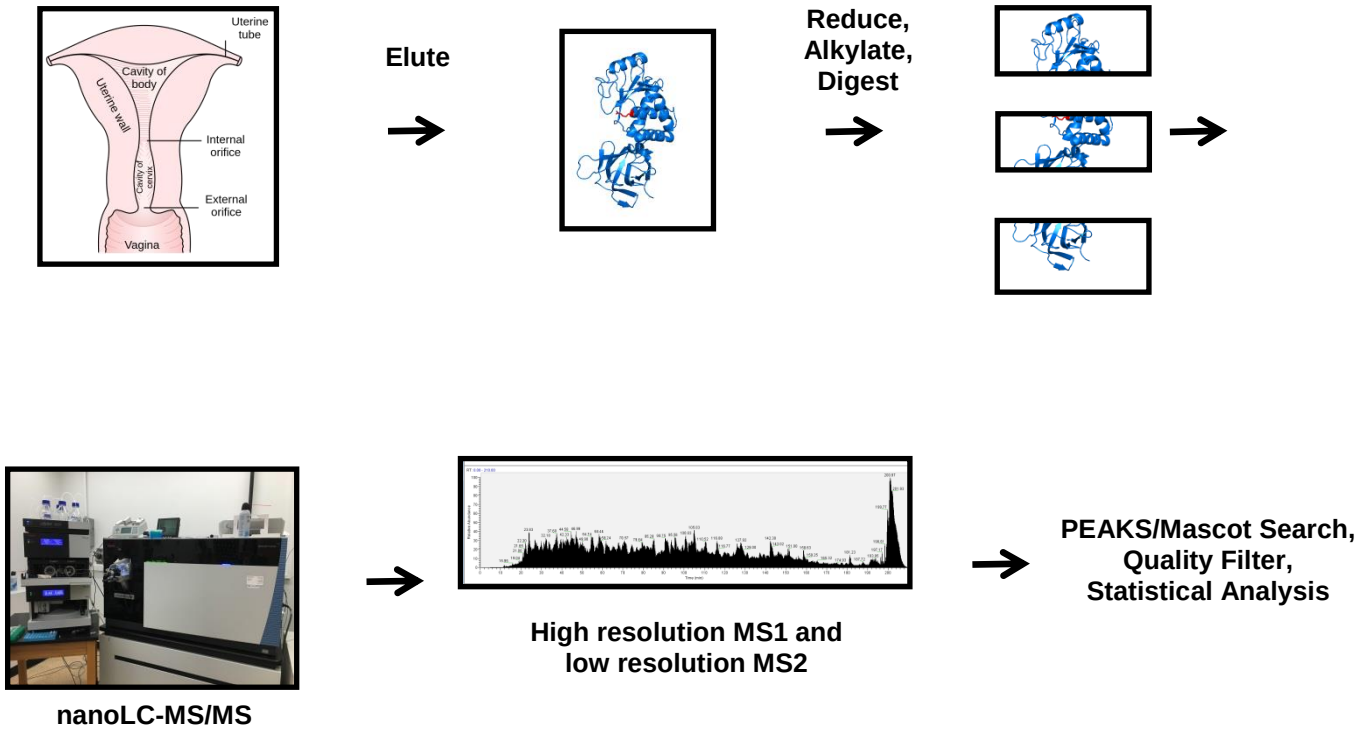

Figure 3.1: Proteomics workflow.

Proteomics was used to identify nitrated proteins found in benign human endomyometrial tissue. Proteins were isolated from tissues, trypsinized into peptide fragments, and analyzed by nanoLC-MS/MS. Peptide fragments identified by MASCOT and PEAKS were manually verified.

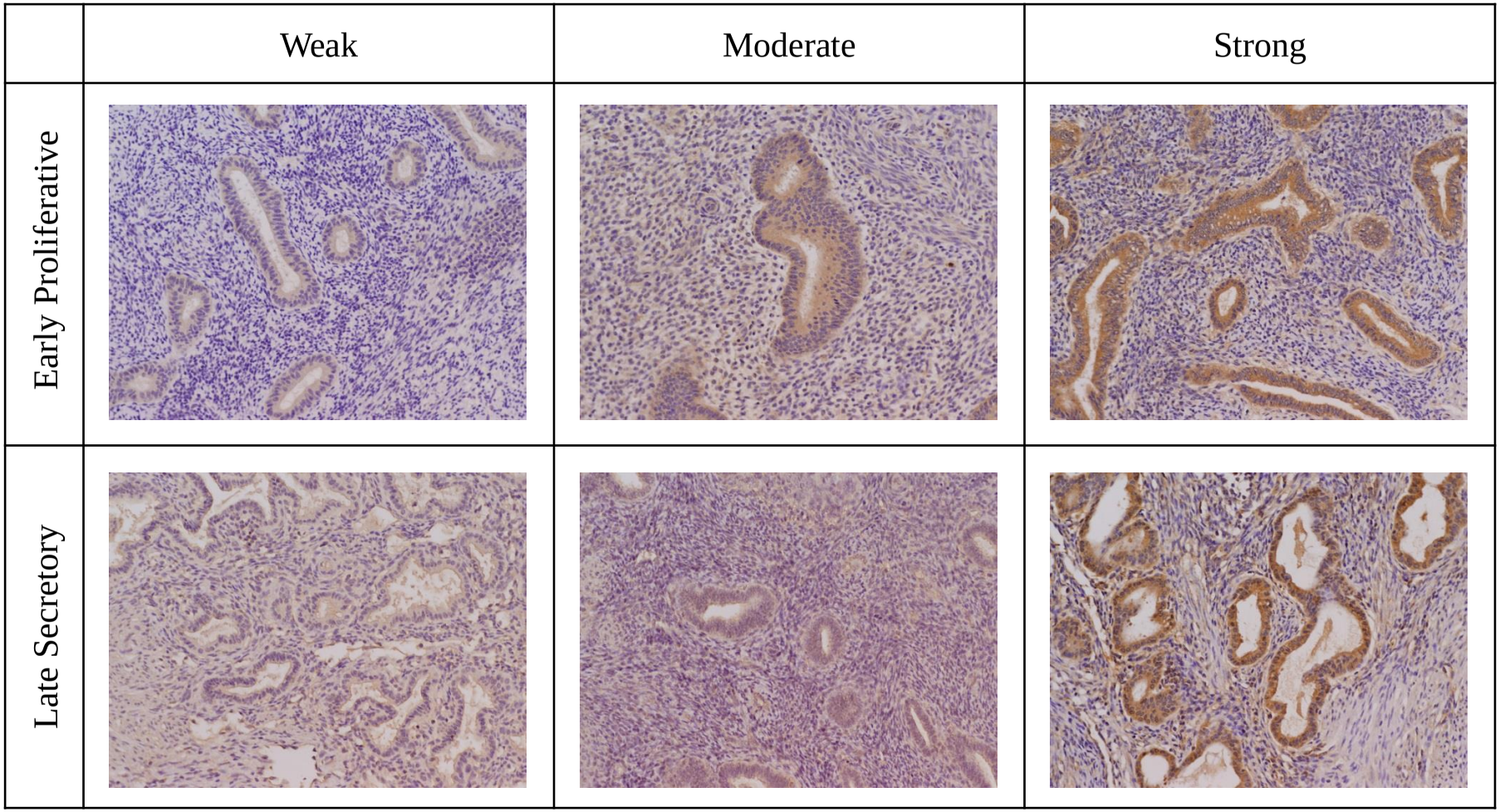

Figure 3.2: Nitrotyrosine immunoreactivity ranges in endometrial glands.

Nitrotyrosine, a marker of peroxynitrite-mediated damage, is observed in benign endometrium by immunohistochemistry. Nitrotyrosine immunoreactivity was scored in the endometrial glands of the basalis. Immunoreactivity was scored as negative (not shown), weak, moderate, or strong.
Sections stained with an antibody against nitrotyrosine (1:2000 dilution). Images are captured at 20x magnification.

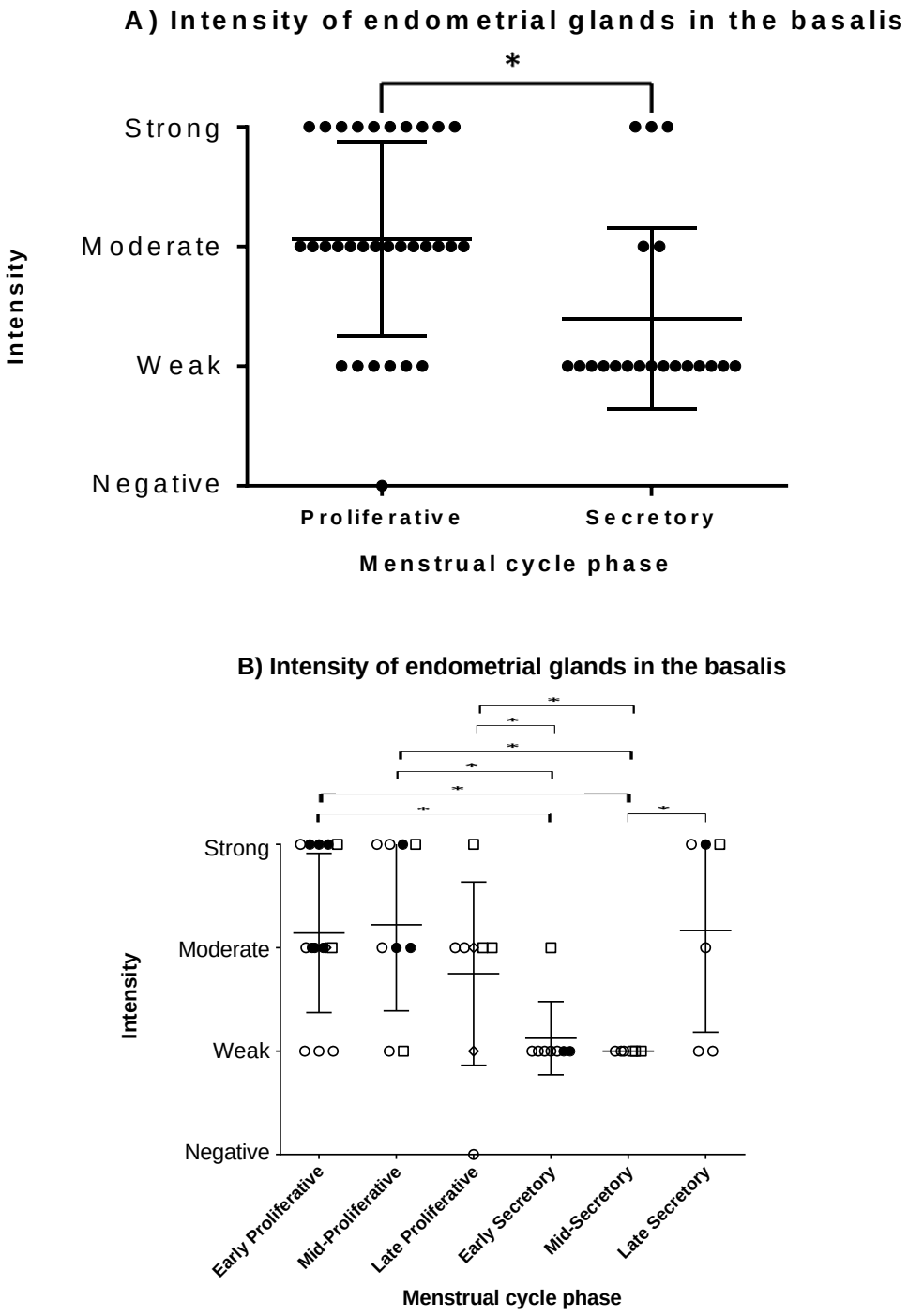

Figure 3.3: Nitrotyrosine intensity fluctuates throughout the menstrual cycle.

The intensity of immunohistochemical nitrotyrosine staining varies throughout the menstrual cycle. Intensity varies widely during the proliferative subphases, is uniformly low during early secretory phase, and varies widely in late secretory phase.

Endometrial glands in the basalis display nitrotyrosine staining regardless of menstrual cycle phase. A) Intensity of nitrotyrosine staining of the endometrial glands of the basalis is significantly lower during the secretory phase than the proliferative phase of the menstrual cycle ($p<0.0001$). B) Representation of race, menstrual cycle subphase and nitrotyrosine scoring intensity. Intensity of endometrial glands decreases as menstrual cycle subphases progress showing a wide range of intensity during the proliferative subphases and a smaller range during the early and mid-secretory subphases. Samples from black patients cluster in the at higher scores of nitrotyrosine immunoreactivity. ○ =white, ● =black, □ =Hispanic, ◇ =unlisted race; *= $p<0.05$

Table 3.2: Staining characteristic of endometrium selected for proteomic analysis.

The three endomyometrial samples selected for proteomic analysis were selected based on nitrotyrosine immunoreactivity score various endometrial structures: the endometrial glands and stroma of the basalis and functionalis.

			Late proliferative	Early Proliferative	Late Secretory
Glands	Functionalis	Intensity	Weak	Strong	Strong
	Basalis	Intensity	Weak	Strong	Strong
	Functionalis	Frequency	<50%	>75%	>75%
	Basalis	Frequency	50-75%	>75%	>75%
Stroma	Functionalis	Intensity	Weak	Strong	Moderate
	Basalis	Intensity	Negative	Moderate	Moderate
	Functionalis	Frequency	<50%	>75%	>75%
	Basalis	Frequency	>75%	>75%	>75%
			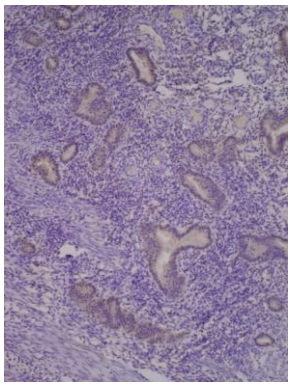	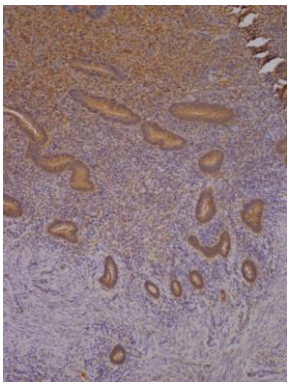	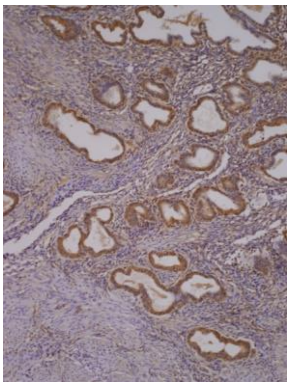

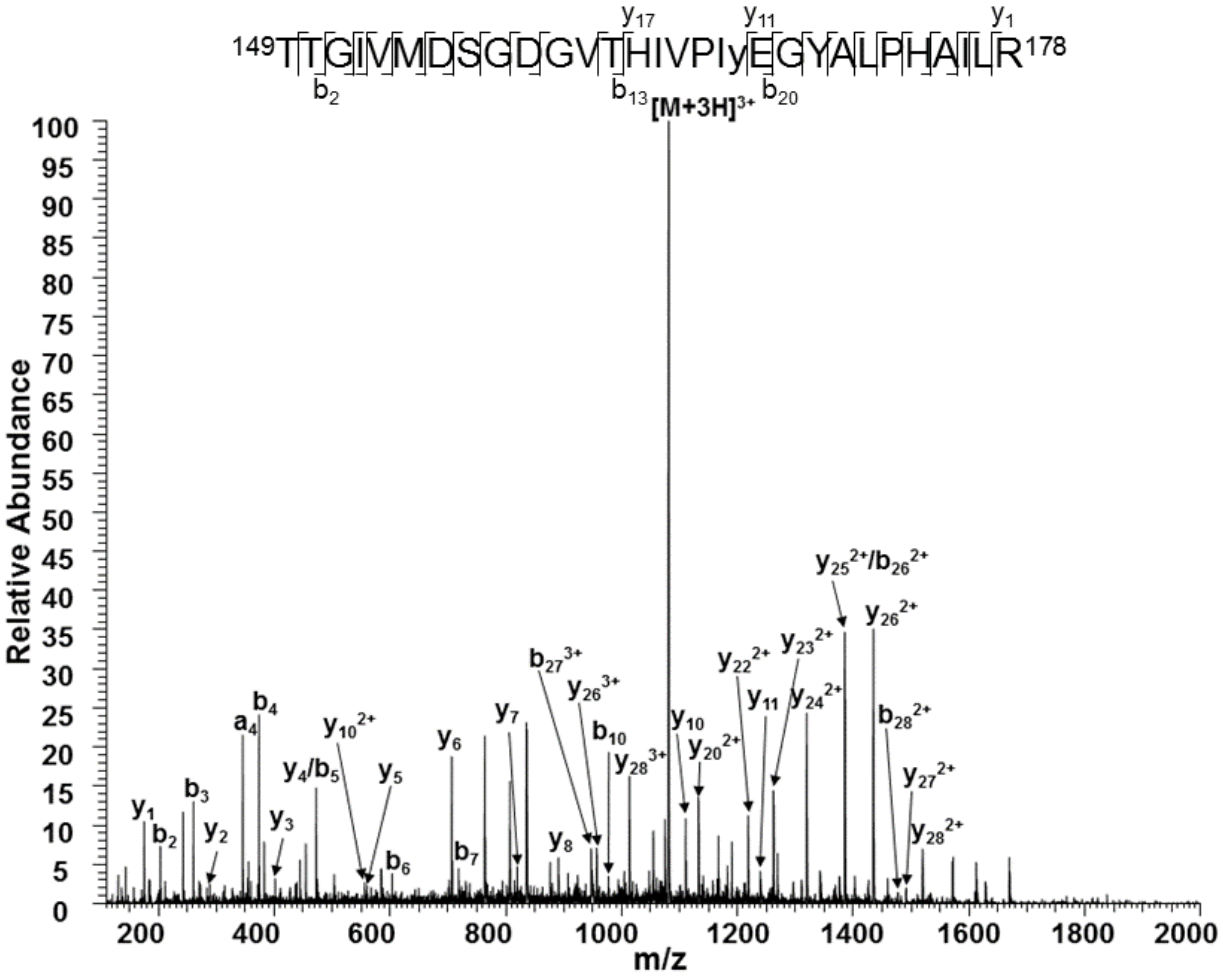

Figure 3.4: ACTBL2 is nitrated in benign human endomyometrial tissue.

The peptide TTGIVMDSGDGVTHIVPIyEGYALPHAILR (theoretical $[M+3H]^{3+}$ = 1080.888, observed 1080.884) encompassing residues 149-178 of ACTBL2 was identified as nitrated in 3 benign human endomyometrial tissues.

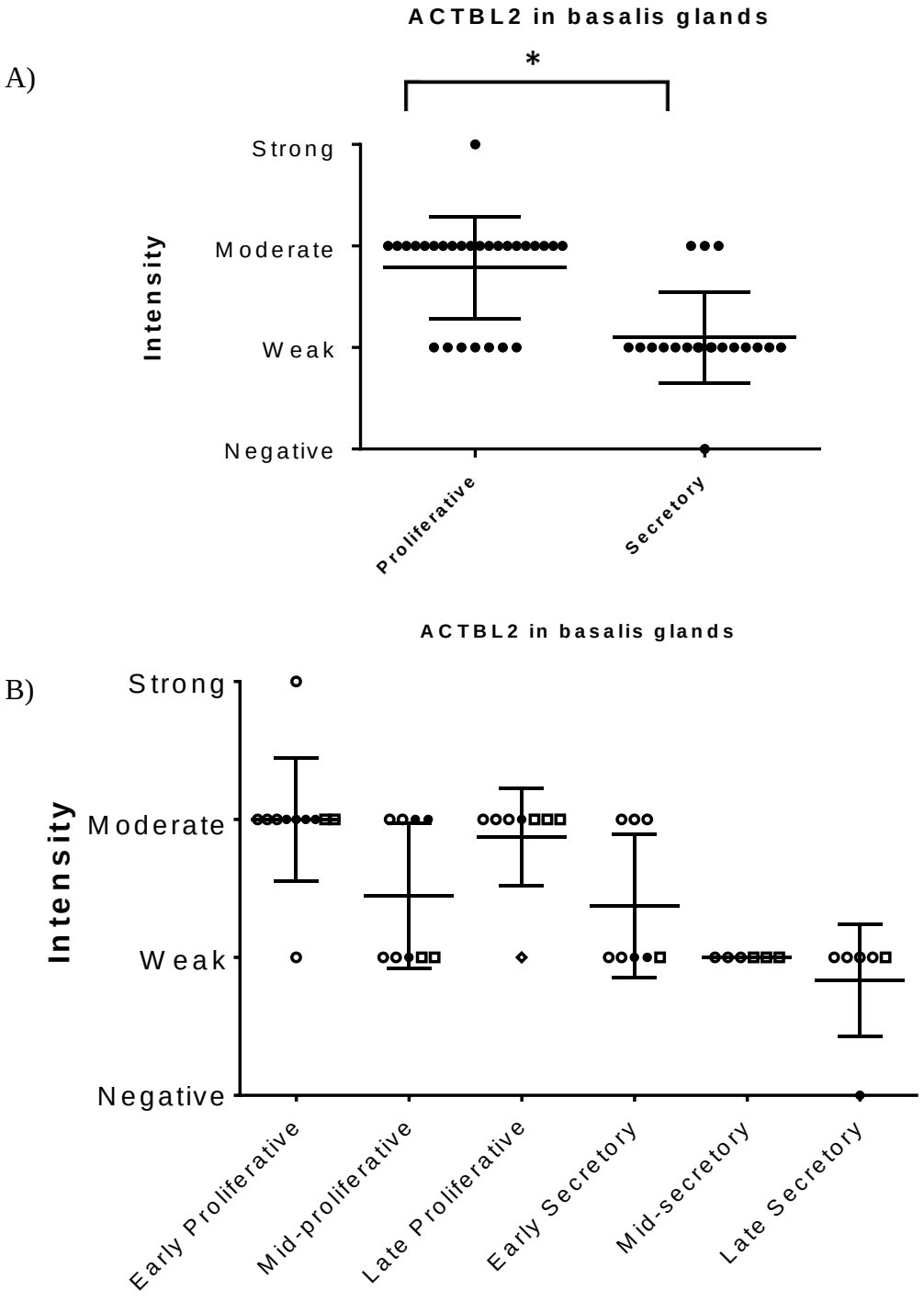

Figure 3.6: ACTBL2 immunoreactivity varies with the menstrual cycle.

ACTBL2 intensity as a function of menstrual cycle. (A) ACTBL2 staining intensity is lower in the secretory phase than in the proliferative phase. p=0.006 (Chi-squared test) (B) ACTBL2

staining, is generally higher in the proliferative subphases of the menstrual cycle than in secretory subphases. ○ =white, ● =black, □ =Hispanic, ◇ =unlisted race

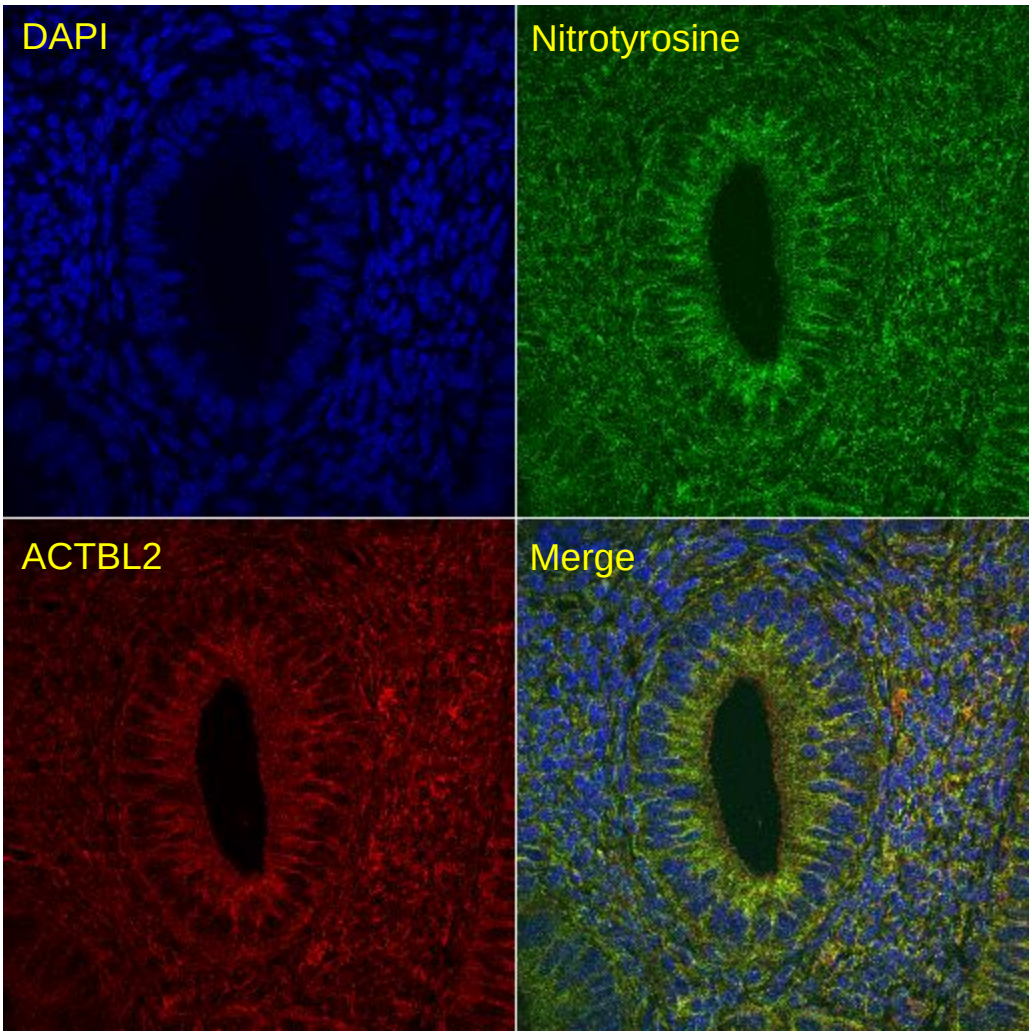

Figure 3.6: ACTBL2 and nitrotyrosine colocalize in benign human endometrial tissue.

Nitrotyrosine and ACTBL2 colocalize by confocal microscopy and IF. Immunofluorescent staining of endometrium for nitrotyrosine (green) and ACTBL2 (red) content reveals that nitrotyrosine and ACTBL2 colocalize (yellow).
ACTBL2 and nitrotyrosine are widespread in endometrial tissue and immunostaining predominantly colocalizes

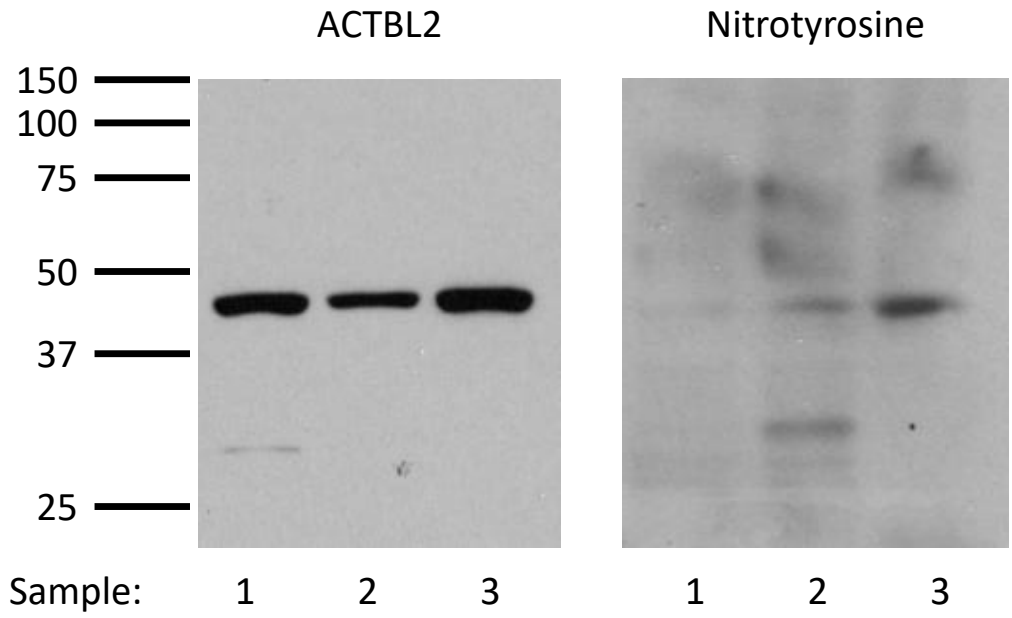

Figure 3.7: Western blotting confirms ACTBL2 as the predominantly nitrated protein in benign endomyometrial tissue.

Proteins isolated from 3 endomyometrial tissue samples were blotted for ACTBL2 and nitrotyrosine content. ACTBL2 is recognized at 42 kDa, the anticipated molecular weight of actin. An additional band is noted in lane 1 of the left panel, which may represent a degradation product of ACTBL2. Blotting for nitrotyrosine content reveals that the predominant band observed aligns with ACTBL2 with additional bands. Additional bands in the membrane blotted for nitrotyrosine may represent additional nitrated proteins or degradation products of nitrated ACTBL2.

Lane 1 represents a sample (late proliferative) low for nitrotyrosine immunoreactivity by immunohistochemistry. Lanes 2 (early proliferative) and 3 (late secretory) are samples of high for nitrotyrosine immunoreactivity by immunohistochemistry.

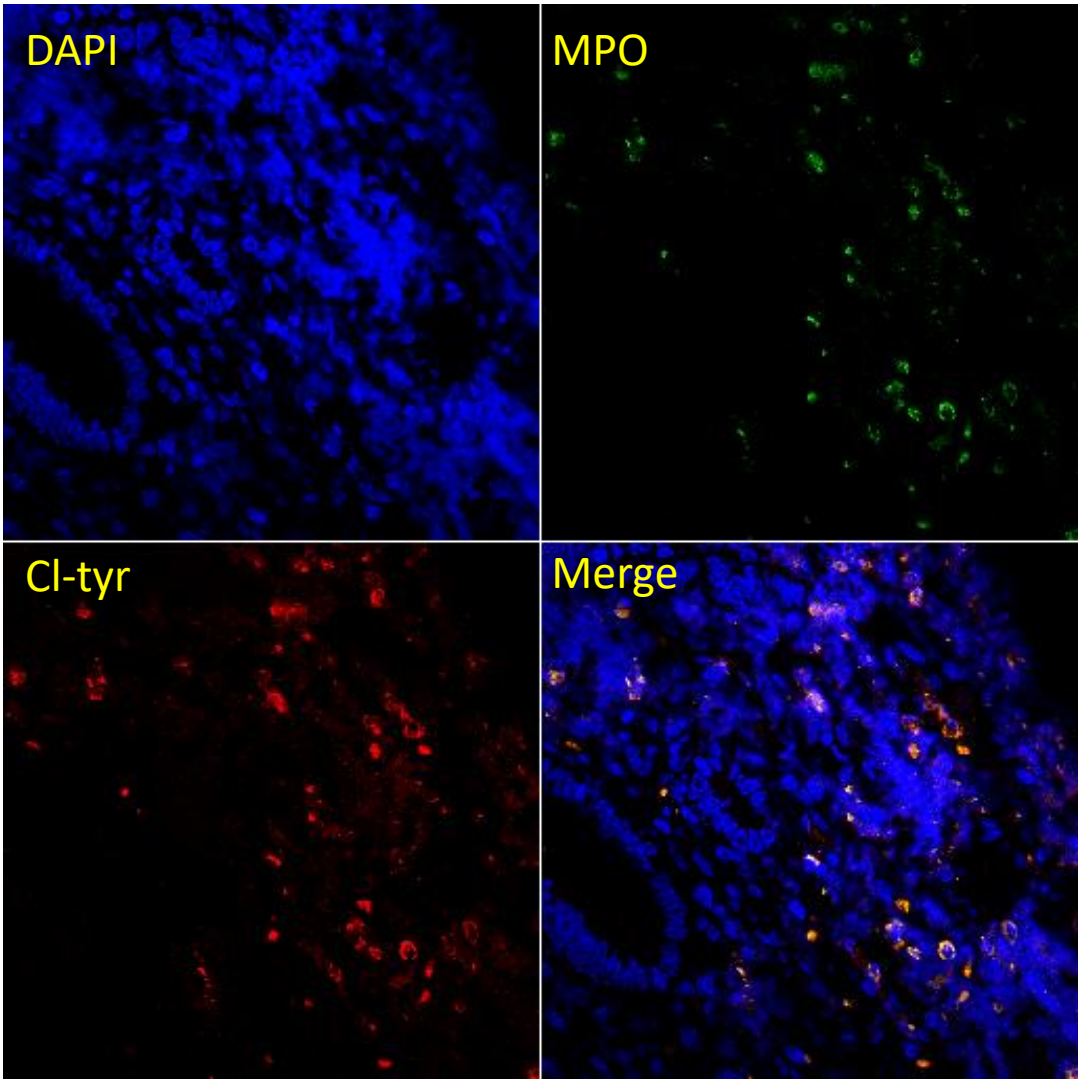

Figure 3.8: Myeloperoxidase and chlorotyrosine colocalized in benign human endometrial tissue.

Myeloperoxidase (MPO) generates HOCl which then reacts with tyrosine to form chlorotyrosine. The colocalized of MPO and chlorotyrosine supports that enzyme mediated formation of the reactive oxygen species responsible for chlorotyrosine presence.

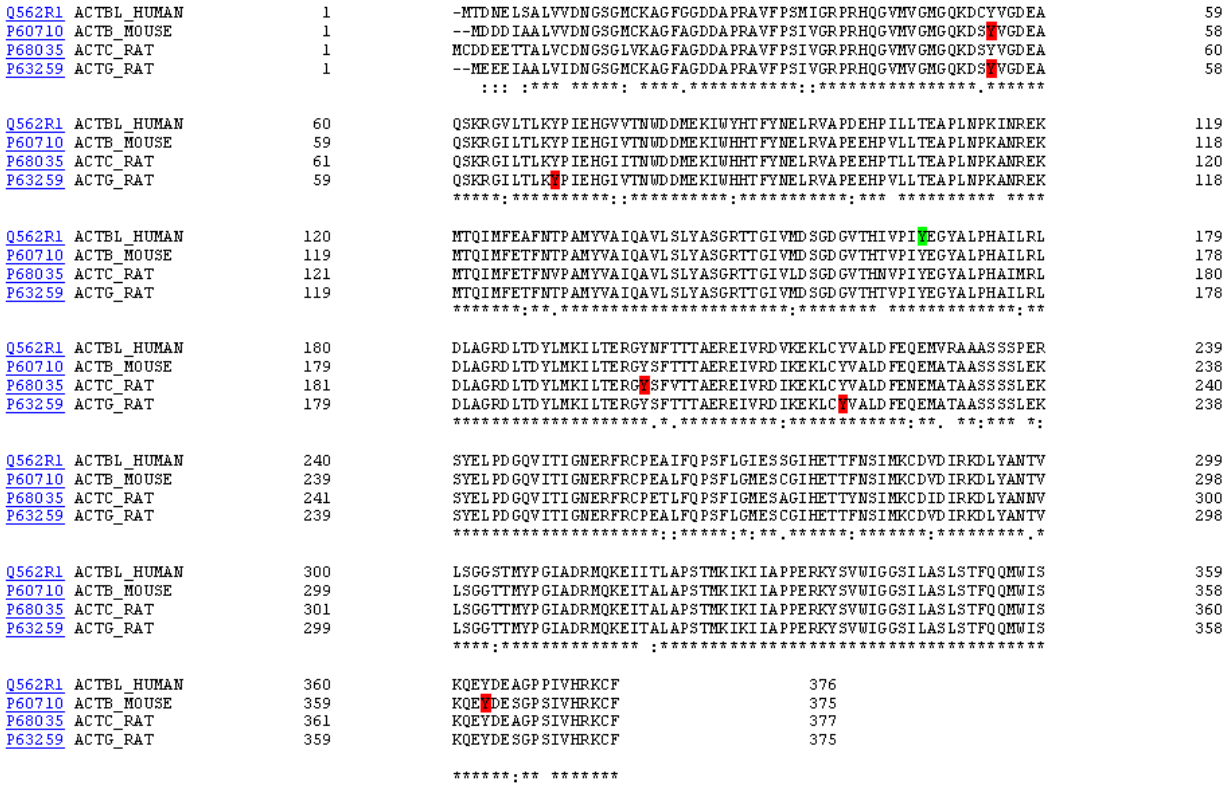

Figure 3.9: Alignment of ACTBL2 and nitrated actin isoforms.

Homology mapping of ACTBL2. While actin has previously been reported to be nitrated, the residue aligning with ACTBL2 Y167 has not previously been reported to be nitrated. Resides highlighted in red represent previously reported sites of tyrosine nitration (121–124). The residue highlighted green represents Y167 in ACTBL2, which we found to be nitrated in benign human endometrial tissue. Actin isoform alignment was assessed by Custal alignment (Clustal Omega). Sequences were obtained from Uniprot (uniprot.org).

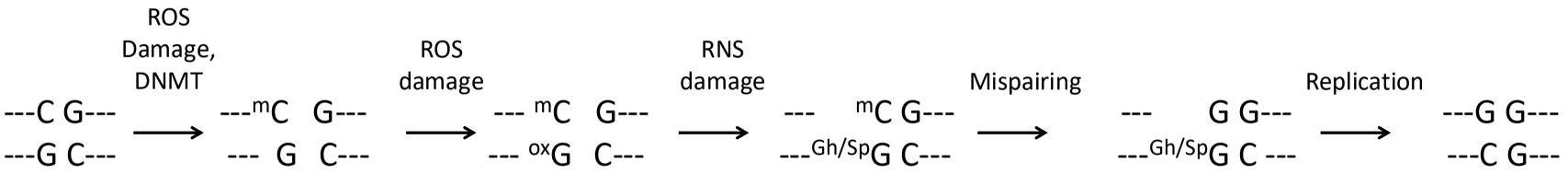

Figure 3.9: Proposed C:G>G:C mutation pathway.

Proposed mutation pathway which contributes to PTEN C->G mutations observed in gynecologic pathology. At PTEN, codon 130, the CpG site is predominantly methylated. G, especially when adjacent to or base paired to ^{m}C, is highly susceptible to oxidation to 8oxoG (oxG). 8oxoG is then particularly prone to further oxidation to form guanidinohydantoin (Gh) and spiroiminodihydantoin (Sp). Gh and Sp are highly mutagenic and have previously been shown to mispair with G. If replication proceeds without repair of the mispairing, the original C:G basepair would be converted into G:C. Through selective advantage, such a mutation at PTEN codon 130 promotes tumorigenesis.

Chapter 4 Leiomyomata

BACKGROUND

Leiomyomata

Leiomyomata, also referred to as fibroids or myomas, are benign neoplasms that arise from smooth muscle. They are typically described as tan, whorled, well-circumscribed lesions in the myometrium (Fig 4.1). Histologically, they are identified by their disorganized cellular orientation, as opposed to linearly oriented normal myometrial cells. Leiomyomas can occur in any area of smooth muscle, but we will limit our discussion to spontaneous myomas of the uterus. Risk factors associated with leiomyoma formation are associated with increased exposure to estrogen, including obesity and early age of menarche (126). Leiomyomas are hyperresponsive to estrogen, often regressing during menopause or through hormonal treatment. Treatment ranges from medical to surgical. Medical treatment can reduce the size of the leiomyoma and improve symptoms, but is not curative and the leiomyoma can recur once treatment is stopped. If severe, leiomyomas can be surgically removed by myomectomy or by hysterectomy. If a myomectomy is performed, it is still possible for leiomyomas to appear in the remaining myometrium. Complications of leiomyomas include abnormal uterine bleeding, potentially leading to anemia. Leiomyomas can also cause recurrent miscarriage and infertility.

Nearly half of all women are diagnosed with leiomyoma by age 50 (127). The rate of incidence in black populations is greater than in white, Hispanic and Asian populations (127). The incidence of leiomyomas is difficult to estimate, as the diagnosis is subject to both under-diagnosis and over-diagnosis. Leiomyomas can be detected by radiology, but the technique is not sensitive enough to diagnose small fibroids, thereby under-diagnosing the condition. Conversely, histology is the definitive method of diagnosis, but use of the technique can over diagnose leiomyomas by identifying very small fibroids that are not of clinical significance. Leiomyomas

range in size, from sub-centimeter to larger than a grapefruit and multiple leiomyomas can form in a single patient.

Leiomyomas can be classified according to their location in the uterine wall, in relation to the endometrium and serosal lining (128). Symptoms commonly include abnormal uterine bleeding; the molecular contributions to bleeding are reviewed by Stewart and Nowak (129). Leiomyoma contribute to anemia and pelvic pain (130,126). They can be managed medically, but are a common indication for hysterectomy.

Mutations observed in leiomyomas

Leiomyomas originate as a stem cell, differentiating into the various cell types observed in in a fibroid. The genetic origin of leiomyomas was unclear, but a few gene aberrations have recently been associated with leiomyoma presence. Mutation in fumarase (fumarate hydratase) has been detected as a germline mutation of multiple cutaneous and uterine leiomyomatosis (MCUL) (131) and in nonsyndromic leiomyomas (132). Pollard et al. have reviewed the likely routes by which mutation of fumarase could promote tumorigenesis:pseudo-hypoxia, dysfunction of apoptosis, and anabolic drive (133). Mutations in HMGA1 and HMGA2 have also been detected in leiomyomas (134–136). The mutation of these genes was detected at low frequency, and it remained unclear what genetic associations the majority of leiomyomas could be linked to.

MED12

Within the last decade, it was found that MED12 mutations could be detected in the majority of leiomyomas. MED12 is found on the X chromosome and encodes for MED12. The MED12 gene contains 45 exons, encoding a 2177 amino acid protein. MED12 functions as a part of the CDK8 submodule of Mediator (137). Association of CDK8 with Mediator represses transcriptional activity (137). Among Mediator's gene-specific functions is the ability to express estrogen receptor target genes (137).

In 2011, Makinen et al. reported the existence of MED12 mutations in 70% of leiomyomas examined (138). These mutations clustered in exon 2 of the MED12 gene, with a hotspot at codon 44 (Fig 4.2) and a second hotspot at codon 36 (138). Mutation at codon 44 and at codon 36 reduces binding with cyclin C, which further affects binding to Mediator (139).

The location of MED12 on the X chromosome presents a dimension of complexity: sequencing of the DNA will be incongruent with MED12 expression due to repressed transcription of one X chromosome in each cell. To study genetic changes with functional outcomes, it is of interest to study transcribed sequences of MED12 rather than just genomic DNA sequences.

The patient population at UTMB has not previously been studied for MED12 mutation status in leiomyomas or adjacent normal myometrium.

Origin of mutations

Though mutated genes have been identified in leiomyomas, it is unclear why these mutations form. The observed MED12 codon 44 mutations occur at guanine, suggesting that oxidative damage plays a role in MED12 mutagenesis. Guanine is highly susceptible to oxidative damage by ROSs and 8oxoG is known to be mutagenic. 8oxoG is susceptible to further oxidation to Gh and Sp, which more mutagenic than 8oxoG.

In this study, we intend to demonstrate that normal myometrium is exposed to $ONOO^-$, which can cause protein nitration and form secondary guanine oxidation products. If ONOO- is present in the myometrium and the endometrium, it is suggestive of a similar mutagenesis pathway in uterine tissues.

NO in myometrium

NO is well known to promote vascular dilation (71), which regulates blood flow in the uterine myometrium. NO is well known to cause vasodilation in vascular smooth muscle. Vasodilation is prompted by NO signaling through cyclic GMP dependent protein kinase

signaling (140,141). Cyclic GMP contributes to smooth muscle relaxation by inhibiting actin cytoskeleton arrangement (140). In uterine tissue, smooth muscle cell relaxation is especially important in the maintenance of pregnancy by promoting myometrial quiescence. The role of NO in regulating myometrial quiescence has been debated though. Some groups have shown that NO influences smooth muscle stretch-induced contraction (142) whereas others argue that low levels of NOS in the myometrium do not account for myometrial contraction and relaxation (143,144). NOS immunoreactivity has been further studied in the uterine myometrium of model animals (78) and humans, showing that NOS is present and argue that NO might promote myometrial quiescence.

MATERIALS AND METHODS

Tissue Collection

Specimens were collected with IRB approval from 17 women treated at the University of Texas Medical Branch in 2015-2016 (Table 4.1). Samples of leiomyomata and adjacent normal myometrium were collected with assistance from a pathologist and pathology residents. Leiomyoma samples were separated from normal myometrium grossly. Tissue samples were weighed and divided into 25-100 mg aliquots in a designated biohazard sample processing area. The tissue was then stored at -80°C until additional processing. The samples were coded and de-identified.

Formalin-fixed, paraffin-embedded blocks from the same patients were obtained from the UTMB pathology department for immunohistochemical analysis.

DNA isolation

Aliquots of tissue (25-30 mg) were incubated in 800 µL lysis buffer overnight at 37°C and 600 rpm. Lysis buffer was composed of 0.1 mL 1M Tris, pH 8.5, 10 µL 0.5M EDTA, 10 µL

20% SDS, 40 µL 5M NaCl, 5 uL 20mg/mL proteinase K, 1 uL 100 mg/mL RNAse, and 840 µL ddH_2O per 1 mL of lysis buffer.

The following day, the tissue was incubated at 55°C for one hour at 700 rpm to facilitate additional lysis and to further solubilize the DNA. Samples are homogenized by pipetting, then divided into two aliquots for further manipulation.

To each aliquot, 37.5 uL of 8M ammonium acetate and 350 µL phenol/chloroform/isoamyl alcohol 25:24:1 buffered with Tris base were added and mixed. The mixture was centrifuged at 18,000 rcf for 5 minutes. The aqueous phase was removed and transferred to 3 volumes of ice-cold 100% ethanol to precipitate DNA. The sample was incubated at -20°C for at least one hour to facilitate DNA precipitation prior to centrifugation at 13,000 rcf for 10 minutes at 4°C. The supernatant was decanted and the pellet washed in 300 µL of ice-cold 70% ethanol. The sample was centrifuged at 13,000 rcf for 5 minutes at $4^{O}C$. The pellet was dried, then resuspended in 500-1000 µL ddH_2O.

Isolating RNA, generating cDNA

Tissue samples of 50-75 mg were homogenized in 1 mL Trizol per sample with a OMNI TH_Q tissue homogenizer using hard tissue Omni tip plastic homogenizing probes. The homogenate was incubated at room temperature for 5 minutes, with intermittent shaking to promote tissue lysis. The homogenate was mixed with 200 µL of chloroform. The mixture is centrifuged for 15 minutes at 12,000 rcf, 4°C. The aqueous phase was transferred to a clean Eppendorf tube, to which 500 µL of molecular grade isopropanol was added. The sample was incubated overnight at -80°C to facilitate RNA precipitation. The next day, after thawing of the sample, the RNA was pelleted by centrifuging the sample 10 minutes, 12,000 rcf at $4^{O}C$. The supernatant is discarded, then the pellet washed with 1 mL room temperature 75% molecular grade ethanol. The sample was centrifuged for 5 minutes at 7600 rcf at 4°C and the supernatant discarded. The RNA was dried then resuspended in 50 µL autoclaved ddH_2O.

To generate cDNA, 2 µg of RNA was incubated with 3 µL 50 ng/µL oligo d(T) mRNA primer, and ddH_2O to a total volume of 37.5 µL at 65°C to melt secondary RNA structures. The sample is cooled to room temperature to allow for primer annealing, then 12 µL of 5X AMV buffer, 6 µL 0.1M DTT, 3 µL 10 mM dNTP mixture, and 1.5 µL AMV reverse transcriptase were added. The reaction was incubated at 42°C for 1 hour for extension of cDNA.

MED12 amplification and sequencing

Exon 2 of MED12 was amplified from genomic DNA and cDNA by the following procedure. 30 ng of genomic DNA or 5 µL of cDNA were used as the template for PCR. The reaction contained 5 uL of 10X PCR buffer, 1 uL of dNTP mix (10 mM of each dNTP), 1 uL each of 10 µM forward and reverse primer, 0.4 µL of HotStarTaq DNA Polymerase (Qiagen product 203205), and ddH_2O to a total volume of 50 µL.

The thermocycler protocol was as follows: 15 minutes at 95°C to activate the HotStarTaq polymerase; then 50 cycles of a 30 second denaturing step at 94°C, 30 seconds at 60° to anneal the DNA, and 30 seconds at 72°C for amplicon extension; with a final extension step at 72°C for 10 minutes.

The following primers were used, based on literature published by Makinen et al (138):

gDNA forward: 5'-GCC CTT TCA CCT TGT TCC TT-3'

gDNA reverse: 5'-TGT CCC TAT AAG TCT TCC CAA CC-3'

cDNA forward: 5'-CTT CGG GAT CTT GAG CTA CG -3'

cDNA reverse: 5'-GAT CTT GGC AGG ATT GAA GC-3'

The genomic DNA primers anneal to intronic sequences that flank exon 2, whereas the cDNA primers anneal to a sequence in exon 1 and to the exon2/exon3 border.

Sanger Sequencing

Amplicons were submitted to the UTMB Molecular Genomics for PCR clean up and Sanger sequencing. The PCR clean up was performed with an ExoSAP-IT PCR product clean up

kit to digest unused primers and dNTPs. Sanger sequencing was performed using the forward and reverse primers used in PCR amplification, described above. The resultant sequencing results are assessed for sequence variants.

Immunohistochemistry

Immunohistochemistry was performed as described above. A primary antibody which recognizes vimentin (Life Technologies, #180052) was used at 1:50 dilution of the stock solution and a primary antibody against caldesmon (Dako, clone h-CD) was used at 1:100. A goat anti-mouse secondary antibody was used against vimentin and caldesmon. The linker used was streptavidin horseradish peroxidase or streptavidin alkaline phosphatase, with DAB or VectorBlue used as the chromagen, respectively.

Nitrotyrosine and ACTBL2 IHC and IF staining were performed as described in the previous chapter.

RESULTS

Fibroids are heterozygous for MED12 mutations, while myometrium is homozygous

To determine the MED12 mutation status of leiomyomas, we first analyzed the MED12 allelic content of apparently normal myometrium. In all but one uterus, the myometrium was wildtype by Sanger sequencing analysis of genomic DNA. In patient 7, MED12 exon 2 contained an indel mutation. The indel mutation was also detected in the leiomyomas sequenced from the same patient.

In all other patients, DNA from up to 17 leiomyomas was tested for MED12 exon 2 mutation status. While 13% of the leiomyomas were wildtype at MED12 exon 2, 15% had an indel mutation in intron 1, exon 2, or intron 2. The remaining samples display substitution mutations: 4% in intron 1, 3% at codon 36, 2% at codon 43, and 62% and codon 44. At codon 44, it has been reported that all possible single base substitutions of guanine were observed

(138). We also observed all 6 possible codon 44 guanine single base substitutions in the UTMB cohort, with G>A mutations most frequently observed (Table 4.2, Fig 4.3). Chi-squared analysis of our codon 44 mutations results to those of Makinen et al. (138) indicated that the two populations are similar in codon 44 mutations spectrum $p>0.05$.

Sanger sequencing of leiomyomas indicated that when a mutation was detected, both a MED12 exon 2 mutated allele and a wildtype allele were detectable indicating that the leiomyomas are heterozygous (Fig 4.4). Comparison of the MED12 codon 44 mutation status with fibroid size does not indicate a correlation between mutation status and size (Table 4.3, Fig. 4.5).

Fibroids from the same patient did not have the same MED12 mutation status. The presence of leiomyomas with different MED12 mutations indicates that leiomyomas are not clonal with respect to each other and likely arise from different stem cells.

Multiple aliquots from a single fibroid have the same MED12 mutations

In 62 fibroids (representing 10 of the patients), multiple aliquots of each fibroid were obtained for gDNA purification and Sanger sequencing. Aliquots were obtained from different areas of the leiomyoma whenever possible: If the leiomyoma was large, aliquots were taken from different sections; if daughter projections were observed, aliquots were taken from each daughter; in one leiomyoma, a calcified area was observed and sampled.

Sequencing of MED12 exon 2 indicated the MED12 mutation observed was consistent across all samplings of the same fibroid. This finding supports the theory of intra-leiomyoma clonality.

Fibroids express the mutated MED12 allele

Because MED12 is found on the X chromosome, only one allele of MED12 is expressed in each cell. Others have published that the mutated MED12 allele is expressed in leiomyoma (138). We examined mRNA purified from myometrium and leiomyomas to demonstrate the

MED12 expression pattern of myometrium and leiomyomas from the same patient. We observed that wildtype MED12 is expressed in myometrium, and the mutated MED12 allele is predominantly expressed in leiomyomas (Fig. 4.6). Wildtype MED12 is also observed to be expressed to a lesser extent in leiomyomas. We were vigilant in collected leiomyomas and myometrium separately, but on the microscopic scale cells homozygous for wildtype MED12 may infiltrate leiomyomas.

Fibroids contain multiple cell types

It has been previously reported that smooth muscle cells and fibroblasts can be observed in leiomyomas (145). We assessed sequenced leiomyomas for cellular composition (Fig. 4.7). Vimentin and caldesmon immunoreactivity signifies smooth muscle cells and fibroblasts, respectively. Dual staining of leiomyoma tissue shows that vimentin positive cells and caldesmon positive cells are present. No discernible difference in frequency of vimentin positivity or caldesmon positivity was noted when leiomyomas with different MED12 mutations were stained.

Nitrotyrosine in leiomyomas and surrounding myometrium

Nitrotyrosine content was also assessed in leiomyomas and myometrium obtained from the same patients included in the sequencing studies. Myometrial tissue was positive for nitrotyrosine immunoreactivity, indicating exposure of smooth muscle to peroxynitrite. Staining also shows that leiomyomas are more highly immunoreactive for nitrotyrosine content than is myometrium from the same patient (Fig 4.8), and was more intense regardless of the MED12 mutation present.

Since nitrotyrosine was observed in myometrial tissue, we asked whether ACTBL2 was nitrated in myometrial tissue as it was in endometrial tissue. As observed in endometrial tissue, nitrotyrosine and ACTBL2 colocalize in myometrium and leiomyomas (Fig 4.9)..

DISCUSSION

Spectrum of MED12 mutations

In agreement with published literature, all single nucleotide substitution possibilities were observed at MED12 c.130G and c.131G (codon 44).

The mutations are predicted to result in mutations of glycine to various amino acids. All mutations are predicted to hinder MED12 function by the bulky replacement of glycine. The most common mutation MED12 codon 44 mutations observed in leiomyomas, p.G44S and p.G44D resulting from G>A mutations, were computationally studied for structural perturbation caused by amino acid changes and found to negatively impact binding of MED12 with CYCC (146) by altering the binding interface (139).

Because all possible substitutions were observed, it appears that there is no selective advantage conferred to any substitution over another. The difference in frequency of codon 44 mutation outcome is possibly a result of the preferential binding of oxidized guanine bases for other bases.

Expression of MED12 mutations

Due to the location of MED12 on the X chromosome, only one allele of MED12 is expected to be expressed in any one cell. Both mutated and wildtype MED12 were detected in leiomyomas. Makinen et al. has previously reported that the mutated allele is predominantly expressed in leiomyomas regardless of the MED12 codon 44 substitution (138). The mutated allele was also predominantly expressed when the MED12 mutation occurred at codon 36 or 43 (138). We observed the same phenomenon with codon 43 and 44 substitution mutations. We also tested cDNA from leiomyomas sequenced to have IVS1_8T>A and a c.123_155del33 mutation and observed an equivalent expression phenomenon. Unlike with autosomal genes, mutation of only one MED12 allele is required to mimic loss of heterozygosity. A gain of function MED12 c.131G>A mouse model indicates that the mutation drives uterine leiomyoma formation (147).

Endogenous events that give rise to MED12 mutations are persistent

As was observed with endometrial tissue, $ONOO^-$ damage is detectable in all samples of normal myometrium. Positive nitrotyrosine immunoreactivity was observed in the myometrium collected from fibroid patients and from patients included in the prior discussed endometrial staining experiments. This indicates that myometrial tissue is persistently exposed to $ONOO^-$, putting DNA at risk of accumulating oxidative damage.

In concordance with our discussion of nitrotyrosine in endometrial tissue, the incidence of leiomyoma is higher in African-American women, than in Caucasian women. One contribution factor may be circulating hormone level differences, particularly estrogen (101,148). Estrogen promotes NOS activity and NO generation, contributing to peroxynitrite generation. The difference in biology would indicate that African-American women are at higher risk of fibroid development than Caucasian counterparts. Exposure of DNA to $ONOO^-$ leads to oxidative DNA damage, and G>A/C/T mutations.

Proposed mechanism of MED12 mutagenesis

We proposed that the persistent exposure of myometrial tissue to peroxynitrite induces secondary oxidation products of guanine and promote mutagenesis (Fig. 4.10). 8oxoG has been detected in myometrial cells and detected at higher level in leiomyomas obtained from the same patients (149). 8oxoG is known to mispair with A, and through replication result in a G>T mutation (64,150). Given that myometrial tissue is persistently exposed to $ONOO^-$, 8oxoG can be further oxidized to Gh of Sp, which have been implicated in G>C and to a lesser extent G>T mutations (64,151). The guanine oxidation lesions can also mispair with G, resulting in the G>A mutations.

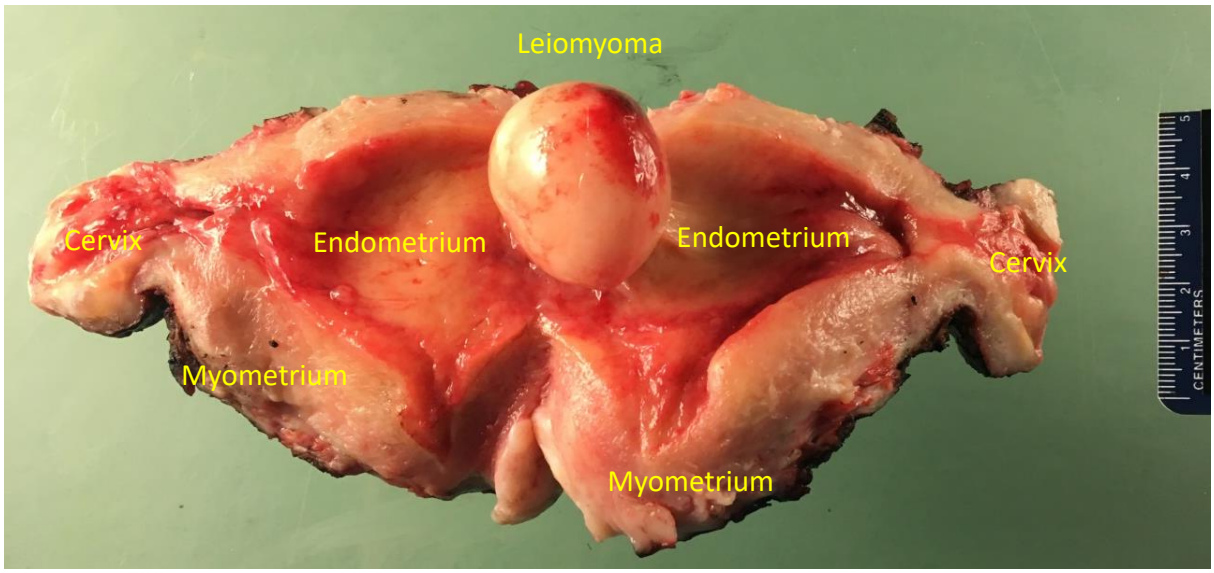

Figure 4.1: Uterine leiomyoma in a uterus.

A uterus has been bivalved to reveal a submucosal leiomyomata. This leiomyoma projects into the endometrial cavity at the fundus of the uterus. Leiomyomas are well-circumscribed, benign tumors that arise from myometrial tissue. Leiomyomas can be submucosal (shown here), intramural, or sub-serosal. Though leiomyomas can be clinically silent, with increasing size they can cause increasing discomfort and pelvic pain.

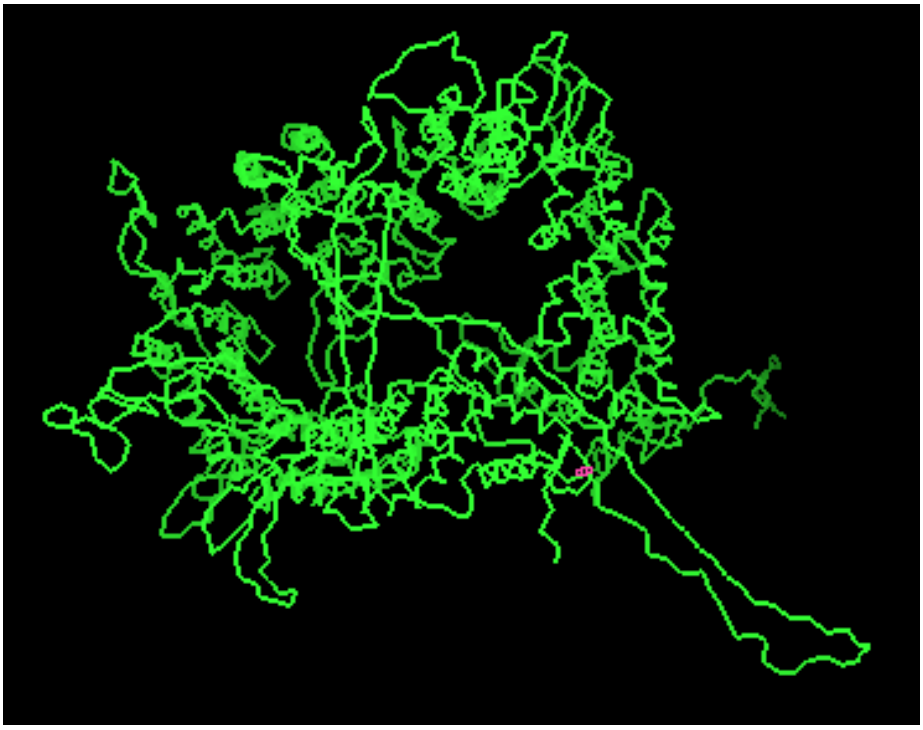

Figure 4.2: Predicted MED12 protein structure.

The MED12 protein structure was predicted by RaptorX (http://raptorx.uchicago.edu) based on the 2177 amino acid sequence of MED12 reported by Uniprot (http://www.uniprot.org/). Gly44 is highlighted in magenta. Gly44 mutation affects MED12 binding to cyclin C and regulation of Mediator.

Table 4.1: Clinical information for patients included in the study.

Leiomyoma tissue was collected from 17 patients that underwent hysterectomy.

Patient #	Age	Ethnicity	Surgical indication	Histopathological findingsrelating to the myometrium
1	53	Hispanic/Latino	Abnormal vaginal bleeding	Adenomyosis and submucosal leiomyoma with focal hemorrhage and infarction
2	49	Hispanic/Latino	Intramural leiomyoma of uterus , menorrhagia	Leiomyomata and adenomyosis
3	50	Asian	Intramural leiomyoma of uterus. Bulky or enlarged uterus.	Cellular leiomyoma
4	47	Black/AA	Intramural leiomyoma of uterus	Leiomyomata with adenomyosis
5	45	Hispanic/Latino	Menorrhagia, mixed incontinence	Intramural and subserosal leiomyomata
6	48	Black/AA	Intramural leiomyoma of uterus, pelvic pain, menorrhagia, iron deficiency anemia due to chronic blood loss	Multiple leiomyomata
7	44	Black/AA	Intramural leiomyoma of uterus	Leiomyomata and adenomyosis
8	45	Black/AA	Submucous leiomyoma of uterus, menorrhagia, iron deficiency anemia due to chronic blood loss	Anterior myometrium with one leyomyoma and posterior myometrium with adenomyosis
9	46	Black/AA	Papanicolaou smear of cervix with low grade squamous intraepithelial lesion, abnormal uterine bleeding , uterine leiomyoma	Leiomyomata
10	47	Black/AA	Not provided	Leiomyomata, adenomyosis
11	48	Hispanic/Latino	Intramural leiomyoma of uterus , abnormal uterine bleeding	Leiomyomata
12	43	Black/AA	Excessive or frequent menstruation, uterine leiomyoma, anemia	Leiomyomata
13	45	White	Uterine leiomyoma	Leiomyomata
14	46	White	Intramural leiomyoma of uterus	Leiomyoma
15	52	Hispanic/Latino	Not provided	Leiomyomata
16	43	Black/AA	Abnormal uterine bleeding	Leiomyomata
17	45	White	Menorrhagia, pelvic pain, polycystic ovary syndrome	Leiomyoma

Table 4.2: Spectrum of MED12 mutations observed in uterine leiomyomas.in the present study, compared with that observed by Makinen et al. (138).

Location	Nucleotide Change	Predicted Protein Change	Nucleotide Change	Count	Percent	Count (Makinen et al.)	Percent (Makinen et al.)
Codon 36	c.107T	p.L36R	CTG->CGG	3	3.30	11	4.89
Codon 43	c.128A	p.Q43P	CAA->CCA	2	2.20	3	1.33
Codon 44	c.130G>C	p.G44R	GGT->CGT	7	7.69	16	7.11
Codon 44	c.130G>A	p.G44S	GGT->AGT	14	15.38	17	7.56
Codon 44	c.130G>T	p.G44C	GGT->TGT	9	9.89	7	3.11
Codon 44	c.131G>C	p.G44A	GGT->GCT	3	3.30	11	4.89
Codon 44	c.131G>A	p.G44D	GGT->GAT	17	18.68	47	20.89
Codon 44	c.131G>T	p.G44V	GGT->GTT	6	6.59	12	5.33
Intronic base substitution	IVS1-8T	p.E33_D34insPQ	T>A	4	4.40	10	4.44
Indel				14	15.38	25	11.11
Wildtype				12	13.19	66	29.33
			Total:	91		225	

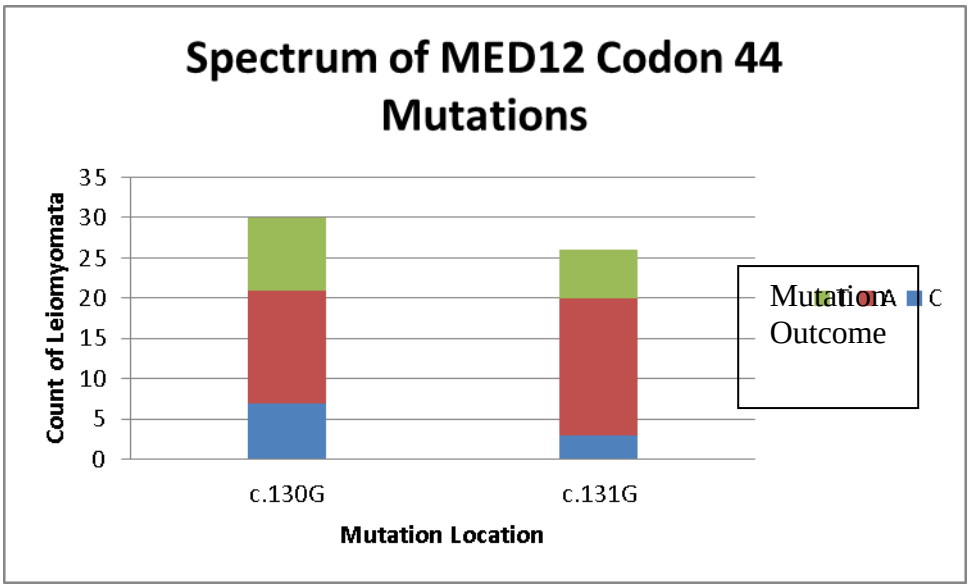

Figure 4.3: Spectrum of MED12 codon 44 mutations observed.

All possible single base substitution mutations were observed at c.130 and c131 of MED12 codon 44. G<A mutations comprise the majority of mutations observed.

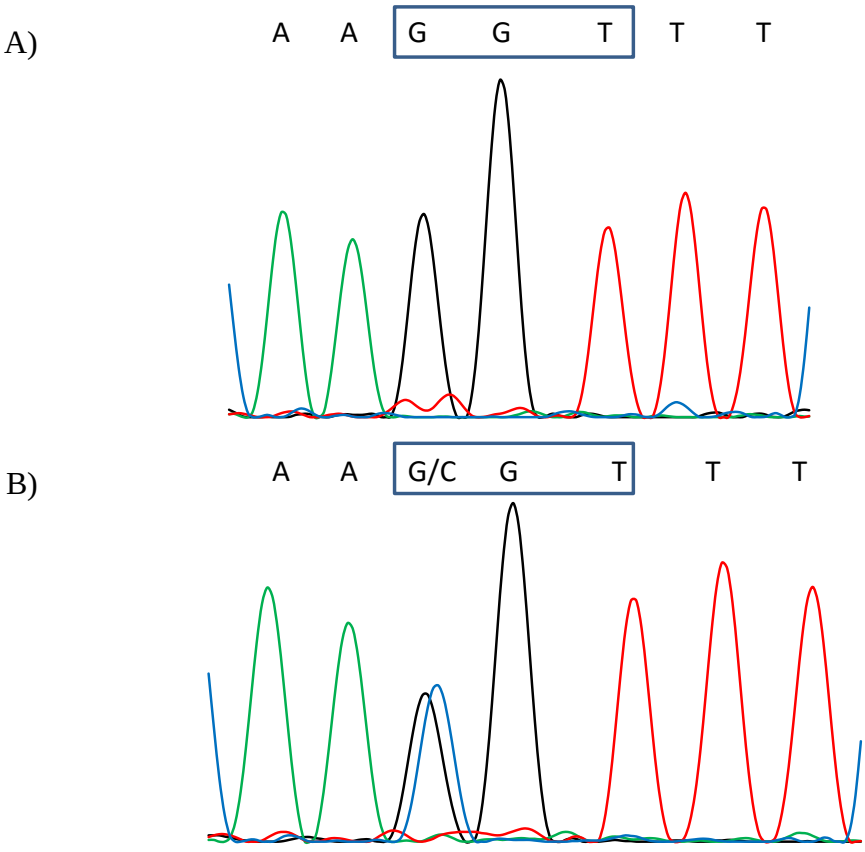

Figure 4.4: MED12 exon 2 is mutated in fibroids.

Fibroids can be heterozygous for MED12 mutation while normal myometrium from the same patient is homozygous wildtype as shown in these DNA sequencing histograms. Sequencing of MED12, exon 2 from the genomic DNA of a patient's tissue reveals that the A) myometrium is wildtype at codon 44 (boxed) while the B) leiomyoma is heterozygous at the same gene location.

Table 4.3: Mutation spectrum and fibroid size.

Fibroids wildtype at MED12 exon 2 were larger than those with a mutation. Of the fibroids mutated at MED12 codon44, there was no difference in average maximal diameter.

Average ± Population Standard Deviation (Range)
Leiomyoma volume was calculated by $V=4/3*\pi*a*b*c$ with a,b,c representing perpendicular diameters of the leiomyoma.

MED12 Sequence status	Predicted Protein	Average Volume (cm^3)	Average max. diameter (cm)
WT	p.G44	1351.2 ± 2353.0 (5.8-7238.2)	5.2 ± 4.1 (1.3-14)
IVS1-8T>A	p.E33_D34insPQ	240.7 ± 300.4 (4.2-748.6)	3.6 ± 2.4 (1.0-7.4)
c.107T>G	p.L36R	465.4 ± 341.1 (6.3-823.3)	5.0 ± 2.5 (1.4-7)
c.128A>C	p.Q43P	31.9 ± 31.0 (0.9-62.8)	1.9 ± 1.2 (0.7-3)
c.130G>C	p.G44R	675.6 ± 1265.3 (9.4-3204.4)	3.7 ± 3.2 (1.5-10)
c.130G>A	p.G44S	169.1 ± 164.7 (3.0-548.9)	3.6 ± 1.9 (1.3-9.1)
c.130G>T	p.G44C	74.0 ± 139.9 (1.2-460.8)	2.3 ± 1.5 (0.7-5.5)
c.131G>C	p.G44A	111.8 ± 111.4 (16.3-268.1)	2.8 ± 0.9 (2.0-4.0)
c.131G>A	p.G44D	60.3 ± 143.8 (0.3-576.0)	1.9 ± 1.4 (0.5-5.5)
c.131G>T	p.G44V	204.0 ± 352.0 (0.9-904.8)	2.7 ± 1.9 (0.7-6)

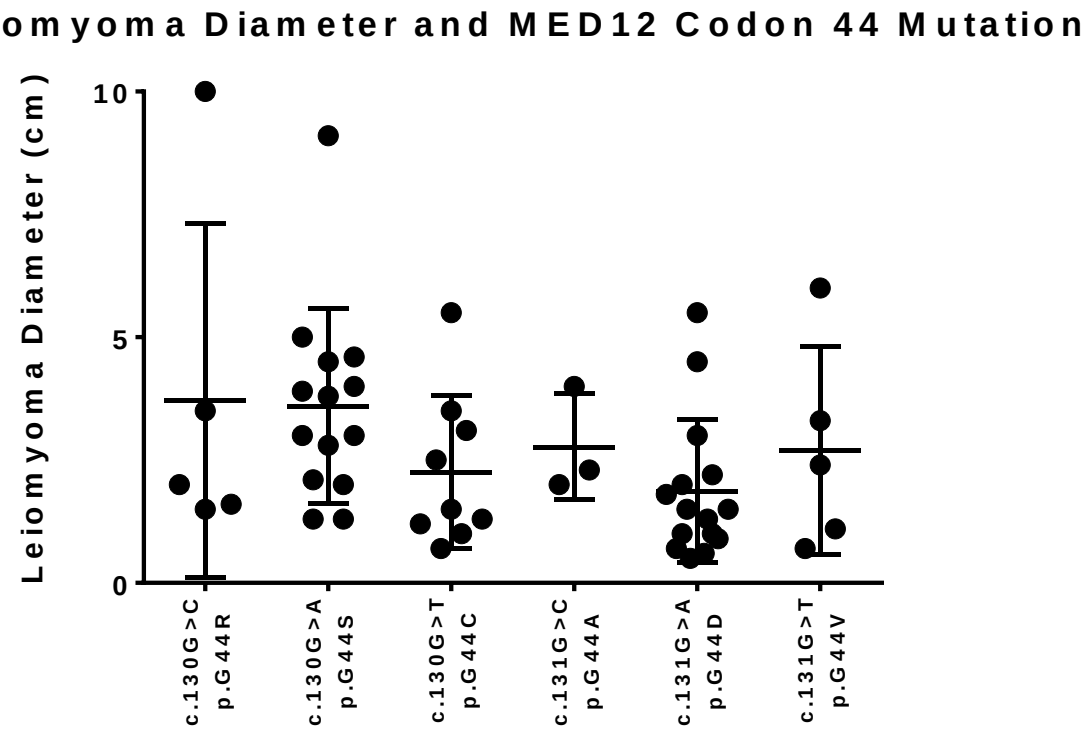

Figure 4.5: Fibroid size does not vary amongst MED12 codon 44 mutated fibroids.

Leiomyoma maximal diameter and MED12 Codon 44 mutation status. The average maximal diameter is similar, regardless of MED12 codon 44 mutation present. Each data point represents the maximal diameter and mutation status of a single fibroid. Bars represent standard deviation.

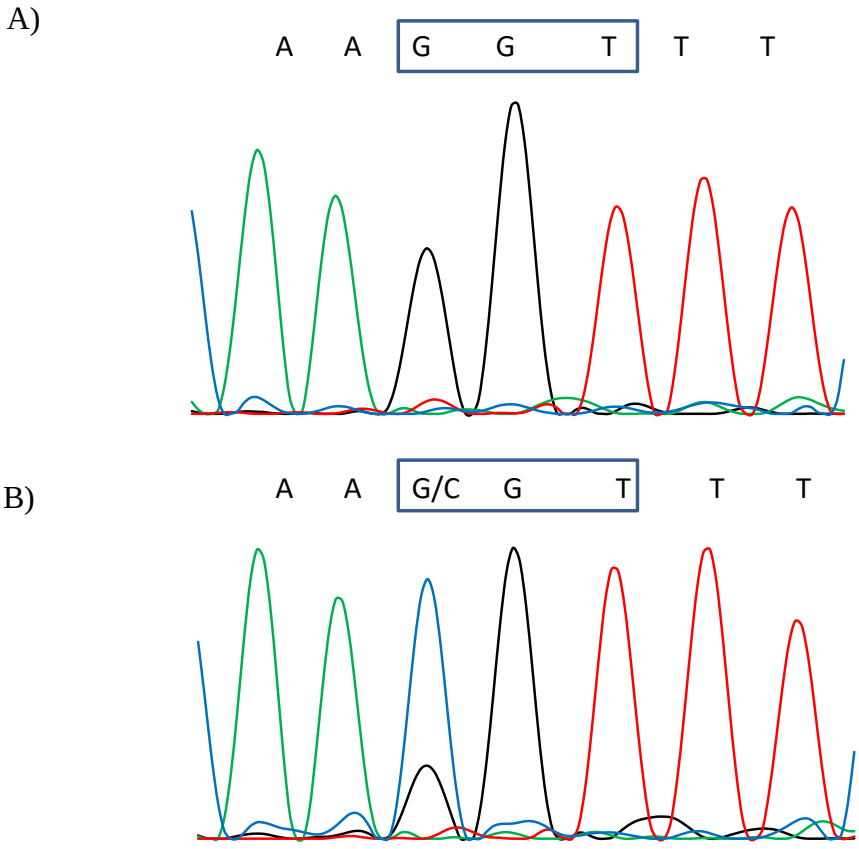

Figure 4.6: The mutated allele is predominantly expressed in fibroids.

The mutated allele of MED12 is expressed in fibroids. Sanger sequencing of cDNA from normal A) myometrium reveals that wild type MED12, codon 44 is expressed while cDNA from B) a leiomyoma from the same patient shows that the mutated allele of MED12 is predominantly expressed.

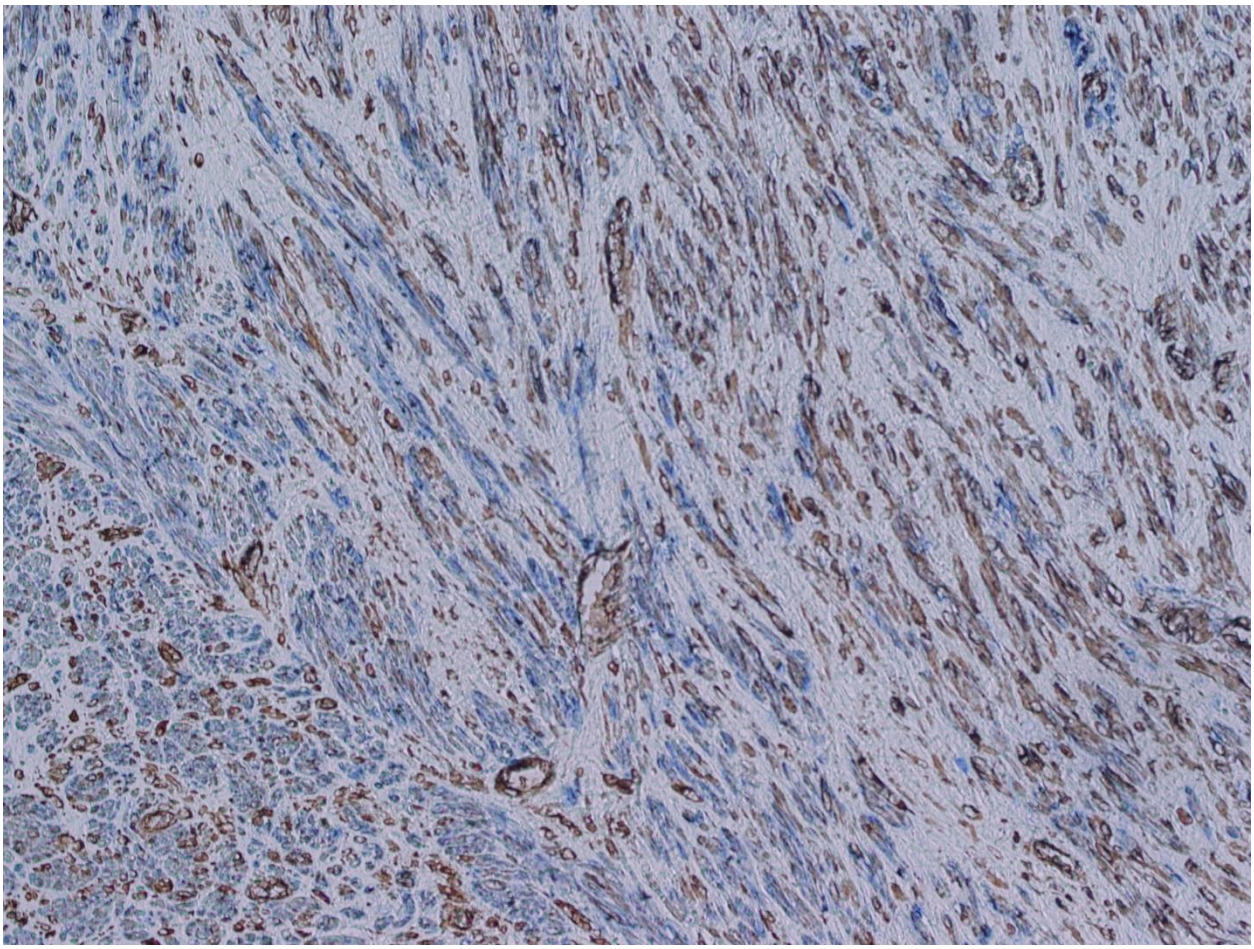

Figure 4.7: Multiple cell types are observed in a fibroid.

A representative section of leiomyoma, immunohistochemically stained for vimentin and caldesmon expression is shown. Brown staining represents vimentin expression (seen in fibroblasts) while blue staining denotes caldesmon expression (observed in smooth muscle cells). Both cell types are observed in leiomyomata.

A)

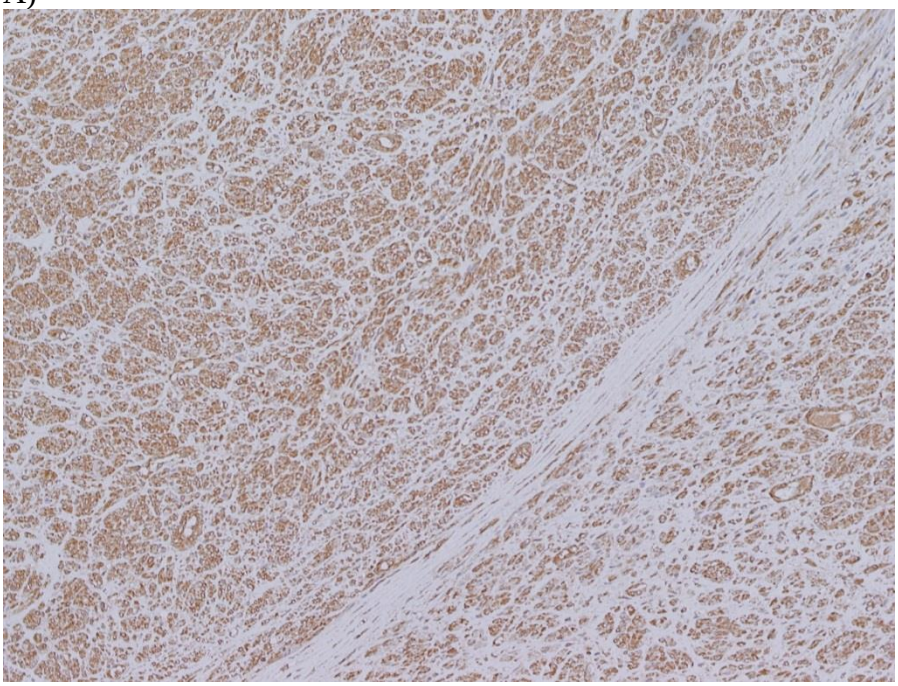

B)

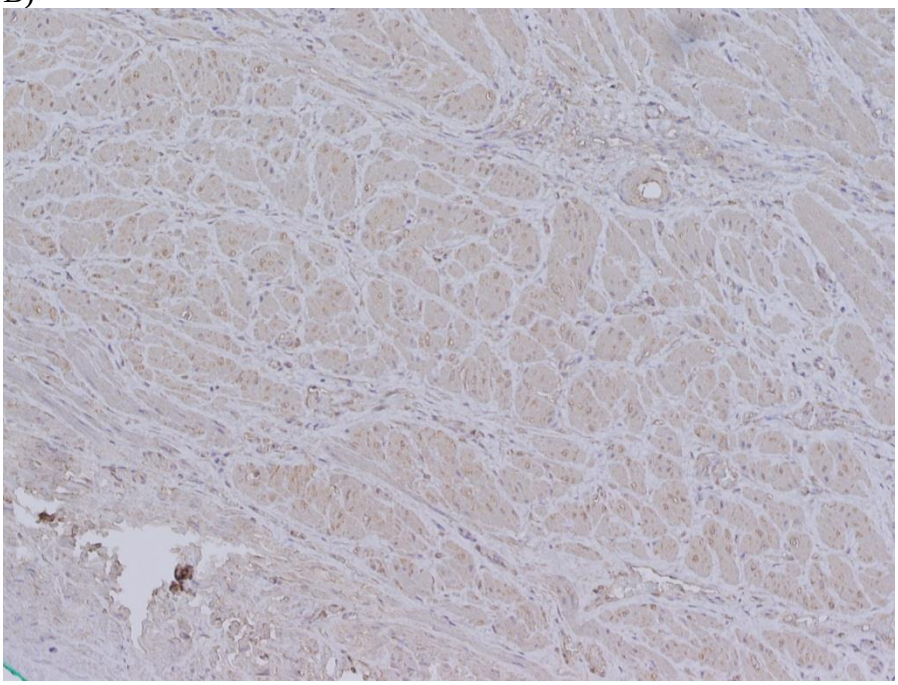

Figure 4.8: Nitrotyrosine intensity is higher in fibroid than surrounding myometrium.

Immunohistochemical staining of a A) leiomyoma and B) myometrium from the same patient reveals that nitrotyrosine staining intensity is greater in the leiomyoma than in the normal myometrium.

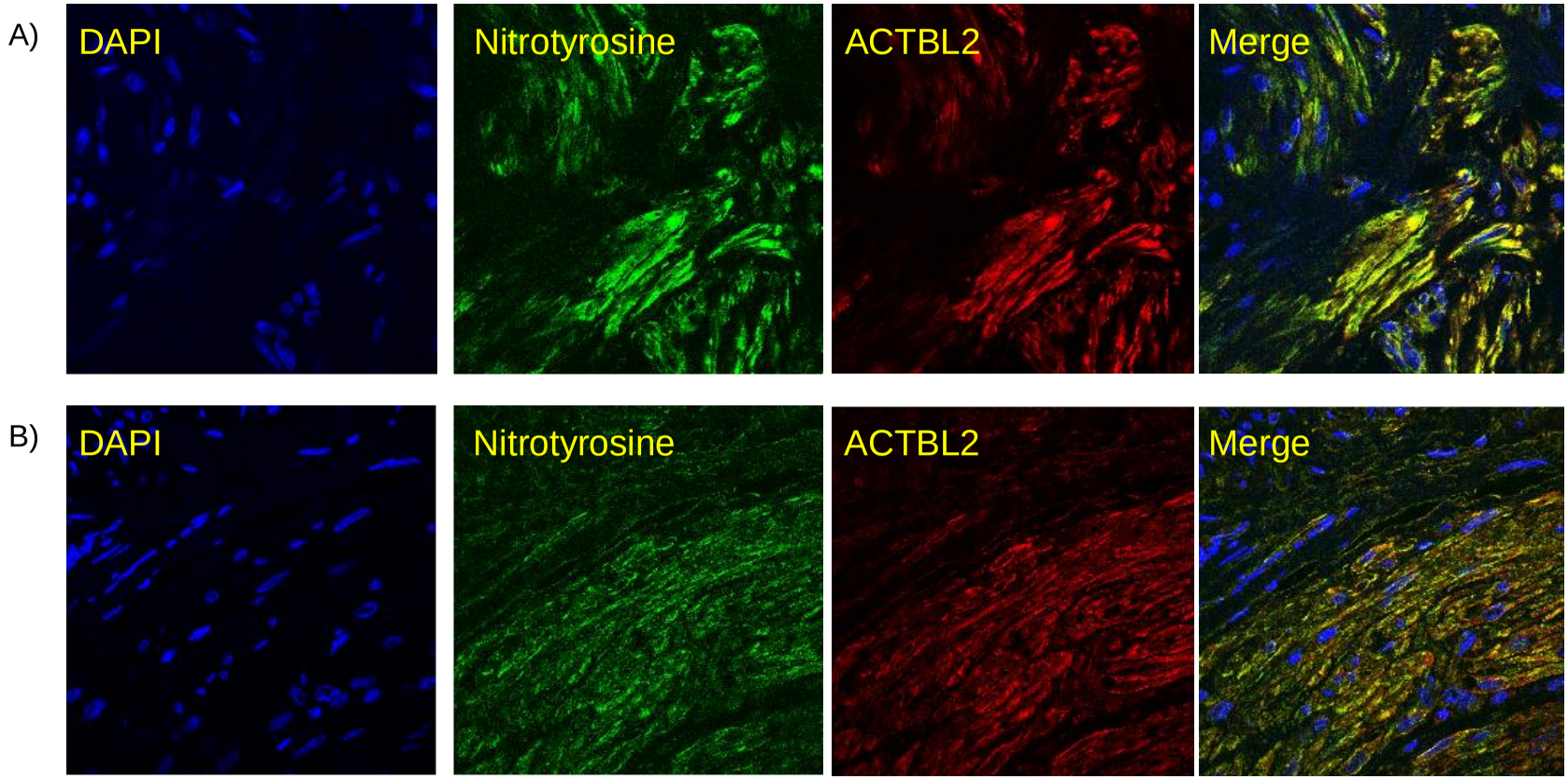

Figure 4.9: Nitrotyrosine and ACTBL2 colocalize in fibroids and in normal myometrium.

Immunostaining of a A) leiomyoma and the B) myometrium of the same patient shows that ACTBL2 (red) and nitrotyrosine (green) predominantly colocalize (yellow).

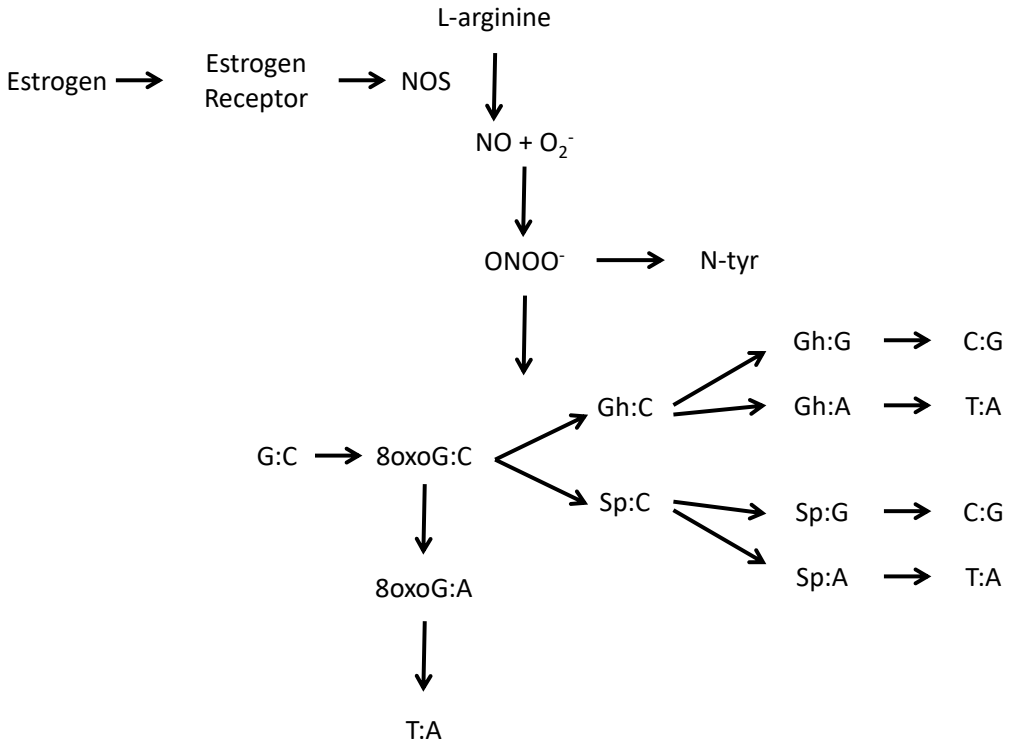

Figure 4.10: Proposed route of mutagenesis in uterine tissue.

Endogenous events that give rise to MED12 mutations are persistent. Estrogen interacts with estrogen receptor to upregulate nitric oxide synthesis expression. Higher estrogen exposure then leads to NO production and $ONOO^-$ exposure. $ONOO^-$ interacts with proteins to nitrate residues and with DNA to form oxidative damage products. Such damage products, guanidinohydantoin (Gh) and spiroiminodihydantoin (Sp), are highly mutagenic and contribute to the mutations observed in gynecologic pathologies.

Chapter 5 Discussion and Future Directions

ENDOMETRIAL CANCER AND LEIOMYOMATA MAY ARISE FROM THE SAME ENDOGENOUS EXPOSURES

Endometrial carcinomas and leiomyomas occur in tissues which are in close proximity. We sought to determine whether $ONOO^-$ exposure might contribute to the mutations observed in both pathologies. We find that both endometrial and myometrial tissues are persistently exposed to peroxynitrite and are at risk of mutagenic insult.

Previous studies have shown that oxidative damage to guanine, detected by 8oxoG presence, occurs in endometrial and myometrial tissue. 8oxoG can be further oxidized to Gh and Sp by exposure to $ONOO^-$. 8oxoG, Gh, and Sp are able to mispair with G and result in G>C mutations, which are observed in both endometrial and myometrial pathology.

We have observed $ONOO^-$ mediated damage in both endometrial and myometrial tissues, adding plausibility to $ONOO^-$ playing a role in uterine mutations. We were further able to identify ACTBL2 as the predominantly nitrated protein in benign endomyometrial tissue.

Mutations observed in pathology are dependent on both the selective advantage conferred by the amino acid change result and the frequency of mutations that occur. The tissue microenvironment can contribute to the spectrum of mutations that form, which may or may not confer a selective protein function advantage. Endometrial and myometrial tissue are persistently exposed to peroxynitrite, putting the DNA of both tissues at risk of forming highly mutagenic secondary guanine oxidation products. NEIL1 excises hydantoin lesions, especially when Gh or SP are opposite a guanine, contributing to G>C mutations rather than preventing them (152).

In endometrial tissues, mutations at the CpG site of PTEN codon 130 result in amino acids changes in the catalytic pocket of the protein. The most frequently observed mutation in endometrial cancer is an arginine to glycine mutation. The PTEN p.R130G mutation results from a cytosine to guanine substitution attributed to $ONOO^-$ mediated damage. PTEN p.R130G allows

mutated PTEN to function in a dominant negative fashion and confers selective advantage over cells with wildtype PTEN or PTEN codon 130 nonsense mutations. In the case of endometrial cancer, it appears that propensity for C>G mutations and the selective advantage conferred by the altered protein function interact to determine the frequency of mutations observed in endometrial cancer.

Myometrial tissue is also exposed to peroxynitrite, promoting the formation of secondary guanine oxidation products. All possible single base substitutions of guanine were observed in our study, confirming that all mutations occur. Single base substitutions at either guanine of MED12 codon 44 substitute bulky amino acids in place of glycine. Though it is unclear whether substitution with one amino acid confers greater selective advantage than any other amino acid at codon 44 of MED12, it is apparent that all possible mutations are deleterious compared to wildtype MED12.

LEIOMYOMATA ARE LIKELY CANDIDATES TO STUDY ENDOMETRIAL CANCER PREVENTION STRATEGIES

As endometrial cancer and leiomyoma associated mutations appear to arise from the same endogenous exposures, one prevention strategy might prevent the occurrence of both pathologies. It might further be possible to use incidence of fibroid formation as a surrogate for studying endometrial cancer formation when assessing prevention strategies.

FUTURE DIRECTIONS

In the future, we intend to extend this exposure study to better understand uterine physiology and development of pathology.

While we have shown that Gh and Sp formation ins uterine tissue is possible, a natural extension of the study would involve demonstrating their presence in benign human uterine issue. Thus far, it has been difficult to quantify Gh and Sp in tissue with reliability. One concern

in the detection of Gh and Sp is the confounding artifactual generation of Gh and Sp by ex vivo oxidation (153).

To a different end, our nitroproteomic study of uterine tissue could be refined to yield more information about the role of protein nitration in uterine tissue. Our analysis was performed on whole tissue lysate, whereas cellular fractionation would aid in understanding of the distribution of nitrated proteins and their role in the membrane, cytoplasm, and nucleus. Deeper coverage may also lead us to identification of additional nitrated proteins. We performed the nanoLC-MSMS analysis on non-enriched samples. Methods for nitrated protein enrichment could be used to obtain deeper coverage of the nitroproteome and lead to identification of addition nitrated proteins.

Deeper coverage of the proteome may identify non-nitrated ACTBL2, contributing to our understanding of the equilibrium and dynamics of ACTBL2 nitration.

We seek to better understand the development of uterine pathology by understanding the benign state of uterine tissue.

References

(1) Burton, G. J., Watson, A. L., Hempstock, J., Skepper, J. N., Jauniaux, E., Cb, C., and Kingdom, U. (2015) Uterine Glands Provide Histiotrophic Nutrition for the Human Fetus during the First Trimester of Pregnancy *87*, 2954–2959.

(2) Noyes, R., Hertig, A., and Rock, J. (1950) Dating the endometrial biopsy. *Fertil. Steril. 1*, 3–25.

(3) Cancer of the Endometrium - SEER Stat Fact Sheets.

(4) Plataniotis, G., and Castiglione, M. (2010) Endometrial cancer: ESMO clinical practice guidelines for diagnosis, treatment and follow-up. *Ann. Oncol. 21*, 41–45.

(5) Nakagawa-Okamura, C., Sato, S., Tsuji, I., Kuramoto, H., Tsubono, Y., Aoki, D., Jobo, T., Oomura, M., Hisamichi, S., and Yajima, A. (2001) Effectiveness of mass screening for endometrial cancer. *Acta Cytol. 46*, 277–83.

(6) Magrina, J. F., and Weaver, A. L. (2004) Laparoscopic treatment of endometrial cancer: Five-year recurrence and survival rates. *Eur. J. Gynaecol. Oncol. 25*, 439–41.

(7) Dubbins, P. a, and Subba, B. (1999) Screening for gynecological malignancy. *Semin. Ultrasound. CT. MR 20*, 231–8.

(8) Jarboe, E. A., and Mutter, G. L. (2010) Endometrial intraepithelial neoplasia. *Semin. Diagn. Pathol. 27*, 215–225.

(9) Bilbao, C., Rodríguez, G., Ramírez, R., Falcón, O., León, L., Chirino, R., Rivero, J. F., Díaz-Chico, B. N., Díaz-Chico, J. C., and Perucho, M. (2006) The relationship between microsatellite instability and PTEN gene mutations in endometrial cancer. *Int. J. Cancer 119*, 563–70.

(10) Sun, H., Enomoto, T., Fujita, M., Wada, H., Yoshino, K., Ozaki, K., Nakamura, T., and Murata, Y. (2001) Mutational analysis of the PTEN gene in endometrial carcinoma and hyperplasia. *Am. J. Clin. Pathol. 115*, 32–8.

(11) McConechy, M. K., Ding, J., Cheang, M. C. U., Wiegand, K. C., Senz, J., Tone, A. a, Yang, W., Prentice, L. M., Tse, K., Zeng, T., McDonald, H., Schmidt, A. P., Mutch, D. G., McAlpine, J. N., Hirst, M., Shah, S. P., Lee, C.-H., Goodfellow, P. J., Gilks, C. B., and Huntsman, D. G. (2012) Use of mutation profiles to refine the classification of endometrial carcinomas. *J. Pathol. 228*, 20–30.

(12) Mutter, G. L., Lin, M.-C. C., Fitzgerald, J. T. J. T., Kum, J. B., Baak, J. P. A., Lees, J. A., Weng, L.-P. P., and Eng, C. (2000) Altered PTEN expression as a diagnostic marker for the earliest endometrial precancers. *J. Natl. Cancer Inst. 92*, 924–931.

(13) Levine, R. L., Cargile, C. B., Blazes, M. S., Cargue, C. B., Rees, B. Van, Kurman, R. J., and Ellenson, L. H. (1998) PTEN Mutations and Microsatellite Instability in Complex Atypical Hyperplasia , a Precursor Lesion to Uterine Endometrioid Carcinoma Advances in Brief PTEN Mutations and Microsatellite Instability in Complex Atypical Hyperplasia , a Precursor Lesion to Ut. *Cancer Res. 58*, 3254–3258.

(14) Mutter, G. L., Monte, N. M., Neuberg, D., Ferenczy, A., and Eng, C. (2014) Emergence, Involution, and Progression to Carcinoma of Mutant Clones in Normal Endometrial Tissues. *Cancer Res.*

(15) Zheng, W., Baker, H. E., and Mutter, G. L. (2004) Involution of PTEN-null endometrial glands with progestin therapy. *Gynecol. Oncol. 92*, 1008–1013.

(16) McConechy, M. K., Ding, J., Senz, J., Yang, W., Melnyk, N., Tone, A. a, Prentice, L. M., Wiegand, K. C., McAlpine, J. N., Shah, S. P., Lee, C.-H., Goodfellow, P. J., Gilks, C. B., and Huntsman, D. G. (2014) Ovarian and endometrial endometrioid carcinomas have distinct CTNNB1 and PTEN mutation profiles. *Mod. Pathol. 27*, 128–34.

(17) Chalhoub, N., and Baker, S. J. (2009) PTEN and the PI3-kinase pathway in cancer. *Annu. Rev. Pathol. 4*, 127–50.

(18) Chen, Z., Dempsey, D. R., Thomas, S. N., Hayward, D., Bolduc, D. M., and Cole, P. A. (2016) Molecular Features of PTEN Regulation by C-Terminal Phosphorylation. *J. Biol. Chem.* jbc.M116.728980.

(19) Lee, J. O., Yang, H., Georgescu, M. M., Di Cristofano, a, Maehama, T., Shi, Y., Dixon, J. E., Pandolfi, P., and Pavletich, N. P. (1999) Crystal structure of the PTEN tumor suppressor: implications for its phosphoinositide phosphatase activity and membrane association. *Cell 99*, 323–34.

(20) Song, M. S., Salmena, L., and Pandolfi, P. P. (2012) The functions and regulation of the PTEN tumour suppressor. *Nat. Rev. Mol. Cell Biol. 13*, 283–96.

(21) Das, S., Dixon, J. E., and Cho, W. (2003) Membrane-binding and activation mechanism of PTEN. *Proc. Natl. Acad. Sci. U. S. A. 100*, 7491–6.

(22) Odriozola, L., Singh, G., Hoang, T., and Chan, A. M. (2007) Regulation of PTEN activity by its carboxyl-terminal autoinhibitory domain. *J. Biol. Chem. 282*, 23306–23315.

(23) Heinrich, F., Chakravarthy, S., Nanda, H., Papa, A., Pandolfi, P. P., Ross, A. H., Harishchandra, R. K., Gericke, A., and Lösche, M. (2015) The PTEN Tumor Suppressor Forms Homodimers in Solution. *Structure 23*, 1952–1957.

(24) Umar, A., Boland, C. R., Terdiman, J. P., Syngal, S., de la Chapelle, A., Rüschoff, J., Fishel, R., Lindor, N. M., Burgart, L. J., Hamelin, R., Hamilton, S. R., Hiatt, R. A., Jass, J., Lindblom, A., Lynch, H. T., Peltomaki, P., Ramsey, S. D., Rodriguez-Bigas, M. A., Vasen, H. F. A., Hawk, E. T., Barrett, J. C., Freedman, A. N., and Srivastava, S. (2004) Revised Bethesda Guidelines for hereditary nonpolyposis colorectal cancer (Lynch syndrome) and microsatellite instability. *J. Natl. Cancer Inst. 96*, 261–8.

(25) Boland, C. R., Koi, M., Chang, D. K., and Carethers, J. M. (2008) The biochemical basis of microsatellite instability and abnormal immunohistochemistry and clinical behavior in Lynch syndrome: from bench to bedside. *Fam. Cancer 7*, 41–52.

(26) Zhou, X.-P., Kuismanen, S., Nystrom-Lahti, M., Peltomaki, P., and Eng, C. (2002) Distinct PTEN mutational spectra in hereditary non-polyposis colon cancer syndrome-related endometrial carcinomas compared to sporadic microsatellite unstable tumors. *Hum. Mol. Genet. 11*, 445–50.

(27) Papa, A., Wan, L., Bonora, M., Salmena, L., Song, M. S., Hobbs, R. M., Lunardi, A., Webster, K., Ng, C., Newton, R. H., Knoblauch, N., Guarnerio, J., Ito, K., Turka, L. a, Beck, A. H., Pinton, P., Bronson, R. T., Wei, W., and Pandolfi, P. P. (2014) Cancer-associated PTEN mutants act in a dominant-negative manner to suppress PTEN protein function. *Cell 157*, 595–610.

(28) Leslie, N. R., and den Hertog, J. (2014) Mutant PTEN in Cancer: Worse Than Nothing. *Cell 157*, 527–529.

(29) Leslie, N. R., Kriplani, N., Hermida, M. A., Alvarez-Garcia, V., and Wise, H. M. (2016) The PTEN protein: cellular localization and post-translational regulation. *Biochem. Soc. Trans. 44*, 273–278.

(30) Amada, K. E. M. Y., Ardo, C. A. C. O., Atoretti, G. I. C., Isher, P. E. E. F., Podsypanina, K., Ellenson, L. H., Nemes, A., Gu, J., Tamura, M., Yamada, K. M., Cordon-Cardo, C., Catoretti, G., Fisher, P. E., Parsons, R., Amada, K. E. M. Y., Ardo, C. A. C. O., Atoretti, G. I. C., Isher, P. E. E. F., Podsypanina, K., Ellenson, L. H., Nemes, A., Gu, J., Tamura, M., Yamada, K. M., Cordon-Cardo, C., Catoretti, G., Fisher, P. E., and Parsons, R. (1999) Mutation of Pten/Mmac1 in mice causes neoplasia in multiple organ systems. *Proc. Natl. Acad. Sci. U. S. A. 96*, 1563–8.

(31) Daikoku, T., Hirota, Y., Tranguch, S., Joshi, A. R., DeMayo, F. J., Lydon, J. P., Ellenson, L. H., and Dey, S. H. K. (2008) Conditional loss of uterine Pten unfailingly and rapidly induces endometrial cancer in mice. *Cancer Res. 68*, 5619–5627.

(32) Cheng, H., Liu, P., Zhang, F., Xu, E., Symonds, L., Ohlson, C. E., Bronson, R. T., Maira, S. M., Tomaso, E. Di, Li, J., Myers, A. P., Cantley, L. C., Mills, G. B., and Zhao, J. J. (2014) A genetic mouse model of invasive endometrial cancer driven by concurrent loss of pten and Lkb1 is highly responsive to mTOR inhibition. *Cancer Res. 74*, 15–23.

(33) Zysman, M. a, Chapman, W. B., and Bapat, B. (2002) Considerations when analyzing the methylation status of PTEN tumor suppressor gene. *Am. J. Pathol. 160*, 795–800.

(34) Dahia, P. L., FitzGerald, M. G., Zhang, X., Marsh, D. J., Zheng, Z., Pietsch, T., von Deimling, A., Haluska, F. G., Haber, D. A., and Eng, C. (1998) A highly conserved processed PTEN pseudogene is located on chromosome band 9p21. *Oncogene 16*, 2403–6.

(35) Cooper, D. N., and Youssoufian, H. (1988) The CpG dinucleotide and human genetic disease. *Hum. Genet. 78*, 151–155.

(36) Tornaletti, S., and Pfeifer, G. P. (1995) Complete and tissue-independent methylation of CpG sites in the p53 gene: implications for mutations in human cancers. *Oncogene 10*, 1493–9.

(37) Pfeifer, G. P. (2000) p53 mutational spectra and the role of methylated CpG sequences. *Mutat. Res. Mol. Mech. Mutagen. 450*, 155–166.

(38) Akhoondi, S., Sun, D., Von Der Lehr, N., Apostolidou, S., Klotz, K., Maljukova, A., Cepeda, D., Fiegl, H., Dofou, D., Marth, C., Mueller-Holzner, E., Corcoran, M., Dagnell, M., Nejad, S. Z., Nayer, B. N., Zali, M. R., Hansson, J., Egyhazi, S., Petersson, F., Sangfelt, P., Nordgren, H., Grander, D., Reed, S. I., Widschwendter, M., Sangfelt, O., and Spruck, C. (2007) FBXW7/hCDC4 is a general tumor suppressor in human cancer. *Cancer Res. 67*, 9006–9012.

(39) Andrews, J. D., Mancini, D. N., Singh, S. M., and Rodenhiser, D. I. (1996) Site and sequence specific DNA methylation in the neurofibromatosis (NF1) gene includes C5839T: the site of the recurrent substitution mutation in exon 31. *Hum. Mol. Genet. 5*, 503–7.

(40) Denissenko, M. F., Chen, J. X., Tang, M. M. -s., and Pfeifer, G. P. (1997) Cytosine methylation determines hot spots of DNA damage in the human P53 gene. *Proc. Natl. Acad. Sci. 94*, 3893–3898.

(41) Feng, Z., Hu, W., Chen, J. X., Pao, A., Li, H., Rom, W., Hung, M.-C., and Tang, M. (2002) Preferential DNA damage and poor repair determine ras gene mutational hotspot in human cancer. *J. Natl. Cancer Inst. 94*, 1527–1536.

(42) Shen, J. C., Rideout, W. M., and Jones, P. a. (1994) The rate of hydrolytic deamination of 5-methylcytosine in double-stranded DNA. *Nucleic Acids Res. 22*, 972–976.

(43) Duncan, B. K., and Miller, J. H. (1980) Mutagenic deamination of cytosine residues in DNA. *Nature 287*, 560–561.

(44) Neddermann, P., and Jiricny, J. (1993) The purification of a mismatch-specific thymine-DNA glycosylase from HeLa cells. *J. Biol. Chem. 268*, 21218–21224.

(45) Bonneau, D., and Longy, M. (2000) Mutations of the human PTEN gene. *Hum. Mutat. 16*, 109–122.

(46) Frommer, M., McDonald, L. E., Millar, D. S., Collis, C. M., Watt, F., Grigg, G. W., Molloy, P. L., and Paul, C. L. (1992) A genomic sequencing protocol that yields a positive display of 5-methylcytosine residues in individual DNA strands. *Proc. Natl. Acad. Sci. U. S. A. 89*, 1827–31.

(47) Ronaghi, M., Karamohamed, S., Pettersson, B., Uhlén, M., and Nyrén, P. (1996) Real-time DNA sequencing using detection of pyrophosphate release. *Anal. Biochem. 242*, 84–89.

(48) Mikeska, T., Candiloro, I. L., and Dobrovic, A. (2010) The implications of heterogeneous DNA methylation for the accurate quantification of methylation. *Epigenomics 2*, 561–573.

(49) Chen, J. X., Zheng, Y., West, M., and Tang, M. (1998) Carcinogens Preferentially Bind at Methylated CpG in the p53 Mutational Hot Spots Carcinogens Preferentially Bind at Methylated CpG in the p53 Mutational Hot Spots1 2070–2075.

(50) Schmutte, C., Yang, A. S., Beart, R. W., Tumors, H. C., and Jones, P. A. (1995) Base Excision Repair of U : G Mismatches at a Mutational Hotspot in the p53 Gene Is More Efficient Than Base Excision Repair of T : G Mismatches in Extracts of Human Colon Tumors Base Excision Repair of U : G Mismatches at a Mutational Hotspot in the p53 3742–3746.

(51) Juedes, M. J., and Wogan, G. N. (1996) Peroxynitrite-induced mutation spectra of pSP189 following replication in bacteria and in human cells. *Mutat. Res. Mol. Mech. Mutagen. 349*, 51–61.

(52) Hailer, M. K., Slade, P. G., Martin, B. D., Rosenquist, T. a., and Sugden, K. D. (2005) Recognition of the oxidized lesions spiroiminodihydantoin and guanidinohydantoin in DNA by the mammalian base excision repair glycosylases NEIL1 and NEIL2. *DNA Repair (Amst). 4*, 41–50.

(53) Hu, C.-W., Cooke, M. S., Tsai, Y.-H., and Chao, M.-R. (2014) 8-Oxo-7,8-dihydroguanine and 8-oxo-7,8-dihydro-2'-deoxyguanosine concentrations in various human body fluids: implications for their measurement and interpretation. *Arch. Toxicol.*

(54) Sheridan, J., Wang, L.-M., Tosetto, M., Sheahan, K., Hyland, J., Fennelly, D., O'Donoghue, D., Mulcahy, H., and O'Sullivan, J. (2009) Nuclear oxidative damage correlates with poor survival in colorectal cancer. *Br. J. Cancer 100*, 381–8.

(55) Ahmed, N. U., Ueda, M., Nikaido, O., Osawa, T., and Ichihashi, M. (1999) High levels of 8-hydroxy-2'-deoxyguanosine appear in normal human epidermis after a single dose of ultraviolet radiation. *Br. J. Dermatol. 140*, 226–31.

(56) Ohtsubo, T., Ohya, Y., Nakamura, Y., Kansui, Y., Furuichi, M., Matsumura, K., Fujii, K., Iida, M., and Nakabeppu, Y. (2007) Accumulation of 8-oxo-deoxyguanosine in cardiovascular tissues with the development of hypertension. *DNA Repair (Amst). 6*, 760–9.

(57) Shimoda, R., Nagashima, M., Sakamoto, M., Yamaguchi, N., Hirohashi, S., Yokota, J., and Kasai, H. (1994) Increased Formation of Oxidative DNA Damage , 8-Hydroxydeoxyguanosine , in Human Livers with Chronic Hepatitis ' ; T : showing that tissue inflammation inthe liver generates oxidative 3171–3173.

(58) Fernando, L., Carvalho, P., Abrão, M. S., Biscotti, C., Sharma, R., Nutter, B., Carvalho, L. F. P., Abrão, M. S., Biscotti, C., Sharma, R., Nutter, B., and Falcone, T. (2013) Oxidative cell injury as a predictor of endometriosis progression. *Reprod. Sci. 20*, 688–98.

(59) Postawski, K., Przadka-Rabaniuk, D., Piersiak, T., Krzysztof, P., Dorata, P.-R., Tomasz, P., Postawski, K., Przadka-Rabaniuk, D., and Piersiak, T. (2013) 8-oxo-7,8-dihydroguanine level - the DNA oxidative stress marker - recognized by fluorescence image analysis in sporadic uterine adenocarcinomas in women. *Ginekol. Pol. 84*, 44–50.

(60) de Carvalho, L. F. P., Abrão, M. S., Biscotti, C., Sharma, R., Agarwal, A., and Falcone, T. (2013) Mapping histological levels of 8-hydroxy-2'-deoxyguanosine in female reproductive organs. *J. Mol. Histol. 44*, 111–6.

(61) Henderson, P. T., Delaney, J. C., Gu, F., Tannenbaum, S. R., and Essigmann, J. M. (2002) Oxidation of 7 , 8-Dihydro-8-oxoguanine Affords Lesions That Are Potent Sources of Replication Errors in Vivo † 914–921.

(62) Cui, L., Ye, W., Prestwich, E. G., Wishnok, J. S., Taghizadeh, K., Dedon, P. C., and Tannenbaum, S. R. (2013) Comparative analysis of four oxidized guanine lesions from reactions of DNA with peroxynitrite, singlet oxygen, and γ-radiation. *Chem. Res. Toxicol. 26*, 195–202.

(63) Niles, J. C., Wishnok, J. S., and Tannenbaum, S. R. (2004) Spiroiminodihydantoin and Guanidinohydantoin Are the Dominant Products of 8-Oxoguanosine Oxidation at Low Fluxes of Peroxynitrite : Mechanistic Studies with 18 O 1510–1519.

(64) Henderson, P. T., Delaney, J. C., Muller, J. G., Neeley, W. L., Tannenbaum, S. R., Burrows, C. J., and Essigmann, J. M. (2003) The hydantoin lesions formed from oxidation of 7,8-dihydro-8-oxoguanine are potent sources of replication errors in vivo. *Biochemistry 42*, 9257–9262.

(65) Shukla, P. K., and Mishra, P. C. (2013) Base pairing patterns of DNA base lesion spiroiminodihydantoin: A DFT study. *Int. J. Quantum Chem. 113*, 2600–2604.

(66) Fleming, A. M., Muller, J. G., Dlouhy, A. C., and Burrows, C. J. (2012) Structural Context Effects in the Oxidation of 8-Oxo-7,8-dihydro-2′-deoxyguanosine to Hydantoin Products: Electrostatics, Base Stacking, and Base Pairing. *J. Am. Chem. Soc. 134*, 15091–15102.

(67) Steenken, S., and Jovanovic, S. V. (1997) How Easily Oxidizable Is DNA? One-Electron Reduction Potentials of Adenosine and Guanosine Radicals in Aqueous Solution. *J. Am. Chem. Soc. 119*, 617–618.

(68) Kawai, K., Wata, Y., Hara, M., Tojo, S., and Majima, T. (2002) Regulation of One-Electron Oxidation Rate of Guanine by Base Pairing with Cytosine Derivatives. *J. Am. Chem. Soc. 124*, 3586–3590.

(69) Ming, X., Matter, B., Song, M., Veliath, E., Shanley, R., Jones, R., and Tretyakova, N. (2014) Mapping Structurally Defined Guanine Oxidation Products along DNA Duplexes: Influence of Local Sequence Context and Endogenous Cytosine Methylation. *J. Am. Chem. Soc.*

(70) Salamonsen, L. A., and Woolley, D. E. (1999) Menstruation: induction by matrix metalloproteinases and inflammatory cells. *J. Reprod. Immunol. 44*, 1–27.

(71) Ignarro, L. J. (2002) Nitric oxide as a unique signaling molecule in the vascular system: a historical overview. *J. Physiol. Pharmacol. 53*, 503–14.

(72) Mellion, B. T., Ignarro, L. J., Ohlstein, E. H., Pontecorvo, E. G., Hyman, A. L., and Kadowitz, P. J. (1981) Evidence for the inhibitory role of guanosine 3', 5'-monophosphate in ADP-induced human platelet aggregation in the presence of nitric oxide and related vasodilators. *Blood 57*, 946–55.

(73) Liaudet, L., Soriano, F. G., and Szabó, C. (2000) Biology of nitric oxide signaling. *Crit. Care Med. 28*, N37–52.

(74) Telfer, J. F., Irvine, G. a, Kohnen, G., Campbell, S., and Cameron, I. T. (1997) Expression of endothelial and inducible nitric oxide synthase in non-pregnant and decidualized human endometrium. *Mol. Hum. Reprod. 3*, 69–75.

(75) Johnson, M. (2004) Differential in vitro actions of nitric oxide on human endometrial cell survival. *Fertil. Steril. 81*, 176–184.

(76) Schaffer, M. R., Tantry, U., Gross, S. S., Wasserburg, H. L., and Barbul, a. (1996) Nitric oxide regulates wound healing. *J. Surg. Res. 63*, 237–40.

(77) Li, H. Y., Chang, S. P., Yuan, C. C., Chao, H. T., Ng, H. T., and Sung, Y. J. (2001) Nitric oxide induces extensive apoptosis in endometrial epithelial cells in the presence of progesterone: involvement of mitogen-activated protein kinase pathways. *Mol. Hum. Reprod. 7*, 755–63.

(78) Roberto da Costa, R. P., Ferreira-Dias, G., Mateus, L., Korzekwa, a, Andronowska, a, Platek, R., and Skarzynski, D. J. (2007) Endometrial nitric oxide production and nitric oxide synthases in the equine endometrium: Relationship with microvascular density during the estrous cycle. *Domest. Anim. Endocrinol. 32*, 287–302.

(79) Mier-Cabrera, J., González-Gallardo, S., and Hernández-Guerrero, C. (2013) Effect of nitric oxide and TH1/TH2 cytokine supplementation over ectopic endometrial tissue growth in a murine model of endometriosis. *Reprod. Sci. 20*, 1332–8.

(80) Wang, J., Zhou, F., Dong, M., Wu, R., and Qian, Y. (2006) Prolonged gonadotropin-releasing hormone agonist therapy reduced expression of nitric oxide synthase in the endometrium of women with endometriosis and infertility. *Fertil. Steril. 85*, 1037–44.

(81) Tschugguel, W., Schneeberger, C., Unfried, G., Bräutigam, G., Stonek, F., Wieser, F., Vytiska-Binstorfer, E., Czerwenka, K., Weninger, W., Kaider, a, Bursch, W., Breitschopf, H., and Huber, J. C. (1999) Elevation of inducible nitric oxide synthase activity in human endometrium during menstruation. *Biol. Reprod. 60*, 297–304.

(82) Tschugguel, W., Schneeberger, C., Unfried, G., Czerwenka, K., Weninger, W., Mildner, M., Bishop, J. R., and Huber, J. C. (1998) Induction of inducible nitric oxide synthase expression in human secretory endometrium. *Hum. Reprod. 13*, 436–44.

(83) Kamada, Y., Nakatsuka, M., Asagiri, K., Noguchi, S., Habara, T., Takata, M., and Kudo, T. (2000) GnRH agonist-suppressed expression of nitric oxide synthases and generation of peroxynitrite in adenomyosis. *Hum. Reprod. 15*, 2512–9.

(84) Huang, J., Roby, K. F., Pace, J. L., Russell, S. W., and Hunt, J. S. (1995) Cellular localization and hormonal regulation of inducible nitric oxide synthase in cycling mouse uterus. *J. Leukoc. Biol. 57*, 27–35.

(85) Goto, T., Haruma, K., Kitadai, Y., Ito, M., Yoshihara, M., Sumii, K., Hayakawa, N., and Kajiyama, G. (1999) Enhanced expression of inducible nitric oxide synthase and nitrotyrosine in gastric mucosa of gastric cancer patients. *Clin. Cancer Res. 5*, 1411–1415.

(86) Hickey, M., Krikun, G., Kodaman, P., Schatz, F., Carati, C., and Lockwood, C. J. (2006) Long-term progestin-only contraceptives result in reduced endometrial blood flow and oxidative stress. *J. Clin. Endocrinol. Metab. 91*, 3633–8.

(87) Li, Z., Min, W., Huang, C., Bai, S., Tang, M., and Zhao, X. (2010) Proteomics-based approach identified differentially expressed proteins with potential roles in endometrial carcinoma. *Int. J. Gynecol. Cancer 20*, 9–15.

(88) Domínguez, F., Garrido-Gómez, T., López, J. A., Camafeita, E., Quiñonero, A., Pellicer, A., and Simón, C. (2009) Proteomic analysis of the human receptive versus non-receptive endometrium using differential in-gel electrophoresis and MALDI-MS unveils stathmin 1 and annexin A2 as differentially regulated. *Hum. Reprod. 24*, 2607–2617.

(89) Nesvizhskii, A. I., Keller, A., Kolker, E., and Aebersold, R. (2003) A Statistical Model for Identifying Proteins by Tandem Mass Spectrometry abilities that proteins are present in a sample on the basis. *Anal. Chem. 75*, 4646–4658.

(90) Delaney, S., Delaney, J. C., and Essigmann, J. M. (2007) Chemical–Biological Fingerprinting: Probing the Properties of DNA Lesions Formed by Peroxynitrite. *Chem. Res. Toxicol. 20*, 1718–1729.

(91) Viera, L., Ye, Y., Estévez, A., and Beckman, J. (1999) Immunohistochemical methods to detect nitrotyrosine. *Methods Enzymol. 301*, 373–381.

(92) Giretti, M. S., and Simoncini, T. (2008) Rapid regulatory actions of sex steroids on cell movement through the actin cytoskeleton. *Steroids 73*, 895–900.

(93) Aslan, M. (2012) Functional consequences of actin nitration: in vitro and in disease states. *Amino Acids 42*, 65–74.

(94) Souza, J. M., Choi, I., Chen, Q., Weisse, M., Daikhin, E., Yudkoff, M., Obin, M., Ara, J., Horwitz, J., and Ischiropoulos, H. (2000) Proteolytic degradation of tyrosine nitrated proteins. *Arch. Biochem. Biophys. 380*, 360–6.

(95) Ota, H., Igarashi, S., Sato, N., Tanaka, H., and Tanaka, T. (2002) Involvement of catalase in the endometrium of patients with endometriosis and adenomyosis. *Fertil. Steril. 78*, 804–9.

(96) Ota, H., Igarashi, S., Hatazawa, J., and Tanaka, T. (1999) Immunohistochemical assessment of superoxide dismutase expression in the endometrium in endometriosis and adenomyosis. *Fertil. Steril. 72*, 129–34.

(97) Sugino, N., Shimamura, K., Takiguchi, S., Ono, M., Nakata, M., Nakamura, Y., Uda, T., Kato, H., Tamura, H., Ono, M., Nakata, M., Nakamura, Y., Ogino, K., Uda, T., Kato, H., Reynolds, A. D., Stone, D. K., Mosley, R. L., Gendelman, H. E., Sugino, N., Shimamura, K., Takiguchi, S., Ono, M., Nakata, M., Nakamura, Y., Uda, T., Kato, H., Tamura, H., Ono, M., Nakata, M., Nakamura, Y., Ogino, K., Uda, T., and Kato, H. (1996) Changes in activity of superoxide dismutase in the human endometrium throughout the menstrual cycle and in early pregnancy. *Hum Reprod 11*, 1073–1078.

(98) Madison, T., Schottenfeld, D., James, S. a., Schwartz, A. G., and Gruber, S. B. (2004) Endometrial Cancer: Socioeconomic Status and Racial/Ethnic Differences in Stage at Diagnosis, Treatment, and Survival. *Am. J. Public Health 94*, 2104–2111.

(99) Cronjé, H. S., Fourie, S., Doman, M. J., Helms, J. B., Nel, J. T., and Goedhals, L. (1992) Racial differences in patients with adenocarcinoma of the endometrium. *Int. J. Gynaecol. Obstet. 39*, 213–218.

(100) Sherman, M. E., and Devesa, S. S. (2003) Analysis of racial differences in incidence, survival, and mortality for malignant tumors of the uterine corpus. *Cancer 98*, 176–86.

(101) Woods, M. N., Barnett, J. B., Spiegelman, D., Trail, N., Hertzmark, E., Longcope, C., and Gorbach, S. L. (1996) Hormone levels during dietary changes in premenopausal African-American women. *J. Natl. Cancer Inst. 88*, 1369–74.

(102) Han, G., Magee, T., and Khorram, O. (2005) Regulation of nitric oxide synthase isoforms by estrogen in the human endometrium. *Fertil. Steril. 84*, 1220–1227.

(103) Bersinger, N. A., Wunder, D. M., Birkhäuser, M. H., and Mueller, M. D. (2008) Gene expression in cultured endometrium from women with different outcomes following IVF. *Mol. Hum. Reprod. 14*, 475–484.

(104) Hood, B. L., Liu, B., Alkhas, a., Shoji, Y., Challa, R., Wang, G., Ferguson, S., Oliver, J., Mitchell, D., Bateman, N. W., Zahn, C. M., Hamilton, C. a., Payson, M., Lessey, B., Fazleabas, a. T., Maxwell, G. L., Conrads, T. P., and Risinger, J. I. (2015) Proteomics of the Human Endometrial Glandular Epithelium and Stroma from the Proliferative and Secretory Phases of the Menstrual Cycle. *Biol. Reprod. 92*, 106–106.

(105) DeSouza, L., Diehl, G., Yang, E. C. C., Guo, J., Rodrigues, M. J., Romaschin, A. D., Colgan, T. J., and Siu, K. W. M. (2005) Proteomic analysis of the proliferative and secretory phases of the human endometrium: Protein identification and differential protein expression. *Proteomics 5*, 270–281.

(106) Fowler, P. A., Tattum, J., Bhattacharya, S., Klonisch, T., Hombach-Klonisch, S., Gazvani, R., Lea, R. G., Miller, I., Simpson, W. G., and Cash, P. (2007) An investigation of the effects of endometriosis on the proteome of human eutopic endometrium: A heterogeneous tissue with a complex disease. *Proteomics 7*, 130–142.

(107) Rai, P., Kota, V., Sundaram, C. S., Deendayal, M., and Shivaji, S. (2010) Proteome of human endometrium: Identification of differentially expressed proteins in proliferative and secretory phase endometrium. *Proteomics - Clin. Appl. 4*, 48–59.

(108) Chang, K.-W., Yang, P.-Y., Lai, H.-Y., Yeh, T.-S., Chen, T.-C., and Yeh, C.-T. (2006) Identification of a novel actin isoform in hepatocellular carcinoma. *Hepatol. Res. 36*, 33–9.

(109) Kabsch, W., and Vandekerckhove, J. (1992) Structure and function of actin. *Annu. Rev. Biophys. Biomol. Struct. 21*, 49–76.

(110) Pantaloni, D., Le Clainche, C., and Carlier, M. F. (2001) Mechanism of actin-based motility. *Science 292*, 1502–6.

(111) Pollard, T. D., Borisy, G. G., and Haven, N. (2003) Cellular Motility Driven by Assemblyand Disassembly of Actin Filaments *112*, 453–465.

(112) Suarez-Huerta, N., Mosselmans, R., Dumont, J. E., and Robaye, B. (2000) Actin depolymerization and polymerization are required during apoptosis in endothelial cells. *J. Cell. Physiol. 184*, 239–245.

(113) Levee, M. G., Dabrowska, M. I., Lelli, J. L., and Hinshaw, D. B. (1996) Actin polymerization and depolymerization during apoptosis in HL-60 cells. *Am. J. Physiol. 271*, C1981–92.

(114) Dominguez, R., and Holmes, K. C. (2011) Actin Structure and Function. *Annu. Rev. Biophys. 40*, 169–186.

(115) Clements, M. K., Siemsen, D. W., Swain, S. D., Hanson, A. J., Nelson-Overton, L. K., Rohn, T. T., and Quinn, M. T. (2003) Inhibition of actin polymerization by peroxynitrite modulates neutrophil functional responses. *J. Leukoc. Biol. 73*, 344–55.

(116) Aslan, M., Ryan, T. M., Townes, T. M., Coward, L., Kirk, M. C., Barnes, S., Alexander, C. B., Rosenfeld, S. S., and Freeman, B. A. (2003) Nitric oxide-dependent generation of reactive species in sickle cell disease: Actin tyrosine nitration induces defective cytoskeletal polymerization. *J. Biol. Chem. 278*, 4194–4204.

(117) Maneen, M. J., and Cipolla, M. J. (2007) Peroxynitrite diminishes myogenic tone in cerebral arteries: role of nitrotyrosine and F-actin. *Am. J. Physiol. Heart Circ. Physiol. 292*, H1042–H1050.

(118) Tajima, M., Harada, T., Ishikawa, T., Iwahara, Y., and Kubota, T. (2012) Augmentation of Arginase Ⅱ Expression in the Human Endometrial Epithelium in the Secretory Phase. *J. Med. Dent. Sci. 59*, 75–82.

(119) Roberto da Costa, R. P., Costa, A. S., Korzekwa, A. J., Platek, R., Siemieniuch, M., Galvão, A., Redmer, D. a, Silva, J. R., Skarzynski, D. J., and Ferreira-Dias, G. (2008) Actions of a nitric oxide donor on prostaglandin production and angiogenic activity in the equine endometrium. *Reprod. Fertil. Dev. 20*, 674–83.

(120) Prat, F., Houk, K. N., and Foote, C. S. (1998) Effect of guanine stacking on the oxidation of 8-oxoguanine in B-DNA. *J. Am. Chem. Soc. 120*, 845–846.

(121) Viera, L., Radmilovich, M., Vargas, M. R., Dennys, C. N., Wilson, L., Barnes, S., Franco, M. C., Beckman, J. S., Est??vez, A. G., Estévez, A. G., and Est??vez, A. G. (2013) Temporal patterns of tyrosine nitration in embryo heart development. *Free Radic. Biol. Med. 55*, 101–108.

(122) Peinado, M. Á., Hernández, R., Peragón, J., Ovelleiro, D., Pedrosa, J. Á., and Blanco, S. (2014) Proteomic characterization of nitrated cell targets after hypobaric hypoxia and reoxygenation in rat brain. *J. Proteomics 109*, 309–321.

(123) Kanski, J., Hong, S. J., and Schöneich, C. (2005) Proteomic analysis of protein nitration in aging skeletal muscle and identification of nitrotyrosine-containing sequences in vivo by nanoelectrospray ionization tandem mass spectrometry. *J. Biol. Chem. 280*, 24261–24266.

(124) Casoni, F., Basso, M., Massignan, T., Gianazza, E., Cheroni, C., Salmona, M., Bendotti, C., and Bonetto, V. (2005) Protein Nitration in a Mouse Model of Familial Amyotrophic Lateral Sclerosis: POSSIBLE MULTIFUNCTIONAL ROLE IN THE PATHOGENESIS. *J. Biol. Chem. 280*, 16295–16304.

(125) Aslan, M., Ryan, T. M., Townes, T. M., Coward, L., Kirk, M. C., Barnes, S., Alexander, C. B., Rosenfeld, S. S., and Freeman, B. A. (2003) Nitric Oxide-dependent Generation of Reactive Species in Sickle Cell Disease *278*, 4194–4204.

(126) Walker, C. L., and Stewart, E. a. (2005) Uterine fibroids: the elephant in the room. *Science 308*, 1589–92.

(127) Marshall, L. M., Spiegelman, D., Barbieri, R. L., Goldman, M. B., Manson, J. E., Colditz, G. A., Willett, W. C., and Hunter, D. J. (1997) Variation in the incidence of uterine leiomyoma among premenopausal women by age and race. *Obstet. Gynecol. 90*, 967–73.

(128) Vilos, G. A., Allaire, C., Laberge, P., Leyland, N., Vilos, A. G., Murji, A., and Chen, I. (2015) The Management of Uterine Leiomyomas. *Soc. Obstet. Gynaecol. Canada 37*, 157–178.

(129) Stewart, E. A., and Nowak, R. A. (1996) Leiomyoma-related bleeding: a classic hypothesis updated for the molecular era. *Hum. Reprod. Update 2*, 295–306.

(130) Kjerulff, K. H., Langenberg, P., Seidman, J. D., Stolley, P. D., and Guzinski, G. M. (1996) Uterine leiomyomas. Racial differences in severity, symptoms and age at diagnosis. *J. Reprod. Med. 41*, 483–90.

(131) Alam, N. a, Rowan, a J., Wortham, N. C., Pollard, P. J., Mitchell, M., Tyrer, J. P., Barclay, E., Calonje, E., Manek, S., Adams, S. J., Bowers, P. W., Burrows, N. P., Charles-Holmes, R., Cook, L. J., Daly, B. M., Ford, G. P., Fuller, L. C., Hadfield-Jones, S. E., Hardwick, N., Highet, a S., Keefe, M., MacDonald-Hull, S. P., Potts, E. D. a, Crone, M., Wilkinson, S., Camacho-Martinez, F., Jablonska, S., Ratnavel, R., MacDonald, a, Mann, R. J., Grice, K., Guillet, G., Lewis-Jones, M. S., McGrath, H., Seukeran, D. C., Morrison, P. J., Fleming, S., Rahman, S., Kelsell, D., Leigh, I., Olpin, S., and Tomlinson, I. P. M. (2003) Genetic and functional analyses of FH mutations in multiple cutaneous and uterine

leiomyomatosis, hereditary leiomyomatosis and renal cancer, and fumarate hydratase deficiency. *Hum. Mol. Genet. 12*, 1241–52.

(132) Lehtonen, R., Kiuru, M., Vanharanta, S., Sjöberg, J., Aaltonen, L.-M., Aittomäki, K., Arola, J., Butzow, R., Eng, C., Husgafvel-Pursiainen, K., Isola, J., Järvinen, H., Koivisto, P., Mecklin, J.-P., Peltomäki, P., Salovaara, R., Wasenius, V.-M., Karhu, A., Launonen, V., Nupponen, N. N., and Aaltonen, L. A. (2004) Biallelic inactivation of fumarate hydratase (FH) occurs in nonsyndromic uterine leiomyomas but is rare in other tumors. *Am. J. Pathol. 164*, 17–22.

(133) Pollard, P., Wortham, N., and Tomlinson, I. (2003) The TCA cycle and tumorigenesis: the examples of fumarate hydratase and succinate dehydrogenase. *Ann. Med. 35*, 634–635.

(134) Hodge, J. C., Cuenco, K. T., Huyck, K. L., Somasundaram, P., Panhuysen, C. I. M., Stewart, E. A., and Morton, C. C. (2009) Uterine leiomyomata and decreased height: A common HMGA2 predisposition allele. *Hum. Genet. 125*, 257–263.

(135) Medeiros, F., Erickson-Johnson, M. R., Keeney, G. L., Clayton, A. C., Nascimento, A. G., Wang, X., and Oliveira, A. M. (2007) Frequency and characterization ofHMGA2 andHMGA1 rearrangements in mesenchymal tumors of the lower genital tract. *Genes, Chromosom. Cancer 46*, 981–990.

(136) Nezhad, M. H., Drieschner, N., Helms, S., Meyer, A., Tadayyon, M., Klemke, M., Belge, G., Bartnitzke, S., Burchardt, K., Frantzen, C., Schmidt, E. H., and Bullerdiek, J. (2010) 6p21 rearrangements in uterine leiomyomas targeting HMGA1. *Cancer Genet. Cytogenet. 203*, 247–252.

(137) Taatjes, D. J. (2010) The human Mediator complex: a versatile, genome-wide regulator of transcription. *Trends Biochem. Sci. 35*, 315–22.

(138) Makinen, N., Mehine, M., Tolvanen, J., Kaasinen, E., Li, Y., Lehtonen, H. J., Gentile, M., Yan, J., Enge, M., Taipale, M., Aavikko, M., Katainen, R., Virolainen, E., Bohling, T., Koski, T. A., Launonen, V., Sjoberg, J., Taipale, J., Vahteristo, P., and Aaltonen, L. A. (2011) MED12, the Mediator Complex Subunit 12 Gene, Is Mutated at High Frequency in Uterine Leiomyomas. *Science (80-.). 334*, 252–255.

(139) Turunen, M., Spaeth, J. M., Keskitalo, S., Park, M. J., Kivioja, T., Clark, A. D., M??kinen, N., Gao, F., Palin, K., Nurkkala, H., V??h??rautio, A., Aavikko, M., K??mpj??rvi, K., Vahteristo, P., Kim, C. A., Aaltonen, L. A., Varjosalo, M., Taipale, J., and Boyer, T. G. (2014) Uterine Leiomyoma-Linked MED12 Mutations Disrupt Mediator-Associated CDK Activity. *Cell Rep. 7*, 654–660.

(140) Sauzeau, V., Le Jeune, H., Cario-Toumaniantz, C., Smolenski, A., Lohmann, S. M., Bertoglio, J., Chardin, P., Pacaud, P., and Loirand, G. (2000) Cyclic GMP-dependent protein kinase signaling pathway inhibits RhoA- induced ca2+ sensitization of contraction in vascular smooth muscle. *J. Biol. Chem. 275*, 21722–91729.

(141) Brady, a J., Warren, J. B., Poole-Wilson, P. a, Williams, T. J., and Harding, S. E. (1993) Nitric oxide attenuates cardiac myocyte contraction. *Am. J. Physiol. 265*, H176–82.

(142) Zheng, J., Zhai, K., Chen, Y., Zhang, X., Miao, L., Wei, B., and Ji, G. (2016) Nitric oxide mediates stretch-induced Ca2+ oscillation in smooth muscle. *J Cell Sci* 2430–2437.

(143) Bartlett, S. R., Bennett, P. R., Campa, J. S., Dennes, W. J., Slater, D. M., Mann, G. E., Poston, L., and Poston, R. (1999) Expression of nitric oxide synthase isoforms in pregnant human myometrium. *J. Physiol. 521 Pt 3*, 705–16.

(144) Mirabile, C. P., Massmann, G. A., and Figueroa, J. P. (2000) Physiologic role of nitric oxide in the maintenance of uterine quiescence in nonpregnant and pregnant sheep. *Am. J. Obstet. Gynecol. 183*, 191–198.

(145) Holdsworth-Carson, S. J., Zaitseva, M., Vollenhoven, B. J., and Rogers, P. A. W. (2014) Clonality of smooth muscle and fibroblast cell populations isolated from human fibroid and myometrial tissues. *Mol. Hum. Reprod. 20*, 250–259.

(146) Banaganapalli, B., Mohammed, K., Khan, I. A., Al-Aama, J. Y., Elango, R., and Shaik, N. A. (2016) A Computational Protein Phenotype Prediction Approach to Analyze the Deleterious Mutations of Human MED12 Gene. *J. Cell. Biochem. 117*, 2023–2035.

(147) Mittal, P., Shin, Y., Yatsenko, S. A., Castro, C. A., Surti, U., and Rajkovic, A. (2015) Med12 gain-of-function mutation causes leiomyomas and genomic instability. *J. Clin. Invest. 125*, 3280–3284.

(148) Flake, G. P., Andersen, J., and Dixon, D. (2003) Etiology and pathogenesis of uterine leiomyomas: A review. *Environ. Health Perspect. 111*, 1037–1054.

(149) Foksinski, M., Kotzbach, R., Szymanski, W., and Olinski, R. (2000) The level of typical biomarker of oxidative stress 8-hydroxy-2′-deoxyguanosine is higher in uterine myomas than in control tissues and correlates with the size of the tumor. *Free Radic. Biol. Med. 29*, 597–601.

(150) Cooke, M. S., Evans, M. D., Dizdaroglu, M., and Lunec, J. (2003) Oxidative DNA damage: mechanisms, mutation, and disease. *FASEB J. 17*, 1195–214.

(151) Hori, M., Suzuki, T., Minakawa, N., Matsuda, A., Harashima, H., and Kamiya, H. (2011) Mutagenicity of secondary oxidation products of 8-oxo-7,8-dihydro-2'-deoxyguanosine 5'-triphosphate (8-hydroxy-2'- deoxyguanosine 5'-triphosphate). *Mutat. Res. 714*, 11–6.

(152) Krishnamurthy, N., Zhao, X., Burrows, C. J., and David, S. S. (2008) Superior removal of hydantoin lesions relative to other oxidized bases by the human DNA glycosylase hNEIL1. *Biochemistry 47*, 7137–7146.

(153) Yu, H., Venkatarangan, L., Wishnok, J. S., and Tannenbaum, S. R. (2005) Quantitation of four guanine oxidation products from reaction of DNA with varying doses of peroxynitrite. *Chem. Res. Toxicol. 18*, 1849–1857.

This dissertation was typed by Michaela Huynh.